

# **On the role of superoxide dismutase and protein phosphatase type-2C $\beta$ in neuronal cell death**

Dissertation

zur

Erlangung des Doktorgrades

der Naturwissenschaften

(Dr. rer. nat.)

dem

Fachbereich Pharmazie

der Philipps-Universität Marburg

vorgelegt von

**Susanna Manuela Grzeschik**

aus Münster

Marburg/Lahn 2003

Vom Fachbereich Pharmazie der Philipps-Universität Marburg als Dissertation am 14. März 2003 angenommen.

Erstgutachter Prof. Dr. Dr. J. Krieglstein

Zweitgutachter Prof. Dr. S. Klumpp

Drittgutachter Prof. Dr. P. H. Chan

Tag der mündlichen Prüfung am 25. April 2003

**To my parents**

## Acknowledgements

This thesis was prepared at the Institute for Pharmacology and Toxicology in the Faculty of Pharmacy of the Philipps-University, Marburg, under the guidance and supervision of **Professor Dr. Dr. Josef Krieglstein**. For his valuable support, his creative ideas, outstanding scientific knowledge and continuous openness for discussions I want to express all my gratitude. By his generosity I did not only gain knowledge and experience from working in his laboratory but was also allowed to profit from pursuing part of the research for my thesis at Stanford University, Palo Alto, CA.

I deeply thank Dr. Pak H. Chan, Professor at the Department of Neurosurgery, Stanford University, for his great generosity and never-ending support. I worked in his laboratory for over two years and was granted the experimental freedom and supervision which allowed me to carry out my experiments, attend international congresses, and write publications.

I especially thank Prof. Susanne Klumpp for all her great scientific and moral support, her encouragement throughout my time as a Ph.D student, for fruitful discussions, and the scientific training I received in her laboratory.

I am indebted to many others for their help and support without which this work would not have been possible. Many thanks go to all my colleagues at Stanford University and Philipps-University Marburg for their support, good cooperation and pleasant working atmosphere which contributed to the success of my scientific studies.

I like to thank Dr. Carsten Culmsee and Dr. Yuan Zhu for valuable advice. I am grateful to all my coworkers at Philipps-University, Marburg, for their direct and fruitful cooperation, constructive discussions and numerous suggestions which helped to improve my experiments.

I also would like to thank Dr. Dagmar Selke and all the other colleagues of Prof. Klumpp's laboratory for their scientific support.

Special thanks go to Dr. Carolina Maier for her great personal and scientific support. She was not only a wonderful colleague but also a dear friend I am happy to have met and worked with.

I want to thank Liza Reola, Ghezal Omar, and Bernard Calagui, Sandra Engel, Michaela Stumpf, Elke Bauerbach, Ute Lehmann and Ulrich Korell for their excellent technical support.

I also want to thank friends who made my stay at Stanford an enjoyable experience. Special thanks go to Waël Nouredine, Felicitas Kausch and Carolina Maier for their friendship and moral support.

Finally, my deepest love and gratitude goes to my family whose love and unwavering support give me the strength and confidence to go through the difficulties of life. All my love to my sisters Nicola and Ricarda and my brother Christian. To my wonderful parents who never hesitated to sacrifice their own well-being for ours, I dedicate this work.

The stay at Stanford University was supported for one year by a fellowship from the German Academic Exchange Service (DAAD). I am very grateful for their support.

# Index

<b>1. Introduction .....</b>	<b>1</b>
<b>1.1. Neuronal cell death in CNS damage.....</b>	<b>1</b>
<b>1.2. Role of SODs in neuronal damage.....</b>	<b>5</b>
1.2.1. Free radicals in brain injury .....	5
1.2.2. Superoxide dismutase family .....	7
1.2.3. SOD knock-out and transgenic mice used in this study.....	8
1.2.4. Cold injury- induced brain trauma .....	9
1.2.5. Intrastratial 3-NP model.....	12
<b>1.3. Role of protein phosphatase type-2C in neuronal cell death.....</b>	<b>14</b>
1.3.1 Phosphatases in cell function .....	14
1.3.2. Connection of PP2C with Bad and neuronal death.....	16
<b>1.4. Outline of the study.....</b>	<b>19</b>
<b>2. Material and Methods.....</b>	<b>22</b>
<b>2.1. Antibodies .....</b>	<b>22</b>
<b>2.2. Chemicals and materials.....</b>	<b>23</b>
<b>2.3. Cold injury-induced brain trauma (CIBT) experiments.....</b>	<b>29</b>
2.3.1. Animals .....	29
2.3.2. Genotyping of the SOD2 knock-out mice.....	29
2.3.3. General principles of surgery .....	33
2.3.4. Performance of CIBT surgery.....	33
2.3.5. Removal of brains and subsequent paraffin embedding .....	35
2.3.6. Histological assessment of infarct size.....	36
2.3.7. Hydroethidine assay .....	37
2.3.8. Perl's iron staining .....	38
2.3.9. MPO immunohistochemistry .....	39
2.3.10. Transferase-dUTP-Nick-End- Labelling (TUNEL-staining).....	41

<b>2.4. Experiments of intrastriatal 3-NP injection.....</b>	<b>43</b>
2.4.1 Animals .....	43
2.4.2. Genotyping of SOD1 transgenic and knock-out mice .....	43
2.4.3. Intrastratial 3-NP injection .....	45
2.4.4. Removal of brains and subsequent paraffin embedding .....	46
2.4.5 Cresyl violet staining of frozen sections and measurement of lesion size and edema .....	47
2.4.6. Transferase dUTP Nick-End Labelling (TUNEL-staining) .....	48
2.4.7. Immunohistochemistry of caspase-3 and caspase-9 in floating sections .....	48
<b>2.5. PP2C/Oleic acid experiments .....</b>	<b>50</b>
2.5.1. Animals .....	50
2.5.2. Preparation and cultivation of rat embryonic cortical neurons .....	50
2.5.3. Primary mixed hippocampal cultures from neonatal rats.....	52
2.5.4. Trypan blue staining.....	54
2.5.5. Quantification of apoptosis in neuronal culture .....	55
2.5.6. Nile blue-staining of lipid droplets in neuronal culture .....	56
2.3.7. Protein quantification .....	56
2.3.8. Western blotting analysis .....	57
2.3.9. Phosphorylation of Bad by PKA .....	62
2.5.10. Immunohistochemistry of PP2C $\beta$ in embryonic cortical neurons .....	62
2.5.11. Drug treatment of rat primary cultures .....	64
<b>2.6. Statistics.....</b>	<b>69</b>
<b>3. Results.....</b>	<b>70</b>
<b>3.1. Effect of SOD2-reduction on cold injury-induced brain trauma.....</b>	<b>70</b>
3.1.1. Lesion size and edema development in SOD2-KO mice and wild-type animals .....	70
3.1.2. Hemorrhagic transformations followed the same pattern in WT and SOD2-KO mice .....	72
3.1.3. Inflammatory response after CIBT in WT and SOD2-KO mice .....	73
3.1.4. TUNE-labelling in SOD2-KO and WT mice .....	77

3.1.5. Hydroethidine oxidation showed no significant difference in superoxide anion production.....	80
<b>3.2. The influence of the SOD1 level on intrastriatal 3-NP lesion.....</b>	<b>81</b>
3.2.1. Establishment of the model in wild type animals .....	81
3.2.2. Detection of apoptosis in WT animals .....	83
3.2.3 Size of lesion and edema formation in SOD1-TG mice, their wild-type littermates and SOD1-KO mice .....	87
<b>3.3. Search for PP2C activation after induction of damage in cultured neurons....</b>	<b>89</b>
3.3.1. Detection of Bad and Bad-155P and PP2C $\beta$ in cultured rat neurons.....	89
3.3.1.1. Detection of Bad/ Bad-155P by Western blotting in embryonic cortical neurons .....	89
3.3.1.2. Detection of PP2C $\beta$ in cultured neurons .....	92
3.3.2. Treatment of cultured rat neurons with oleic acid.....	94
3.3.2.1 Influence of B27 supplement on damaging effects of oleic acid .....	94
3.3.2.2 Influence of BSA or $\beta$ -cyclodextrine on solubility of oleic acid and damaging effect.....	99
2.3.2.3. Characterisation of neuronal damage after treatment of primary cultures with oleic acid/ DMSO in NB-B27.....	106
3.3.3. Nile blue staining of embryonic cortical neurons after oleic acid treatment....	110
3.3.4. Western blotting on Bad, Bad-155P and PP2C $\beta$ after oleic acid treatment in embryonic cortical and hippocampal cultures .....	111
3.3.5. Apoptotic effect of ginkgolic acids in rat neuronal cultures .....	113
3.3.5.1. Induction of apoptosis in rat neuronal culture by ginkgolic acids.....	114
3.3.5.2. Detection of Bad, Bad-155P and PP2C $\beta$ protein levels by Western blotting after Ginkgolic acids treatment of primary cultures.....	117
3.3.6. Treatment of embryonic cortical culture with elaidic acid .....	118
<b>4. Discussion .....</b>	<b>121</b>
<b>4.1. Neuroprotective effect of SOD1 in a model of intrastriatal 3-nitropropionic acid injection.....</b>	<b>121</b>
<b>4.2. Effect of SOD2 reduction on cold injury-induced brain trauma.....</b>	<b>125</b>
<b>4.3. Role of PP2C<math>\beta</math> in neuronal apoptosis .....</b>	<b>131</b>



<b>5. Summary .....</b>	<b>136</b>
<b>6. Zusammenfassung .....</b>	<b>138</b>
<b>7. Publications.....</b>	<b>141</b>
<b>7.1 Journals.....</b>	<b>141</b>
<b>7.2 Meetings .....</b>	<b>141</b>
<b>8. References .....</b>	<b>142</b>
<b>9. Abbreviations.....</b>	<b>161</b>
<b>10. Curriculum vitae .....</b>	<b>164</b>

# **1. Introduction**

## **1.1. Neuronal cell death in CNS damage**

The central nervous system (CNS) is an exceptional organ in many aspects: It functions as the control unit of the organism by recording and evaluating information from in- and outside and regulating body functions. There are over 100 billion neurons in the human CNS which interact with each other; they are the smallest units in a dense network that processes immense amounts of information. A single neuron can receive signals from up to 100,000 other cells and transfer the signal to a maximum of 10,000 cells by branches of its axon. An incredible amount of signals are exchanged, and by today, the function of the brain remains a miracle in a lot of aspects. In humans, the final number of neurons is reached shortly after birth, from then on they mature, interact with each other but do not divide and multiply. Although limited neurogenesis has been observed in some parts of the brain in adult primates by activation of stem cells, neurogenesis does not significantly influence the total number of cerebral neurons in mature animals. Neurons as carriers of information are meant to last a life time and when they are damaged and die, there is no replacement for them. Through improved life conditions in industrial countries the life expectation rose to 80 years for women and 74 years for men, however, the life span of neurons has not been extended. With increasing age chances are getting higher that neurons cannot maintain their physiological function and degenerate like all kind of cell types. The number of aged people in the population of western countries increased with the prolonged life expectation, which is associated with larger numbers of patients with neurodegenerative disorders like Morbus Alzheimer and Morbus Parkinson, or other age-dependent neuronal diseases like stroke and dementia. Stroke, for example, is the third frequent cause of death worldwide after cancer and cardiovascular diseases, and surviving patients often need lifelong intensive care as a result of insufficient regeneration from neuronal loss, not allowing full recovery (Bronner et al., 1995) (de Freitas et al., 2001).

Visualizing the impact of these diseases on patients and on expenses of health care shows how important the study of mechanisms of neuronal cell death is. Gaining knowledge about the pathophysiology of ischemia and neurodegenerative disorders could help to find potent therapies which could improve the prognosis and the life quality of patients.

### *Neuronal apoptosis versus necrosis*

All multicellular organisms including humans experience cell death as part of their existence during their developmental phase and their adult life. During development, cell death is absolutely necessary to shape organs and tissues. A genetic masterplan determines which cells survive or die in different developmental phases to allow the patterning of tissues and organs, thereby building a functional organism. Cell death also constantly occurs in adult organisms: Damaged or dysfunctional cells die and are removed; a delicate balance is kept between cell proliferation and death. The lifespan of a cell is determined by its function in the organism, and neurons are exceptional cells designed to maintain their function throughout the organism's life. However, acute brain damage and pathological neurodegeneration can cause cell death and the irreplaceable loss of neurons. Neuronal death in neurodegenerative diseases and brain damage can follow one of two different modes, necrosis or apoptosis. These types of cells death are two extremes at the opposite ends of a wide-ranged scale of possible mechanisms of cell death. Neuronal apoptosis, one the one hand, is defined as an active form of cell death. Biochemically, protein biosynthesis and activated death pathways can be detected including activation of caspases and nucleases which leads to DNA fragmentation. Morphologically, apoptosis shows typical features such as nuclear condensation, cell shrinkage and formation of apoptotic bodies. The process ends with disintegration of the cell and phagocytosis, ideally without involving inflammation. Neuronal necrosis, on the other hand, is passive, uncontrolled cell death due to lack of energy in which oxidative stress, excitotoxicity, disruption of the cellular  $\text{Ca}^{2+}$  homeostasis, mitochondrial dysfunction, ATP depletion and failure of  $\text{Na}^+/\text{K}^+$  ion pumps lead to cell swelling, lysis and release of its intracellular content into the surrounding tissue. It is followed by inflammatory response that further damages the surrounding cells. Cell death in different diseases or experimental models often can not be assigned, unequivocally, to one of these two categories since the cells do not display all typical features. This can partly be explained by the fact that a cell's determination to undergo apoptosis or necrosis is very often a matter of its energy supply. The intracellular ATP level determines the damaged cells for either necrosis (ATP level below 15 %) or apoptosis (25-75 % normal ATP level). Cells initially undergoing apoptosis can switch to necrosis any time the cell runs out of energy (Eguchi et al., 1997) (Lieberthal et al., 1998) (Nicotera et al., 1998). Considering just the two extreme categories might be too simple to grasp the whole concept of cell death, however, it is helpful in the elucidation of the mechanisms involved and it is acceptable as long as one is aware that a fluent transition from apoptosis to necrosis is possible.

So far, a vast amount of information has been gathered about both types of cell death, especially apoptosis. Programmed cell death has been shown to play an important role in the development and homeostasis of multicellular organisms by triggering an intrinsic cellular death program when cells are damaged, infected, aged or no longer receiving survival signals from their extracellular environment (Raff, 1998) (Vaux and Korsmeyer, 1999). Environmental stimuli that induce apoptosis are irradiation leading to DNA damage, oxidative stress, toxins, viruses and withdrawal of neurotrophic support. Apoptosis has been shown in numerous degenerative CNS diseases like Huntington's disease (Butterworth et al., 1998) and contributes to trauma and stroke (Mattson et al., 2000) (Li et al., 1995a); (MacManus et al., 1993) (Rink et al., 1995).

Induction of apoptosis in mammalian cells has been described to be mediated via two major pathways: a) Via death receptor stimulation and b) via a mitochondrial pathway in which apoptotic stimuli trigger the release of apoptogenic molecules from the mitochondria (Peter and Kramer, 1998) (Scaffidi et al., 1998) (Fig. 1).

A series of molecular key players of the apoptotic program are known so far which allow insight in the complexity of this process. Among them are the following ones:

- Apoptosis-inducing or death receptors (*e.g.* Apo-1/Fas) whose activation triggers apoptosis.
- Apaf-1 (apoptotic protease-activating factor 1) and other apoptosis-initiating factors (AIFs), molecules which activate cell death cascades.
- Small proteins released from damaged mitochondria into the cytoplasm in early stages of cell death like cytochrome c which activate postmitochondrial cascades of apoptosis. In general, release of cytochrome c from the mitochondrial inner membrane into the cytosol initiates the mitochondrial-dependent apoptosis pathway (Liu et al., 1996b) (Yang and Cortopassi, 1998).
- The Bcl-2 and p53 oncogene families and mitogen-activated protein kinase pathways regulated by neurotrophins which are key modulators of the cells response on apoptotic signals.
- Proteins/proteases of the caspase/calpain families which can activate each other and cleave death substrates. Amongst them are upstream instigator caspases (caspase-8) which activate other caspases, named effector caspases. They are important regulators of postmitotic neuronal homeostasis. Downstream caspases like caspase-3 or -9 and their proteolytic products are recognized markers of apoptosis, their activation representing an irreversible step in the cell death cascade ("point of no return"). Cells expressing these enzymes are prone to

death. Once activated, many but not all of these enzymes induce proteolysis of specific cellular substructures and consequently amplify the death signal cascade (Hengartner, 2000).

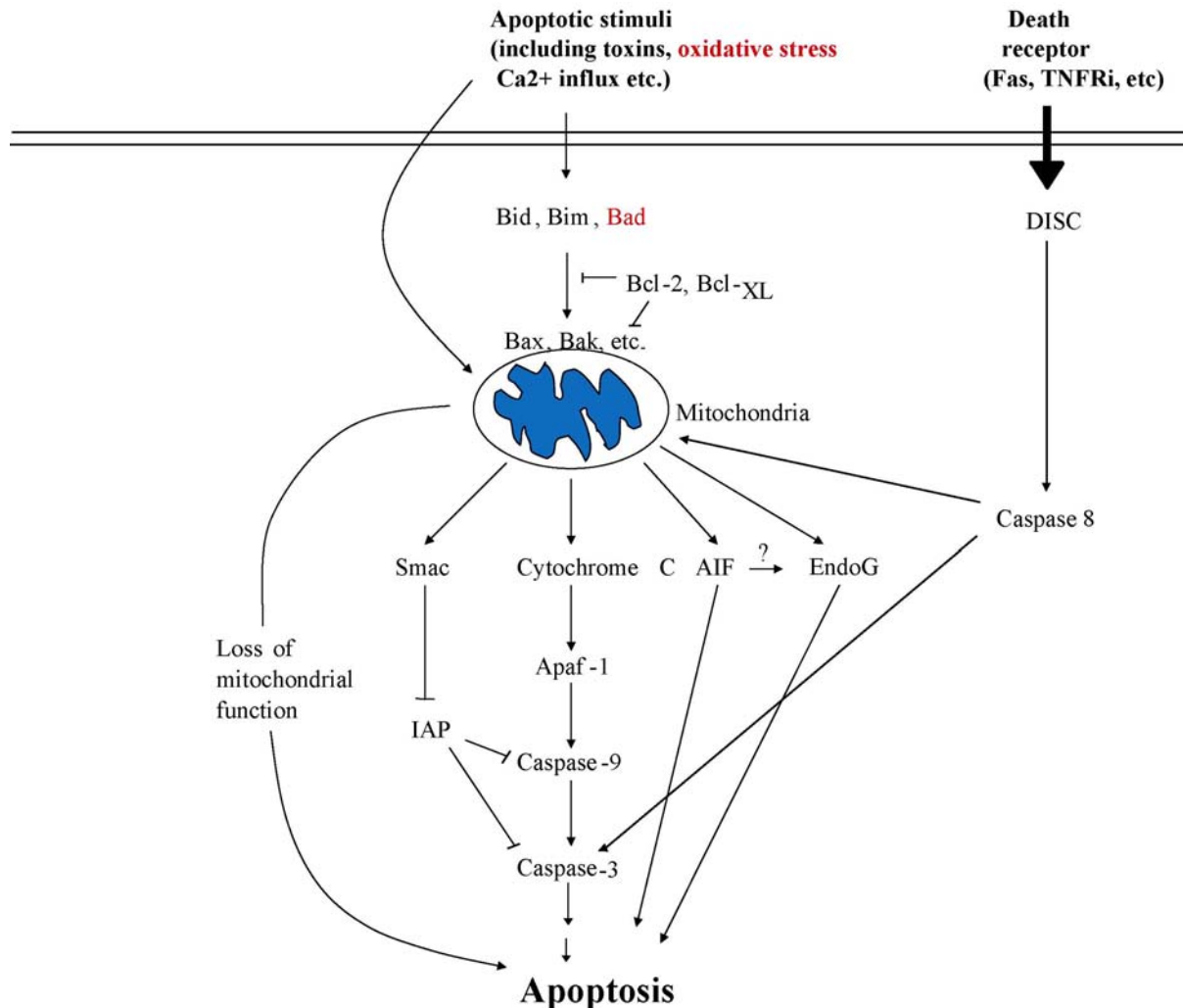


**Figure 1: Schema of apoptotic pathways in mammalian cells**

Apoptosis can be induced by different pathways which result in caspase activation, cleavage of cellular substrates, DNA fragmentation and cell death. One pathway includes mitochondrial damage caused by proapoptotic Bcl-2 family members or other apoptotic stimuli. This triggers the release of apoptogenic proteins such as cytochrome c, Smac, AIF, and EndoG. Cytochrome c leads to caspase activation through Apaf-1, and Smac relieves IAP inhibition of caspases. AIF and EndoG cause chromatin condensation and fragmentation in a caspase-independent manner. Bcl-2 family members which can transduce apoptotic stimuli to mitochondria are pro-apoptotic members, such as Bad, Bim or Bax. These signals, if not

*neutralized by antiapoptotic proteins, such as Bcl-2 or Bcl-x<sub>L</sub>, are further transferred to the mitochondria by proapoptotic proteins such as Bax or Bak.*

*Apoptosis can also be triggered via activation of death receptors such as Fas which leads to caspase activation and apoptosis. The steps studied in this thesis, modulation of oxidative stress by quantitative variation of scavenging enzymes SOD and the phosphorylation of Bad, are highlighted by coloured letters.*

*(Modified from Wang, 2001)*

Activation of proteins which participate in the cell death cascade can either happen by cleavage of proforms, by increased protein expression or by reversible phosphorylation since the activity of many proteins and enzymes depends on their state of phosphorylation.

The wide interest in especially mechanisms of programmed cell death is understandable: It is established that apoptosis can be inhibited or reversed at an early stage before the “point of no return”, and the elucidation of the apoptotic processes might provide targets for neuroprotection. However, since necrosis is a major component of acute neuronal damage as stroke or trauma, observation and elucidation of its mechanisms is important, as well. In this thesis, different models of neuronal cell death are applied to study specific factors involved in programmed cell death and necrosis. The two different “in vivo” models of neuronal damage, cold injury-induced brain trauma (CIBT) and intrastriatal injection of the toxin 3-nitropropionic acid (3-NP) in mice, were employed to study the influence of quantitative modulation of superoxide dismutases (SODs) on brain damage. In addition, the role of the enzyme protein phosphatase type-2C (PP2C) which participates in the reversible phosphorylation of proteins during neuronal apoptosis was studied in cultured rat neurons.

## **1.2. Role of SODs in neuronal damage**

### **1.2.1. Free radicals in brain injury**

Free radicals are produced in tissues under physiological as well as under pathological conditions. They are defined as molecules with free, unpaired electrons; a compound which contains oxygen with a single, unpaired electron in an outer orbital shell is called oxygen free radical. Oxygen free radicals, belong to a group of with reactive oxygen species (ROS) which can oxidize and damage cell structures like lipids, nucleic acids, proteins and saccharides (Lewen et al., 2000). Among potentially cytotoxic ROS are superoxide anion radicals (O<sub>2</sub><sup>-</sup>),

hydroperoxyl radicals ( $\text{HO}_2^\cdot$ ), hydrogen peroxide ( $\text{H}_2\text{O}_2$ ), hydroxyl radicals ( $\text{HO}^\cdot$ ), lipid peroxide radicals ( $\text{R-OO}^\cdot$ , R= lipid), singlet oxygen ( $^1\text{O}_2$ ), nitric oxide ( $\text{NO}^\cdot$ ) and peroxynitrite ( $\text{ONONO}_2$ ). Under physiological conditions, the electron chain of the mitochondria is a constant source of free radical production, about 2-5 % of oxygen is not fully utilized but transformed into ROS, preferentially superoxide anion radicals and hydrogen peroxide. The energy demand of the brain and its  $\text{O}_2$  consumption is especially high since its high metabolism rate is essential for pumping ions associated with synaptic communication. Although its weight is just 2 % of the total body weight, about 20 % of the body's oxygen intake is used by the brain, mainly for the production of high energy molecules like adenosine-triphosphate (ATP). Its respiration rate is about 10 times higher than that of other body tissues and even under physiological conditions ROS production is high. Additionally, the brain is a likely source of reactive oxygen species since it contains high levels of iron and copper metals which can lead to the production of the especially aggressive hydroxyl radical by the Fenton reaction. Finally, the brain contains a high percentage of lipids and is therefore an easy target for oxidation and generation of free oxygen radicals. Unsaturated bonds of fatty acids in lipids and membrane cholesterol can react with free radicals and undergo peroxidation (Bast and Goris, 1989); each of the resulting peroxides is a potential free radical which can start an autocatalytic reaction that peroxidizes the neighbouring lipids and starts a cascade of free radical production.

To protect themselves from oxidative stress created by a high metabolism rate, brain cells employ protective mechanisms which include superoxide dismutases (SODs), enzymes which are able to scavenge superoxide anion radicals, glutathione peroxidase, catalase, and antioxidative compounds like vitamin E, glutathione or ascorbic acid. Under pathological conditions, production of ROS can be strongly increased to a level which exceeds the capacities of the endogenous antioxidative defence and have deleterious effects to the cell leading to both apoptosis and necrosis. Superoxide anion radicals react with  $\text{NO}^\cdot$ , constantly produced by the nitric oxide synthase, to peroxynitrite which degrades to aggressive hydroxyl radicals and nitrogen dioxide or leads to nitration of cellular tyrosines (Beckman et al., 1990).

Especially the pathomechanism of neuronal necrosis has been shown to be closely associated with both free radical production and excitotoxicity. Free radicals can increase the extracellular concentration of excitatory neurotransmitters like glutamate by inhibiting its re-uptake (Trotti et al., 1998). Intracellular  $\text{Ca}^{2+}$  overload is triggered via activation of glutamate receptors associated with  $\text{Ca}^{2+}$  ion channels (Carriedo et al., 1998). Destruction of the intracellular ion homeostasis leads to mitochondrial dysfunction resulting in a stop of ATP

production. As long as the cell is still supplied with oxygen, mitochondrial dysfunction causes ROS production, and without full detoxification from these free radicals the mitochondria themselves become targets of free radical attacks. This leads to the *circulus vitiosus* of further impairment of ATP generation causing energy depletion followed by enhanced free radical production (Hillered and Chan, 1988a) (Coyle and Puttfarcken, 1993). There are other free radical pathways activated by high  $\text{Ca}^{2+}$  levels, including the conversion of xanthine dehydrogenase to xanthine oxidase, nitric synthase and the phospholipase  $\text{A}_2$ -cyclooxygenase pathways which, again, lead to the formation of superoxide anion radicals, hydrogen peroxide, nitric oxide and peroxyxynitrite (Lewen et al., 2000). By oxidation of cellular structures like lipids, DNA, and proteins, ROS destroy and alter their functions. Even high intracellular levels of ROS do not kill cells directly but through  $\text{Ca}^{2+}$  as demonstrated in previous studies revealing that even under high peroxide concentrations (level 100 times higher than under physiological conditions) neuronal cells survived if their  $\text{Ca}^{2+}$  intake was inhibited (Maher and Schubert, 2000).

### **1.2.2. Superoxide dismutase family**

The SOD family, endogenous free radical scavengers, includes three well known members in mammalian cells: Copper/zinc-superoxide dismutase (SOD1, Cu,Zn-SOD) a homodimer constitutively expressed in the cytosol; inducible manganese-superoxide dismutase (Mn-SOD, SOD2) which is localized in the mitochondrial matrix as a homotetramer; high-molecular weight tetrameric glycosylated Cu,Zn- SOD which can be found in the extracellular space (E-SOD, SOD3) and is present only in low levels in the brain (Fridovich, 1995). All of the SODs dismutate superoxide anion radicals to hydrogen peroxide which is subsequently converted to molecular oxygen and water by catalase and selenium-dependent glutathione peroxidase. First experiments to understand the role of SODs in the functionality of the cells and their role in CNS damage revealed a protective effect of liposome-entrapped SOD1 in traumatic and ischemic injuries (Chan et al., 1987) (Imaizumi et al., 1990) (Michelson et al., 1988) (Phelan and Lange, 1991). Other investigators obtained various degrees of success (Wei et al., 1981) (Pigott et al., 1988; Liu et al., 1989) (Levasseur et al., 1989) (Zhang and Ellis, 1991) or failure (Forsman et al., 1988) (Haun et al., 1991) (Ikeda et al., 1989) (Ment et al., 1985) (Schurer et al., 1990) when using free, non-modified SOD or modified SOD (PEG-SOD) in various models of neuronal injury. SOD1's short half life in circulating blood (6 min) and its inability to pass the blood brain barrier (BBB) explain, partly, the contradicting results about



neuroprotection by SODs. A more elegant approach to unveil the direct role of SODs in the pathogenesis of brain damage, however, is the use of genetically engineered animals in which the level of SOD expression has been altered by either “transgenically” increasing their level or decreasing the level by deletion or mutation of the genes in “knock-out” approaches. One has to be aware that by genetic modulation of protein expression cells possibly develop mechanisms to compensate or counteract the genetic change and therefore, in some cases, the physiology of genetically modified cells is different from normal cells. Still, knock-out and transgenic animals offer the great opportunity to examine underlying mechanisms of cell physiology and damage. In this thesis, three different strains of genetically engineered mice were used to test the effect of SOD in brain damage, heterozygous SOD2 knock-out (SOD2-KO, het), homozygous SOD1 knock-out mice (SOD1-KO) and SOD1 transgenic mice (SOD1-TG) mice.

### **1.2.3. SOD knock-out and transgenic mice used in this study**

#### *1) SOD2-KO:*

In SOD2-KO mice *Sod2* was mutated with a replacement type targeting vector that deleted exon 3 of the SOD2 gene which resulted in a shortened m-RNA and loss of enzymatic activity. Homozygous SOD2-KO mice showed a lethal phenotype, animals only survived until postnatal day 10, showed dilated cardiomyopathy and steatosis. Therefore, instead of homozygous animals, heterozygous mice were more suitable for brain injury experiments. At the age of 9 month, heterozygous animals revealed no discernible phenotypic difference compared to their wild-type littermates other than that their enzymatic SOD2 activity was reduced to 50 % (Li et al., 1995b). These mice have been tested in various models of brain and neuronal injury including traumatic brain injury (TBI) (Lewen et al., 2001), transient focal ischemia (Noshita et al., 2001) (Kim et al., 2002), permanent focal ischemia (Murakami et al., 1998b) (Fujimura et al., 1999b) subarachnoid haemolysate exposure (Matz et al., 2001), systemic 3-NP intoxication (Kim and Chan, 2002), and glutamate toxicity in neuronal culture (Li et al., 1998). The role of SOD2 as a neuroprotective enzyme was evident in all models since a decrease in protein level resulted in exacerbated damage, mostly correlating with increased cytochrome c release from the mitochondria. Not in all models an increase in apoptosis was associated with exacerbated brain injury in SOD2-KO mice, e.g. after TBI the number of apoptotic cells was reduced although the total number of damaged cells had increased, as had the cytochrome c release.

## 2) *SOD1-TG*:

The second kind of genetically modified animals used in this study were SOD1-TG mice of the strain TgHs/SF-218 carrying the human CuZn-SOD (h-SOD-1) gene and being bred on a CD-1 background. The genome of this strain carried several copies of the h-SOD-1 gene, presumably in a tandem array and showed a threefold increase in SOD1 activity. There were no observable phenotypic differences between SOD1-TG mice and their non-transgenic littermates (Chan et al., 1991). SOD1 overexpression had revealed neuroprotective effects in a number of brain injury models including global and focal cerebral ischemia (Kinouchi et al., 1991) (Kinouchi et al., 1998) (Yang et al., 1994) (Murakami et al., 1997) (Fujimura et al., 1999a) (Fujimura et al., 2000), cold injury-induced brain trauma (Chan et al., 1991), neurotoxicity in neuronal culture (Chan et al., 1990b), methamphetamine neurotoxicity (Cadet et al., 1994), systemic 3-nitropropionic acid toxicity (Beal et al., 1995), photothrombotic ischemia (Kim et al., 2001), traumatic brain injury (Mikawa et al., 1996), subarachnoid hemorrhage (Kamii et al., 1999) and spinal cord injury (Sugawara et al., 2002). However, not in all types of brain injury models SOD1 overexpression improved the outcome, as in a model of permanent focal ischemia the damage was not attenuated (Chan et al., 1993).

## 3) *SOD1-KO*:

The third strain of animals used for this study were SOD1-KO mice of the strain *Sod1*<sup><tm1 Cep></sup> created by a targeted deletion of the *Sod1* gene in embryonic stem cells of 129/CD1 mice using a positive-negative selection scheme that replaced all *Sod1* coding sequences with a neomycin resistance gene. Homozygous knock-out mutants were bred on a CD1 background for at least 8 generations, they showed 100 % reduction of SOD1 activity while their phenotype was not distinct from their wild-type littermates'. Although in a model of transient focal and global ischemia the damage was exacerbated in SOD1-KO mice (Kondo et al., 1997b) (Kawase et al., 1999) and the animals revealed increased neuronal damage induced by kainic acid (Kondo et al., 1997a), the reduction of SOD1 did not affect the infarction after permanent focal cerebral ischemia (Fujimura et al., 2001).

### 1.2.4. Cold injury-induced brain trauma

Cold injury-induced brain trauma (CIBT), synonymous with cryogenic injury, is a model for early development of vasogenic cerebral edema which is the most common form of brain edema observed after many brain injuries like trauma and stroke (Tanno et al., 1992)

(Baskaya et al., 1997) (Kogure et al., 1981). Characterized by increased brain water and sodium content, it is associated with increased permeability of the blood brain barrier (BBB) for macromolecules like serum proteins which is normally limited due to the tight barrier of capillary endothelial cells. Brain injuries concomitant with vasogenic edema can be explained by several pathophysiological mechanisms: Primary damage can be caused by swelling of the edematous tissue and brain herniation which can lead to critical conditions. Additionally, swelling of the injured tissue can increase the intracranial pressure leading to decreased cerebral perfusion and ischemia. Furthermore, the distance between cells and vessels gets extended by extravasation of fluid into the extracellular space, as gets the diffusion distance for oxygen and nutrition. Therefore, the edema forces the tissue into an ischemic state and leads to a declined ATP production. Furthermore, vasogenic edema has been shown to release arachidonic acid from membrane lipids, potentially inducing a cascade of free radical production and excitotoxicity (Chan et al., 1990a). Finally, humoral components extravasate from the vessels into the tissue and can possibly damage the cells, as well.

CIBT induces trauma by application of low temperature on the exposed cortex and was first established in cats by Klatzo et al., 1958, then modified for rats and later developed for mice (Chan et al., 1991). In the latter modification, craniotomy is not necessary since the skull of mice is thin enough to allow damage of the underlying cortex; therefore this procedure is less invasive. The development and severity of the lesion after CIBT varies in different studies due to use of different protocols of CIBT induction and different experimental animals. In general, the vessels in the core of the lesion area are mechanically disrupted by freezing. Subsequently, capillaries in the lesion become permeable for molecules from the vascular compartment by secondary damage mechanisms. Thus, serum elements extravasate and spread by hydrostatic forces from the systemic circulation (Reulen et al., 1977). Cells, amongst them astrocytes, take up serum proteins after extensive extravasation (Maeda et al., 1997). During the phase of early edema, massive cell death, both necrosis and apoptosis, occurs inside the lesion. After closure of the injured small vasculature, healing processes take place around the cold lesion with proliferation of the microvasculature, and edema fluids and serum proteins gradually disappear (Orita et al., 1988).

The model of CIBT used in this study has been well established by Chan et al. (Chan et al., 1991): Following CIBT, an early (1 to 4 hours) increase in water content in the injured hemisphere was demonstrated that reached its maximum level at 24 h and remained elevated for 3 days. BBB breakdown, while also acute, returned to baseline values by 24 h post-CIBT (Chan et al., 1991) (Murakami et al., 1998a) (Murakami et al., 1999). Apoptosis,

characterized by appearance of TUNEL-positive cells, was maximal at 72 h post-insult in the periphery of the injury and was thought to contribute to secondary brain damage and lesion expansion in both early and late phases after cold injury. Cytochrome c release from the mitochondria was demonstrated as well as caspase activation indicating that apoptosis, indeed, contributed to cell death after CIBT (Morita-Fujimura et al., 1999b) (Morita-Fujimura et al., 1999a).

Oxidative stress seems to be a major component in CIBT damage: Liposome-entrapped SOD1 reduced BBB breakdown, transgenic mice overexpressing copper-zinc (Cu/Zn) SOD (SOD1) revealed significant attenuation of brain edema, neurological deficits and a reduction of blood-brain barrier (BBB) permeability following CIBT (Chan et al., 1987; Chan et al., 1991) supporting the notion that ROS are implicated in traumatic brain injury development. Release of arachidonic acid occurring after CIBT has been associated with free radical production and subsequent excitotoxicity causing enhanced repeated ROS generation (Chan et al., 1988).

Pathophysiology and biochemical sequelae of focal neuronal and glial damage after cold-induced brain trauma are thought to be quite similar to traumatic brain injury (TBI) since vascular compartments are the major targets for free radical attack (Chan et al., 1983) (Chan et al., 1987) (Kontos, 1985). Therefore, findings from TBI can, with restrictions, be transferred to the CIBT model as well. Like in CIBT, experimental evidence has associated reactive oxygen species (ROS) formation as one of the various biochemical events leading to cell death with TBI (Lewen et al., 2000). Brain injury in cats has been reported to increase the production of superoxide anion which is normally scavenged by superoxide dismutase (Kontos and Wei, 1986; Patel et al., 1996) Several studies have demonstrated apoptotic cell death following TBI, and two major pathways have been identified in mammalian cells: the Fas/TNF-R receptor pathway and the mitochondrial pathway (Rink et al., 1995) (Clark et al., 1997; Skoglosa et al., 1999). The mitochondrial electron transport chain is one of the many sources of ROS (Phillis, 1994) and plays a significant role in the pathogenesis of TBI. In general, release of cytochrome c from the mitochondrial inner membrane into the cytosol initiates the mitochondrial-dependent apoptosis pathway (Liu et al., 1996b) (Yang and Cortopassi, 1998). It has been shown that oxidative stress-dependent mechanisms after severe TBI result in the release and translocation of cytochrome c from the mitochondria to the cytosol 1 hour (Lewen et al., 2001) before DNA fragmentation. Manganese superoxide dismutase (SOD2)-deficient mice in particular, expose massive mitochondrial cytochrome c release after controlled cortical impact leading to large cortical lesions but less apoptotic cell death 4 and 24 hours after injury compared with WT animals (Lewen et al., 2001).

Regarding the exacerbation of damage after TBI in SOD2-KO mice compared to WT animals and manifestation of increased secondary and delayed BBB breakdown at 72 h post-insult in a model of transient focal ischemia, it was hypothesized that SOD2-KO mice would be more susceptible to secondary brain damage and hemorrhage in CIBT, as well. In this thesis SOD2-KO mice were subjected to CIBT to test the role SOD2 in the development of the lesion, especially focussing on the late effects and delayed BBB breakdown.

### **1.2.5. Intrastratial 3-NP model**

The mycotoxin 3-nitropropionic acid (3-NP, mildewed sugar cane toxin) is an irreversible inhibitor of succinate dehydrogenase, an electron transport enzyme in complex II of the mitochondria. By blocking both mitochondrial electron transport and Krebs Cycle, it leads to cellular depletion of adenosine triphosphate (ATP) (Ludolph et al., 1992). Therefore, hypoxic (energy-deficient) brain damage such as specific, striatal lesions is induced after chronic or subacute systemic treatment (Alston et al., 1977) (Palfi et al., 1996).

3-NP intoxication provides an interesting model of CNS damage since it can produce selective striatal lesions resembling the histological, neurochemical, and clinical features of Huntington's Disease (HD) (Palfi et al., 1996) (Borlongan et al., 1997; Brouillet et al., 1999). Huntington's Disease is a progressive neurodegenerative disorder associated with severe degeneration of basal ganglia neurons, especially intrinsic neurons of the striatum and characterized by progressive dementia and involuntary abnormal choreiform movements (Martin and Gusella, 1986). The degeneration of basal ganglia is associated with a decrease of mitochondrial function most notable in the caudate nucleus (Brennan et al., 1985). The way of administering 3-NP seems to be a crucial aspect determining how closely the model reflects the features of HD: Chronic, systemic treatment with low doses of 3-NP, on the one hand, can produce selective striatal lesions sparing aspiny NADPH-diaphorase-positive neurons and replicating some features of HD (Beal et al., 1993b) (Brouillet et al., 1995) (Palfi et al., 1996). Apoptosis has been shown to be the most prominent type of cell death after this kind of treatment (Sato et al., 1997a).

Acute systemic or intrastratial treatment with 3-NP, on the other hand, does not closely correlate with HD (Beal et al., 1993b). Intrastratial injection of 3-NP leads to degeneration of both intrinsic striatal neurons and the nigrostriatal dopaminergic system, suggesting that this lesion may provide an animal model of a form of multiple system atrophy rather than Huntington's disease (Nakao and Brundin, 1997). It is characterized by severe loss of

neuronal cell bodies and marked glial infiltration in the medial aspect of the striatum. In comparison with systemic chronic administration, it results in more profound hypoactivity, greater loss of passive avoidance retention, and more severe striatal damage (Koutouzis et al., 1994) (Borlongan et al., 1997). Rapid cell death after intrastriatal injection may be due to excitotoxic necrosis as suggested by previous studies (Ankarcrona et al., 1995), however, apoptosis has been described as an underlying mechanism of cell death as well (Sato et al., 1997b) (Sato et al., 1998).

Investigations of cell death mechanisms in HD have identified energy depletion and increased sensitivity for excitatory amino acids (EAA, e.g. glutamate) as a primary cause of neuronal cell death (Zorumski and Olney, 1993). One hypothesis is that cells degenerate due to increased cellular vulnerability to glutamate excitotoxicity. This increased toxicity is caused by deficits in mitochondrial energy production which are evident, too, after 3-NP intoxication (Albin and Greenamyre, 1992) (Ankarcrona et al., 1995) (Beal et al., 1993b). Energy depletion induced by 3-NP has been described to potentate the glutamatergic intoxication especially via NMDA receptors as well as non-NMDA receptors (Simpson and Isaacson, 1993) (Beal et al., 1993b) (Hamilton and Gould, 1987), and blood brain barrier (BBB) dysfunction followed by serum proteinaceous deposits might modulate the severity of the lesion (Hamilton and Gould, 1987) (Nishino et al., 1995). Supporting the hypothesis that 3-NP neurotoxicity might be mediated by an overproduction of ROS, previous findings showed increased peroxynitrite production after 3-NP treatment (Schulz et al., 1996), in vivo protein oxidation in striatal synaptosomes (Fontaine et al., 2000), reduction of the striatal lesion after subacute, systemic treatment in SOD1-overexpressing animals, and increased vulnerability in heterozygous Mn-SOD knockout mice (Beal et al., 1995) (Andreassen et al., 2001) (Kim and Chan, 2002). Oxidative stress associated with 3-NP toxicity could possibly be produced via by three mechanisms:

1) Enhanced ROS production by increased O<sub>2</sub> flux from the electron chain in mitochondria; 2) induction of enhanced excitotoxicity; 3) inflammatory responses to neuronal degeneration. 3-NP inhibition of succinate dehydrogenase of the Krebs cycle in the mitochondria increases the production of ROS via a direct mechanism by functional impairment of the electron transport chain. An excitotoxic mechanism of ROS production has been described to be mediated via NMDA receptor activation (Lafon-Cazal et al., 1993): Decreased ATP levels lead to the loss of membrane depolarisation (Riepe et al., 1992) which relieves the voltage dependant Mg<sup>2+</sup> block of NMDA (N-methyl-D-aspartate) receptor ion channels (Henneberry et al., 1989). Unblocking these receptors allows ambient glutamate concentrations to push the intracellular

ion homeostasis out of balance, triggers  $\text{Ca}^{2+}$  influx which can not be counteracted by the cell due to energy depletion. At first,  $\text{Ca}^{2+}$  may be taken up by mitochondria and endoplasmatic reticulum, but when their capacity is exceeded, high intracellular  $\text{Ca}^{2+}$  concentrations further impair mitochondrial function, increase ROS production via mitochondrial and cytoplasmatic pathways and activate caspases, phospholipases, kinases and endonucleases (Brouillet et al., 1999). All these events ultimately lead to cell death through different pathways which are related to apoptosis or necrosis depending on cell type, severity of energy depletion and possible compensatory mechanisms.

Oxidative stress can also occur in association with inflammatory response induced by 3-NP. Neutrophil infiltration, immunoreactivity to serum/immune complement factors like C3b/C4B4 have been observed after 3-NP intoxication suggesting inflammation taking place in the lesion (Nishino et al., 1995). Additionally, levels of pro-inflammatory cytokines, tumor necrosis factor alpha (TNF- $\alpha$ ) (Geddes et al., 1996) and expression of inducible nitric oxide synthase (Nishino et al., 1996) have been found to be increased.

Since increased excitotoxicity is just one of many pathways, thought to be involved in the pathogenesis of HD, neither systemic acute or chronic administration of 3-NP nor models of intrastriatal injection fully mimic HD-related cell death. However, they are well established models to study excitotoxic cell death after inhibition of mitochondrial ATP production. In the present study, a model of intrastriatal 3-NP injection was employed to study whether SOD1 influences the outcome of the lesion. Since overexpression of SOD1 decreases the lesion in a more moderate model of subacute systemic 3-NP treatment (Beal et al., 1995), we set out to determine whether in an acute model of intrastriatal 3-NP injection SOD1 might play a protective role as well, using SOD1-TG mice as well as SOD1-KO animals.

### **1.3. Role of protein phosphatase type-2C $\beta$ in neuronal cell death**

#### **1.3.1 Phosphatases in cell function**

Reversible phosphorylation, the phosphorylation of proteins by protein kinases (PKs) and subsequent dephosphorylation by protein phosphatases (PPs), is an important cellular mechanism to regulate the function of proteins. This regulation includes modulation of enzymatic activities, marking proteins for destruction, enabling them to move from one cellular compartment to another or changing their association with other proteins. Kinases and phosphatases themselves are possible targets for reversible phosphorylation. By modulation

of kinase and phosphatase activities the cell can regulate different cellular pathways, including programmed cell death/apoptosis. A number of disorders have been implicated with mutations in protein kinases and phosphatases and deleterious effects of some naturally occurring toxins and pathogens can be explained by them altering protein phosphorylation. Understanding processes which are regulated by reversible phosphorylation will reveal new therapeutical targets for the treatment of various diseases. For example, progress has been made in developing specific inhibitors of protein kinases for the treatment of cancer and chronic inflammatory diseases (Cohen, 2001).

About 600 kinases are known to be encoded by the human genome but only an estimated number of 200 phosphatases (Cohen, 2001). However, since single phosphatase catalytic units are often associated with several different regulatory or targeting subunits, it is believed that the number of functional phosphatase holoenzymes adds up to the number of protein kinases. Whereas, so far, the focus of research interest was predominantly on protein kinases, it is evident that protein phosphatases as their counterparts play an equally important role. There are 4 potential sites for phosphorylation and dephosphorylation in proteins: the amino acids serine, threonin and tyrosine which contain a free –OH residue whose phosphorylation leads to O-phosphates and histidine which can be phosphorylated at its -NH group creating N-phosphoamidates. Thus, 3 different superfamilies of protein O-phosphatases exist: The protein tyrosine phosphatases (PTP) including members such as dual-specificity phosphatase and serine/threonine phosphatases which are grouped into members of the PPP family (phosphoprotein phosphatases) and PPM family (protein phosphatase  $Mg^{2+}$ -dependent) which are defined by molecular structure and conserved amino acid sequences (Klumpp et al., 2002). PP1, PP2A or PP2B belong to the family of PPPs whereas five PP2C isoforms and the pyruvate dehydrogenase with similar amino acid sequences are part of the PPM family (Ingebritsen and Cohen, 1983). Additionally, protein histidine phosphatases have been discovered which can dephosphorylate N-phospho-histidine. The nomenclature of serine/threonin phosphatases has been established according to their biochemical properties before gaining more knowledge about structural similarities: Type 1 enzymes were inhibited by heat-stable inhibitor proteins and preferentially dephosphorylated the  $\beta$ -subunit of phosphorylase kinase. Type 2 protein phosphatases, on the contrary, were insensitive to these inhibitors and preferentially dephosphorylated the alpha unit of the phosphorylase kinase. Type 2 was divided in different subtypes which were activated under special conditions: While PP2A was spontaneously active, PP2B activity was  $Ca^{2+}$ -dependent and PP2C  $Mg^{2+}$ -dependent. An additional parameter by which phosphatases could be differentiated from each



other was their sensitivity to certain toxins, such as okadaic acid, a fatty acid derivative, or microcystin, a cyclic heptapeptide. Both natural toxins known to be potent inhibitors of most Ser/Thr phosphatases in different concentrations (Cohen et al., 1990). PP1, PP2A and PP2B activity could be inhibited by these toxins whereas PP2C as well as members of the PTP superfamily stayed unaffected.

### 1.3.2. Connection of PP2C with Bad and neuronal death

Protein phosphatase type 2C enzymes (PP2Cs), members of the PPM family, are monomeric molecules with a relative molecular weight ( $M_r$ ) of 42,000- 48,000 Da. PP2C $\alpha$  and PP2C $\beta$  are the two most prominent PP2C enzymes, produced from distinct genes, while each of them can be divided in several isoforms due to different splicing variants. Since full PP2C activity was detectable only in the presence of unphysiologically high concentrations of  $Mg^{2+}$ -ions (10-20 mM  $Mg^{2+}$  or  $Mn^{2+}$ -ions) *in vitro*, for a long time the importance of PP2C was underestimated (Tsuiki et al., 1988). When Klumpp et al. discovered that certain unsaturated fatty acids like oleic acid or ginkgolic acids increased the activity of PP2C *in vitro* and that in the presence of these kinds of fatty acids much lower  $Mg^{2+}$  concentrations were sufficient for activation, the physiological role of PP2C had to be re-evaluated (Ahlemeyer et al., 2001) (Klumpp et al., 1998).

These fatty acids or derivatives which were able to activate PP2C had common chemical and structural features: They were unsaturated, lipophilic compounds with a minimum chain length of 15 C-atoms and had a negatively charged group. Interestingly, the same fatty acids which activated PP2C *in vitro* induced apoptosis in chick neuronal culture (Klumpp et al., 2002). This astonishing finding gave reason to hypothesize that PP2C activation could play an important role in neuronal apoptosis.

It is unresolved how the apoptotic pathway is influenced by PP2C, however, there is strong indication that the dephosphorylation of Bad (Bcl-2/Bcl-x<sub>L</sub>-antagonist, causing cell death) might be one of the underlying pro-apoptotic mechanisms (Klumpp and Krieglstein, 2002). Bad belongs to the Bcl-2 family which consists of pro- (Bax, Bid, Bad, Bak, Bcl-x<sub>S</sub>) and anti-apoptotic members (Bcl-2, Bcl-x<sub>L</sub>) which control a critical intracellular checkpoint within an evolutionary preserved cell death pathway (Wang and Reed, 1998) (Fig. 1). They are key regulators of apoptosis whose function as cell death agonists or antagonists is modulated by transcriptional and posttranscriptional modifications. The relative ratio between anti- and pro-

apoptotic members of this family determines the ultimate sensitivity to cell apoptotic signals (Oltvai et al., 1993). Many of the Bcl-2 family proteins are capable of interacting with each other by a shared sequence homology with Bcl-2 in the BH3 (**Bcl-2 homology 3**) domain, an amphipathic helix required to interact with other Bcl-2 family members (Huang and Strasser, 2000). They are normally located in other cellular compartments and translocate to the mitochondria in response to apoptotic stimuli. Once translocated to the mitochondria, they interact with each other, causing mitochondrial damage and release of apoptogenic proteins possibly through the formation of a permeability transition pore in the mitochondrial membranes. Cytochrome c, one of the pro-apoptotic proteins released from mitochondria, forms a cytoplasmic complex including Apaf-1 and caspase-9. This results in caspase-9 activation and subsequent caspase-3 activation which leads to cleavage of death substrates and apoptosis (Fig. 1). In order to avoid a suicidal fate by dimerisation of pro- and anti-apoptotic members of this protein family, cells require continuous survival signals from their surface receptors to support cell survival. The mechanism of post-translational modification (e.g. phosphorylation) which inactivates pro-apoptotic members of the Bcl-2 family and prevents them from interacting with anti-apoptotic members is supported by survival factors such as insulin-like growth factor, platelet-derived growth factor, nerve growth factor, and interleukin-3 (Datta et al., 1999).

The proapoptotic molecule Bad is able to heterodimerize with a wide range of anti-apoptotic members like Bcl-x<sub>L</sub> in the outer mitochondrial membranes, neutralizing their anti-apoptotic activities, thereby promoting cell death (Yang et al., 1995) (Bae et al., 2001). This heterodimerization with Bcl-x<sub>L</sub> is regulated by its state of phosphorylation (Hirai and Wang, 2001) (Fig. 2). So far at least five different phosphorylation sites of Bad have been discovered in the murine protein: Ser<sup>112</sup>, Ser<sup>136</sup>, Ser<sup>155</sup>, Ser<sup>170</sup> and Ser<sup>128</sup>. While phosphorylation at Ser<sup>128</sup> seems to be a proapoptotic signal (Konishi et al., 2002), Ser<sup>112</sup>, Ser<sup>136</sup>, Ser<sup>155</sup> and Ser<sup>170</sup> phosphorylations have been proposed to have anti-apoptotic functions. The mechanism by which phosphorylation inhibits binding of Bad to Bcl-x<sub>L</sub> has been closely examined of several groups (Zha et al., 1996) (Zha et al., 1997) (Datta et al., 2000) (Yaffe and Elia, 2001) (Masters et al., 2001): According to a current model, unphosphorylated Bad forms a stable complex with Bcl-x<sub>L</sub> via its BH3 domain; this complex is localized on the outer surface of the mitochondrial membrane and functions as an apoptotic signal. Ser<sup>155</sup> as part of the BH3 domain is unphosphorylated in this complex. Phosphorylation at sterically approachable Ser<sup>112</sup>/Ser<sup>136</sup> by kinases allows binding of Bad to 14-3-3 ligands, dimeric alpha-helical pSer/Thr-binding proteins, via its phospho-serine-136 domain. Although Bad has a

substantially higher affinity to Bcl-x<sub>L</sub>, the binding to 14-3-3 protein weakens the Bad/Bcl-x<sub>L</sub> complex enough to allow phosphorylation at Ser<sup>155</sup> which destroys the Bad/Bcl-x<sub>L</sub> complex by disrupting the interaction the hydrophobic face of the BH3 domain and the hydrophobic groove of Bcl-x<sub>L</sub>. Bad then translocates from the outer mitochondrial membrane to the cytoplasm where it forms a stable complex with 14-3-3 proteins. Dephosphorylation of Bad by phosphatases reverses this process, Bad dissociates from 14-3-3 proteins and translocates to the mitochondrial membrane where it can dimerize with Bcl-x<sub>L</sub>. (Fig. 2)

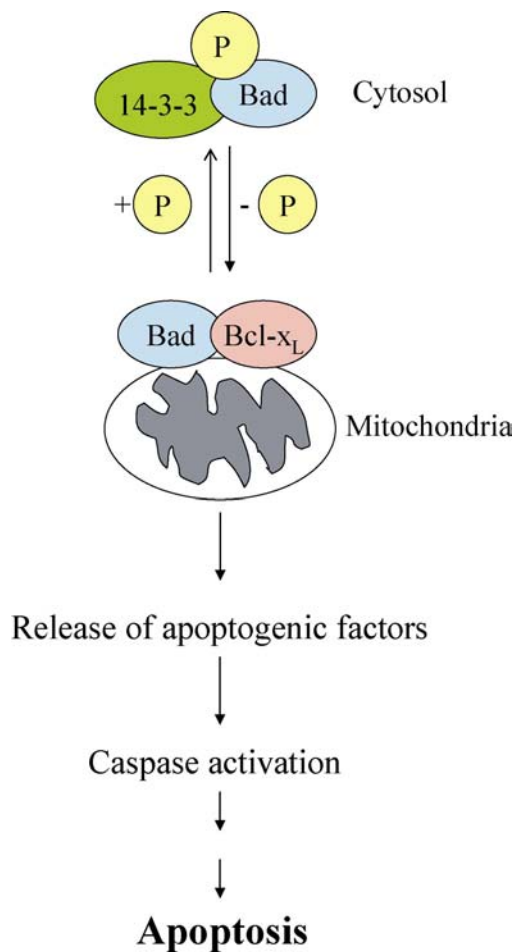


**Figure 2:**

*Bad, unphosphorylated at Ser<sup>155</sup>, binds to anti-apoptotic Bcl-x<sub>L</sub>, causing the release of mitochondrial factors like cytochrome c into the cytosol which triggers caspase activation followed by apoptotic cell death. This mechanism is reversed by phosphorylation of Bad at Ser<sup>155</sup> which opens the Bad/ Bcl-x<sub>L</sub> complex and allows Bad to diffuse into the cytosol where it can bind to 14-3-3 binding proteins if it is phosphorylated at Ser<sup>136</sup> and Ser<sup>112</sup>.*

Phosphorylation at Ser<sup>112</sup>, Ser<sup>136</sup> and Ser<sup>155</sup> is regulated by growth factors through activation of different survival kinases such as Raf-1 when targeted to mitochondria (Wang et al., 1999) (Wang et al., 1996) (Salomoni et al., 1998) (Neshat et al., 2000), Akt/protein kinase B (Datta et al., 1997) (del Peso et al., 1997) (Blume-Jensen et al., 1998), protein kinase A (Harada et al., 1999) (Datta et al., 2000) (Virdee et al., 2000) (Zhou et al., 2000) (Lizcano et al., 2000), the p21-activated kinases (Schurmann et al., 2000) or the mitogen-activated protein kinase Rsk (Lizcano et al., 2000) (Bonni et al., 1999). However, it is not fully resolved which protein

kinase phosphorylates which site of Bad *in vivo*. Although some published findings are conflicting, it is likely that phosphorylation of Bad Ser<sup>112</sup>, Ser<sup>136</sup> and Ser<sup>155</sup> is mediated by multiple pathways of kinase activation. *In vivo*, Ser<sup>112</sup>-phosphorylation by the MAP-kinase Rsk and protein kinase C has been described. Involvement of protein kinase A in Ser<sup>112</sup>-phosphorylation is not fully understood since contrasting findings have been published. Reports about protein kinase B (PKB) involvement are equally contradictory (Harada et al., 1999) (Tan et al., 1999) (del Peso et al., 1997) (Liu et al., 1996a). Phosphorylation of Ser<sup>136</sup> is mediated mainly through either PKB (del Peso et al., 1997) or a so far unknown kinase (Lizcano et al., 2000) (Scheid and Duronio, 1998). Ser<sup>155</sup> phosphorylation seems to predominantly be performed by c-AMP-mediated protein kinase A (Lizcano et al., 2000).

Different phosphatases like Ser/Thr-protein phosphatases type-1 (PP1), 2A (PP2A) and 2B (Calcineurin, PP2B) are responsible for the dephosphorylation of Bad at Ser<sup>112</sup>, Ser<sup>136</sup> and Ser<sup>155</sup>. PP1, PP2A and PP2B have been shown to dephosphorylate Bad at phospho-serine-112 and -136 (Wang et al., 1999) (Ayllon et al., 2000) (Chiang et al., 2001). Recently it has been observed that PP2C dephosphorylates Ser<sup>155</sup> *in vitro* (Kriegelstein, Klumpp, unpublished data) and that phospho-Bad-112 and -136 are substrates for PP2C as well. Thus, the underlying mechanisms by which PP2C could be involved in apoptosis could be that PP2C, after activation by unsaturated fatty acids, dephosphorylates Bad which unleashes Bad's proapoptotic properties.

The aim of this part of this study was to elucidate the role of PP2C in neuronal apoptosis *in vivo*. Protocols were established to detect Bad, Bad-155P and PP2C proteins in primary neuronal culture and to induce damage and apoptosis in these neurons by treatment with unsaturated fatty acid like oleic acid or ginkgolic acids. With these tools changes in protein levels of Bad, Bad-155P and PP2C due to treatment were analyzed to search for possible changes in Bad-phosphorylation due to PP2C activation.

#### **1.4. Outline of the study**

The purpose of this study was to evaluate the involvement of specific enzymes, superoxide dismutases and PP2C, in neuronal cell death. To this end, different experimental models of neuronal damage were used. The role of superoxide dismutases (SODs), endogenous free radical scavengers, was tested in two *in vivo* models of neuronal damage, cold injury-induced brain trauma (CIBT) and intrastriatal injection of the toxin 3-nitropropionic acid in mice. The

function of enzyme protein phosphatase type 2C $\beta$  (PP2C $\beta$ ) which participates in the reversible phosphorylation of proteins was studied during apoptosis in primary rat neuronal cultures induced by oleic acid and ginkgolic acids.

### *1) A possible protective role of superoxide dismutases*

#### *Influence of SOD2 downregulation on CIBT*

ROS have been shown to play a pivotal role in the development of CIBT, a traumatic model with vasogenic edema as the most obvious parameter. Since overexpression of cytosolic SOD1 could ameliorate the outcome of CIBT, one major aim of this thesis was to elucidate the role of mitochondrial SOD2 in CIBT by using SOD2-KO mice and compare their outcome of the lesion with that in wild-type littermates at 1, 3 and 7 days post-insult. Parameters to describe the development of the lesion were as follows:

- Lesion size as the percentage of damaged tissue measured up to 7 days post injury
- Edema formation as hemisphere enlargement up to 7 days after CIBT to examine BBB breakdown
- Number and distribution of apoptotic cells by TUNEL-staining to reveal the severity of the lesion
- Number and distribution of inflammatory cells, neutrophil infiltration following CIBT, which are another major source for ROS, examination up to 7 days
- Grade and distribution of hemorrhagic transformations (HT) up to 7 days
- *In situ* superoxide anion production by hydroethidine oxidation 2 hours following CIBT to assess whether there were any differences in the level of ROS production in both animal groups early in development of the tissue injury

#### *Role of SOD1 on intrastriatal damage after 3-NP injection*

The aim of the 3-NP experiments was to testing a possible influence of SOD1 in this intrastriatal 3-NP model using SOD1 transgenic and knockout mice. The model was established in mice inducing a middle-sized lesion within the borders of the striatum of wild type mice and the development of the lesion established. Parameters to define the lesion were

- Size of the lesion at 4 h, 24 h, 72 h and 7 days
- Edema formation at the same time points as for measurement of lesion size
- Detection of apoptotic cells by TUNEL-staining to reveal the severity of the lesion and define the predominant type of cell death

- Immunohistochemistry of active caspase-3 and caspase-9 as biochemical markers for apoptosis to confirm findings of TUNEL-staining

After establishing the model, mice overexpressing SOD1 (SOD1-TG), wild type littermates and animals which had the SOD1 gene homozygously knocked out (SOD1-KO) were subjected to 3-NP injection, and the severity of their lesions was compared. Measured parameters were:

- Size of lesion
- Edema development
- Detection and quantification of apoptotic cells by TUNEL-staining

## 2) PP2C, a potential target for prevention of apoptosis

Since PP2C has been shown to be activated by certain toxic unsaturated fatty acids which also induce apoptosis, induction of PP2C enzymatic activity might play a pivotal role in mechanisms of apoptosis. The aim of this study was to elucidate the role of PP2C in neuronal apoptosis also focussing on Bad phosphorylation as possible target for PP2C *in vivo*. The study had the following tasks:

- To establish protocols to detect Bad, Bad-155P and PP2C $\beta$  proteins in rat neuronal culture by either Western blotting or immunohistochemistry and hence prove that PP2C $\beta$  and Bad are co-localized.
- To establish treatment conditions to induce cell damage, preferably apoptosis in cultured neurons (neonatal hippocampal or embryonic cortical neurons) by treatment with unsaturated fatty acid like oleic acid or ginkgolic acids.
- To detect possible changes in protein levels of Bad, Bad-155P and PP2C $\beta$  after treatment with oleic acid or ginkgolic acids in order to elucidate a possible role of PP2C in neuronal apoptosis probably by involving Bad dephosphorylation.

## 2. Material and Methods

### 2.1. Antibodies

#### Primary antibodies:

Anti-active caspase-3, rabbit, polyclonal

1) Promega GmbH, Mannheim, Germany

2) PharMingen International, San Diego, CA, USA

Anti-active caspase-9, p35, rabbit, polyclonal

Santa Cruz Biotechnology, Santa Cruz, CA, USA

Anti-Bad, rabbit, polyclonal

1) Cell Signaling/ New England Biolabs, Frankfurt a.M., Germany

2) Santa Cruz Biotechnology, Heidelberg, Germany

Anti-Bad-155P, rabbit, polyclonal

Cell Signaling/ New England Biolabs, Frankfurt a.M., Germany

Anti-myeloperoxidase (MPO), rabbit, polyclonal

DAKO, Carpinteria, CA, USA

Anti-PP2C $\beta$ , rabbit, polyclonal

Provided by Prof. Klumpp, Münster, Germany

#### Secondary antibodies:

Biotinylated anti-mouse IgG (H+L)

1) Vector Laboratories, Burlingame, CA, USA

2) Amersham, Braunschweig, Germany

Biotinylated anti-rabbit IgG (H+L)

1) Vector Laboratories, Burlingame, CA, USA

2) Amersham, Braunschweig, Germany

## 2.2. Chemicals and materials

Acrylamide/ Bisacrylamide	Carl Roth GmbH & Co, Karlsruhe, Germany
Agarose	Sigma Aldrich, Milwaukee, WI, USA
Amino-n-caproic acid	Sigma, Taufkirchen, Germany
Ammonium persulfate, APS	AppliChem, Gatersleben, Germany
ATP	Sigma, Taufkirchen, Germany
Axioplan 2 Imaging microscope/Axiovision software	Carl Zeiss MicroImaging, Thornewood, NY, USA
B-27 supplement, 50x,	Life Technologies, Karlsruhe, Germany
Betadine solution, 10 % povidone iodine	Purdue Frederick, Norwalk, CT, USA
Boric acid	Sigma, Taufkirchen, Germany
Bovine serum albumin - fraction V, BSA	Sigma Aldrich, Milwaukee, WI USA
Bromophenol blue	Sigma, Taufkirchen, Germany
Calpain inhibitor	Sigma, Taufkirchen, Germany
cA-PK	Sigma, Taufkirchen, Germany
Citric acid	Sigma Aldrich, Milwaukee, WI, USA
Cresyl violet	Sigma Aldrich, Milwaukee, WI, USA
DAB-tablets, N-N'-Diaminobenzamidine	Sigma Aldrich, Milwaukee, WI, USA
Dihydroethidium, Hydroethidine	Molecular Probes, Eugene, OR, USA
Disodium hydrogenphosphate, Na <sub>2</sub> HPO <sub>4</sub>	Fluka Chemie AG, Neu Ulm, Germany
DNase-/RNase-free water	Sigma Aldrich, Milwaukee, WI, USA



dNTPs	Roche diagnostics, Indianapolis, IN, USA
16-dUTP	Roche diagnostics, Indianapolis, IN, USA
Dimethylformamide, DMF	Sigma Aldrich, Milwaukee, WI, USA
Dimethylsulfoxide, DMSO	Sigma, Taufkirchen, Germany IN, USA
Developer for Kodak films	Sigma, Taufkirchen, Germany
EDTA	Sigma, Taufkirchen, Germany
EGTA	Sigma, Taufkirchen, Germany
Eosine dye Y	Sigma Aldrich, Milwaukee, WI, USA
Ethidium bromide	Sigma Aldrich, Milwaukee, WI, USA
Filter paper	Schleicher und Schüll, Dassel, Germany
Fisherbrand Superfrost/Plus Microscope Slides, precleaned	Fisher Scientific, Tustin, CA, USA
Fisher Histomatic Tissue Processor, Model 166	Fisher Scientific, Tustin, CA, USA
Fixator for Kodakt films	Agfa Gevaert, Leverkusen, Germany
Fetal calf serum	PAA, Linz, Austria
Fluorescence microscope, Axiovert 100	Zeiss, Göttingen, Germany
Fmax fluorometer	Molecular Devices Corp., Sunnyvale, CA, USA
Formaldehyde 37 %	Sigma Aldrich, Milwaukee, WI, USA
D-Glucose	Merck, Darmstadt, Germany
Gentamycine	Sigma, Taufkirchen, Germany
Glacial acetic acid	Sigma Aldrich, Milwaukee, WI, USA
Glycerol	Sigma, Taufkirchen, Germany
Glycine	Sigma, Taufkirchen, Germany

Goat serum	Sigma, Taufkirchen, Germany
Hamilton syringe, 5 $\mu$ l	Hamilton, Reno, NV, USA
Heparine Sodium injection, 1000 Units/ml	Pharmacia & Upjohn, Kalamazoo, MI, USA
HEPES	Sigma, Taufkirchen, Germany
Homeothermic control unit	Harvard Instruments, Holliston, Maine, USA
Hoechst-33258 dye	Sigma, Taufkirchen, Germany
Horse serum	PAN Biotechnologies GmbH, Aidenbach, Germany
Hydrochloric acid, HCl	Sigma, Taufkirchen, Germany
Hydroethidine (= Dihydroethidium)	
Hydrogen peroxide 30 %, H <sub>2</sub> O <sub>2</sub>	Sigma Aldrich, Milwaukee, WI, USA
Isoflurane, AErrane®	Inhalon Pharmaceuticals Inc. Lehigh Valley, PA, USA
Image analysis system, MCID	Imaging Research Inc., Ontario, Canada
Kodak X-Omat film	Sigma, Taufkirchen, Germany
L-Glutamine	Sigma, Taufkirchen, Germany
Lithium carbonate, Li <sub>2</sub> CO <sub>3</sub>	Sigma Aldrich, Milwaukee, WI, USA
Laser scanning microscope, LSM 510	Zeiss, Göttingen, Germany
Magnesium chloride, MgCl <sub>2</sub>	Sigma Aldrich, Milwaukee, WI, USA
Magnesium sulfate, MgSO <sub>4</sub> ,	Sigma Aldrich, Milwaukee, WI, USA
Mayer's hematoxylin	Sigma Aldrich, Milwaukee, WI, USA
2-Mercaptoethanol	Sigma, Taufkirchen, Germany
Methanol	Sigma, Taufkirchen, Germany
Methyl green solution	Vector laboratories, Burlingame, CA, USA

Microtome, 820 Spencer	VWR Scientific, West Chester, PA, USA
Milk powder, fat-free	Heirler Cenovis GmbH, Radolszell, Germany
Mineral oil	Sigma Aldrich, Milwaukee, WI, USA
Minimal essential medium (MEM)	Life Technologies, Karlsruhe, Germany
Micro BCA Protein Assay Reagents	Pierce, Rockford, USA
Model 5000 Microinjection unit	David Kopf Instruments, Tujungam, CA, USA
MOPS	Sigma, Taufkirchen, Germany
3-Nitropropionic acid (3-NP)	Sigma Aldrich, Milwaukee, WI, USA
Neurobasal medium	Life Technologies, Karlsruhe, Germany
Nickel sulfate, NiSO <sub>4</sub>	Sigma Aldrich, Milwaukee, WI, USA
Nile blue A	Sigma, Taufkirchen, Germany
Nitro-blue tetrazolium (NBT)	Sigma Aldrich, Milwaukee, WI, USA
Nitrocellulose membrane, Hybond	Amersham, Braunschweig, Germany
Nitrogen dioxide, N <sub>2</sub> O	Praxair, Danbury, CT, USA
Novex precast gel, Tris-Glycine gel 10 % NP-40	Invitrogen, Carlsbad, CA, USA Sigma Aldrich, Milwaukee, WI, USA
Oxygen, O <sub>2</sub>	Praxair, Danbury, CT, USA
Oleic acid	Sigma, Taufkirchen, Germany
Papain	Sigma, Taufkirchen, Germany
Pap pen, Kiyota	Sigma, Taufkirchen, Germany
Parafilm M	Fisher Scientific, Tustin, CA, USA
Paraffin, solid	Sigma, Taufkirchen, Germany
PCR machine, Robocycler Gradient 40	Stratagene, La Jolla, CA, USA

PCR nucleotide mix	Invitrogen/Life Technologies, Grand Island, NY, USA
Penicillin/Streptomycin	PAA, Linz, Germany
Permount	Fisher Scientific, Tustin, CA, USA
Petri dishes (Ø 35 mm, 60 mm)/ 24-multiwells	Fisher Scientific, Schwerte, Germany
Phenol red	Sigma, Taufkirchen, Germany
Phenylmethylsulfonyl fluoride (PMFS)	Sigma, Taufkirchen, Germany
Polyethylenimine, PEI	Sigma, Taufkirchen, Germany
Poly-L-lysine	Sigma, Taufkirchen, Germany
Ponceau S red	Serva Feinbiochemica GmbH&Co, Heidelberg, Germany
Potassium chloride, KCl	Sigma Aldrich, Milwaukee, WI, USA
Potassium ferrocyanide	Sigma Aldrich, Milwaukee, WI, USA
Potassium phosphate	Sigma Aldrich, Milwaukee, WI, USA
Potassium dihydrogenphosphate, $\text{KH}_2\text{PO}_4$	Merk, Darmstadt, Germany
Premium cover glass	Fisher Scientific, Tustin, CA, USA
Proteinase K	DAKO Corporation, Carpinteria, CA, USA
Pyruvate	Sigma Aldrich, Milwaukee, WI, USA
Riboflavin	Sigma Aldrich, Milwaukee, WI, USA
Silk suture, 6-0	Ethicon, Cornelia, GA, USA
Small stereotactic frame	David Kopf Instruments, Tujungam, CA, USA
Sodium acetate	Sigma Aldrich, Milwaukee, WI, USA
Sodium azide, $\text{NaN}_3$	Sigma Aldrich, Milwaukee, WI, USA

Sodium chloride, NaCl	Sigma Aldrich, Milwaukee, WI, USA
Sodium dihydrogenphosphate, NaH <sub>2</sub> PO <sub>4</sub>	Sigma, Taufkirchen, Germany
Sodium dodecylsulfate, SDS	Sigma, Taufkirchen, Germany
Sodium hydrogencarbonate, NaHCO <sub>3</sub>	Sigma, Taufkirchen, Germany
Sodium tetraborate	Sigma, Taufkirchen, Germany
Staurosporine	Sigma, Taufkirchen, Germany
Streptavidin Oregon Green	Molecular Probes, Oregon, USA
Taq DNA polymerase, recombinant	Invitrogen/Life Technologies, Grand Island, NY, USA
TEMED	Sigma, Taufkirchen, Germany
TdT buffer	Invitrogen/Life Technologies, Grand Island, NY, USA
TdT, recombinant	Invitrogen/Life Technologies, Grand Island, NY, USA
Trichloroacetic acid	Sigma, Taufkirchen, Germany
Tris-HCl	Sigma Aldrich, Milwaukee, WI, USA
Triton-X 100	Sigma, Taufkirchen, Germany
Trypan blue	Sigma, Taufkirchen, Germany
Trypsin	Sigma, Taufkirchen, Germany
Trypsin inhibitor	Sigma, Taufkirchen, Germany
Tween-20	Sigma, Taufkirchen, Germany
Vectamount Mounting Medium	Vector Laboratories, Burlingame, CA, USA
Vectastain ABC- Kit (with peroxidase)	Vector Laboratories, Burlingame, CA, USA
Vectastain ABC-AP Kit (with alkaline phosphatase)	Vector Laboratories, Burlingame, CA, USA
Vector Red Alkaline Phosphatase Substrate Kit I	Vector Laboratories, Burlingame, CA, USA
Vector Vip Substrate Kit for Peroxidase	Vector Laboratories, Burlingame, CA, USA

XCELL Surelock Electrophoresis Cell	Novex/Invitrogen, Carlsbad, CA, USA
Xylene	Sigma Aldrich, Milwaukee, WI, USA
Xylene cyanole	Sigma Aldrich, Milwaukee, WI, USA

## **2.3. Cold injury-induced brain trauma (CIBT) experiments**

### **2.3.1. Animals**

Heterozygous SOD2 knock-out mice with a CD1/SV129 background (Li et al., 1995) were used for the cold injury brain trauma (CIBT) experiments. They were backcrossed with CD-1 mice for at least 5 generations and obtained from local stocks. In these animals mouse-SOD2 was mutated with a replacement type targeting vector that had deleted exon 3 out of 5 exons. This resulted in the production of a shortened mRNA and loss of enzymatic activity. Heterozygous SOD2 knock-out (SOD2-KO) animals had a ~ 50 % reduction of SOD2 expression in various tissues including brain tissue. No abnormalities in phenotype compared to their wild-type littermates could be observed in these animals up to 9 month. Homozygous SOD2-KO showed high neonatal lethality, animals did not survive 2 weeks and could, therefore, not be used for CIBT experiments. Knock-out mice and their wild- type littermates (WT) with identical genetic background were kept under controlled conditions (12 h light/dark circle,  $23 \pm 1^\circ\text{C}$ ,  $55 \pm 5$  % humidity) and had free access to food and water.

### **2.3.2. Genotyping of the SOD2 knockout mice**

#### *DNA Preparation:*

Animals were labelled with a numbered earring clip to allow identification. A sample of tail tissue (2-3 mm length) was obtained and transferred into a 1.5 ml Eppendorf tube. 20  $\mu\text{l}$  of lysis buffer (working solution) was added and the tissue incubated for 1 h at  $55^\circ\text{C}$ . Afterwards samples were diluted with 180  $\mu\text{l}$  of DNase-/RNase-free water, incubated at 100

°C for 10 min and centrifuged at 20,000 x g for 10 min. The supernatant was used for the polymerase chain reaction (PCR).

*Polymerase chain reaction:*

DNA-fragments were amplified by a hot start PCR protocol using a primer pair described by Li and colleagues (Li et al., 1995b). In a 0.5 ml Eppendorf tube 19 µl of primer mixture and 1 µl of sample supernatant were combined. After vortexing and short centrifugation, a drop of mineral oil was added to prevent a reduction of volume by evaporation. The sample tubes were placed in the PCR machine and the PCR was started.

PCR was performed in a Robocycler (RoboCycler Gradient 40, Stratagene, La Jolla, CA, USA) as follows:

RoboCycler Gradient 40, Stratagene, Program #1, SOD2 KO PCR

Step 1	98°C, 5 min	80°C, 2 min
	1 cycle	

After cooling down the probes to 80°C, the RoboCycler was stopped to allow an addition of 5 µl of hot start PCR solution in each tube and the PCR continued.

Step 2	94°C, 30 sec	62°C, 60 sec	75°C, 90 sec
	1 cycle		

Step 3	94°C, 30 sec	62°C, 60 sec	75°C, 90 sec
	30 cycles		

Step 4	75°C, 5 min	6°C, 10 min
	1 cycle	

*Genotype identification*

After PCR, the amplified fragments were separated on a 1 % agarose gel. For preparation of the gel 1 g agarose was mixed with 200 ml 1xTBE buffer and then cooked in a microwave for 2 min. Afterwards, 7 µl ethidium bromide solution were added under laminar flow protection. The solution was poured in the gel chamber (Model H5, Horizontal Gel Electrophoresis

System, Life technologies, Grand Island, NY, USA), and allowed to solidify for 1 h. The gel was transferred to an electrophoresis tank and covered with 1xTBE buffer. 10 µl of amplified sample were added to 3 µl loading buffer and 10 µl of this mixture was loaded on the gel. The electrophoresis was performed at 140 V for approximately 1 h in 1x TBE buffer. The DNA bands were visualized under UV illumination and recorded on Polaroid (Fotodyne, Fotodyne Incorp., New Berlin, WI, USA) (Fig. 3).

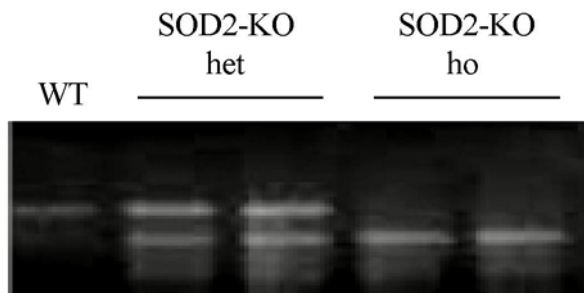


**Figure 3: Genotypic identification of SOD2-KO mice**

*WT animals showed one band for multiplied mouse SOD2 DNA, heterozygous SOD2 knock-out mice (SOD2-KO het) showed two bands, one for the mouse SOD2, another for the DNA-fragment that disrupted the SOD2 gene. Homozygous SOD2 knock-out mice (SOD2-KO ho) show one band for the vector that disrupted the SOD2 gene.*

*Solutions for PCR:*

*Hot start PCR solution*

DNase/RNase free water	4.5 µl
10 mM dNTPs	0.5 µl
Taq polymerase (added just before use)	0.1 µl

*Loading buffer*

Bromophenol blue	2.5 g
Xylene cyanole	2.5 ml
Glycerol	3.0 ml
Sterile water	ad 10 ml



*10x lysis buffer (stock)*

1 M Tris HCl pH 8.0	5 ml
0.5 M EDTA	0.2 ml
NaCl	117 mg
SDS	1 g
Sterile water	ad 100 ml

*10x lysis buffer (working solution)*

Proteinase K	21.4 ml
Lysis buffer (stock)	278.5 ml

*10x PCR buffer*

1 M Tris-HCl, pH 9.0	1 ml
1 M KCl in sterile water	0.5 ml
1 M MgSO <sub>4</sub> in sterile water	0.5 ml
10 mg/ml BSA solution	0.5 ml
10 % Triton-X in sterile water	0.5 ml
DNase-/RNase-free water	1.85 ml

*Primer cocktail*

<b>1. Primer A, Mn SOD-Exon3/Up</b>	
5'-TTA GGG CTC AGG TTT CAG AA,	
200 µM	50 µl
<b>2. Primer B, 1.7 Short/Down</b>	
5'-CGA GGG GCA TCT AGT GGA GAA,	
200 µM	50 µl
<b>3. Primer C, Pall/Up</b>	
5'-CAC ACA TCG GGA AAA TGG TTT G,	
200 µM	50 µl
<b>4. DNase/RNase free water</b>	850 µl

*Primer mixture*

DNase/RNase-free water	14 µl
Primer cocktail	2.5 µl

10x PCR buffer	2.5 µl
<i>Proteinase K</i>	
in 10 mM Tris-HCl, pH 7.5	14.0 mg/ml
<i>1x TBE buffer</i>	
5x TBE	200 ml
Sterile water	ad 1 l
<i>1 M Tris HCl, pH 8.0</i>	
Tris	12.11 g
Sterile water	100 ml
adjust to pH 8.0 with 1 M HCl	
<i>1 M Tris HCl, pH 9.0</i>	
Tris	12.11 g
Sterile water	100 ml
adjust to pH 9.0 with 1 M HCl	

### **2.3.3. General principles of surgery**

Throughout the surgery, maximal asepsis was achieved by using autoclaved instruments and disinfecting the surgery place with 70 % ethanol before each use. In all performed surgeries mice were anesthetized with an initial inhalator mixture of 5 % isoflurane/30 % oxygen/70 % nitrogen dioxide and anesthesia was maintained with 2 % isoflurane/30 % oxygen/70 % nitrogen dioxide. Chan et al. had used chloral hydrate anesthesia during the surgery inducing CIBT (Chan et al., 1991). This modification allowed us to reduce the time of anesthesia from about 30 min after chloral hydrate anesthesia (35 mg/g bodymass).

### **2.3.4. Performance of CIBT surgery**

The induction of CIBT in mice was performed according to a method described by Chan et al. (Chan et al., 1991). This procedure created a unilateral, highly reproducible lesion in the cortex that did not extend into the hippocampus. After inducing anaesthesia, the heads of the

mice were shaved with an electric shaver and disinfected with iodine. The animal's heads were placed in a small stereotactic frame for mice (David Kopf Instruments) and they were kept under anaesthesia using a face mask. They rested on a heating pad throughout the surgery and were covered with a blanket. Rectal temperature was monitored throughout the surgery and maintained at  $37 \pm 0.5^\circ\text{C}$ . (Homeothermic control unit, Harvard instruments). After scalp incision on the midline, the skull was exposed and cleaned from tissue. A metal probe (100 g, 4 mm diameter, constantly cooled with powdered dry ice) (Fig. 4) applied on the right side of the bony skull for 30 seconds (Fig. 5).

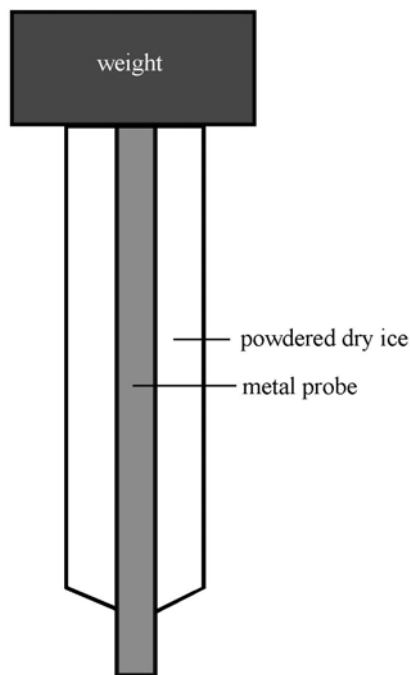


**Figure 4: Metal probe to induce CIBT**

*The metal probe was constantly cooled with powdered dry ice; a weight was added on top to increase the total weight to 100 g. Placing this probe on the intact bony skull produced a lesion in the underlying cortex.*

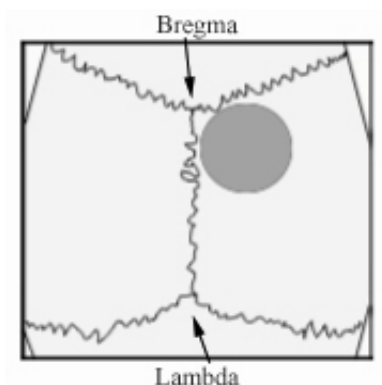


**Figure 5: Surface of skull with the spot of CIBT induction**

*The center of the cold injury probe was placed 2 mm posterior and 2 mm lateral to bregma (marked as a round spot).*

The skin wound was closed by a suture (silk suture, 6-0), and the animals were kept on the heating pad until regaining consciousness. After surgery, they were kept in a clean cage under controlled conditions (12 h light/dark cycle,  $23 \pm 1^\circ\text{C}$ ,  $55 \pm 5\%$  humidity) and had free access to food and water.

### **2.3.5. Removal of brains and subsequent paraffin embedding**

At different time points up to 7 days after CIBT animals were sacrificed in deep isoflurane anaesthesia. Immediately after the respiration stopped, the thorax was opened allowing free access to the heart. After opening the right chamber of the heart with scissors, the mice were slowly transcardially perfused with 50 ml heparinized saline (10 Units/ml) to clear the vessels from blood and 50 ml 3.7 % formalin/PBS. After waiting 10 min to let the formalin harden the brain, the mice were decapitated with scissors. Their scalp was incised on the midline, the skin removed and the skull carefully opened with small scissors to allow the brain to be removed with a spatula. The brains were postfixed by storing them in 3.7 % formalin/PBS solution in glass vials for one week and afterwards paraffin-embedded using an automatic tissue processor (Fisher Histomatic Tissue Processor, Model 166). The paraffin-embedded brains were cut into 6  $\mu\text{m}$  sections by microtome (820 Spencer Microtome); the brain sections were transferred onto glass slides (Fisherbrand Superfrost/Plus Microscope Slides, precleaned) in 150  $\mu\text{m}$  intervals and used for histological assessment. Adjacent sections were used for haematoxylin and eosin staining, myeloperoxidase (MPO)-immunohistochemistry, Perl's iron staining, and TUNEL staining.

#### *Heparinized saline 10 Unit /ml*

Heparine 1000 U/ml	10 ml
NaCl	9 g
Demineralized water	ad 1000 ml

#### *3.7 % Formalin/PBS solution*

Formaldehyde 37 %	100 ml
PBS-tablets	5
Demineralized water	ad 1000 ml

### 2.3.6. Histological assessment of infarct size and edema

To assess the size of the lesion, hematoxylin and eosin (H&E) staining was performed on 9 paraffin sections per animals in defined anatomical distances. H&E is a routine staining of purple color that allows the detection of lesion as a relatively pale area. Hematoxylin is a basic stain with deep purple or blue color; it stains basophilic structures such as chromatin (i.e. cell nuclei) and ribosomes. Eosin is an acidic stain with a red color and stains acidophilic cell structures and dead neurons. The glass slides containing the paraffin brain sections (-> 2.3.5.) were placed in a slide holder and subjected to the following washing/staining steps:

- 3 min resting in 100 % xylene
- 3 min washing in 100 % xylene
- 3 min washing in 100 % xylene /100 % ethanol (1:1)
- 3 min washing in 100 % ethanol
- 3 min washing in 100 % ethanol
- 3 min washing in 95 % ethanol
- 3 min washing in 70 % ethanol
- 1 min washing under running tap water
- 5 min incubation in Mayer's hematoxylin
- 12 dips in Demineralized water
- 1 quick dip in 1 % acid alcohol (1 % HCl in 70 % ethanol)
- 5 min washing under running water tap water (H<sub>2</sub>O)
- 5 dips in 1 % saturated lithium carbonate solution
- 5 sec brief dip in distilled water H<sub>2</sub>O
- 30 sec dip in 1 % saturated lithium carbonate solution
- 5 min washing under running tap water
- 1 quick dip in Eosin Y dye
- 12 dips in demineralized water
- 15 dips in 95 % ethanol
- 15 dips in 100 % ethanol
- 15 dips in 100 % ethanol
- 15 dips in 100 % ethanol
- 3 min washing in 100 % xylene /100 % ethanol (1:1)
- 5 min washing in 100 % xylene

After the H&E staining, the sections were sealed with Permount and covered with glass coverslips (Premium Cover Glass, Fisher Scientific). Digital pictures of the stained sections were taken and printed out on paper. The area of traumatic injury was first defined by examining the stained sections under light microscopy and later outlined on the print outs. Ipsilateral hemisphere, contralateral hemisphere and cortical area of traumatic injury were measured on the printouts using an image analysis system (MCID). Lesion size was calculated as average % of ipsilateral hemisphere in 9 defined sections. The size of edema was evaluated as average hemisphere enlargement in 4 defined core sections.

### **2.3.7. Hydroethidine assay**

The production of superoxide anion radicals ( $O_2^{\cdot-}$ ) after CIBT was investigated by intravenously administering hydroethidine (HEt) which diffuses into the CNS parenchyma and is selectively oxidized by superoxide anion radicals ( $O_2^{\cdot-}$ ) to ethidium (Et). HEt has been shown to be a good tool to measure and detect free radical production in brain tissue after various insults (Murakami et al., 1998b). Ethidium shows red fluorescence at 590 nm when excited at 544 nm. Light- and air-sensitive hydroethidine was stored at  $-20^{\circ}\text{C}$  in darkness under argon as a stock solution in dimethylsulfoxide. For the hydroethidine assay HEt-stock solution was freshly diluted 1:100 in PBS (working solution 1 mg/ml in PBS), sonicated until it was a milky, homogenous suspension and kept in darkness until use.

Animals were anesthetized, their chests shaved with an electric shaver and disinfected with iodine. They were placed on a heating pad and anesthesia was maintained using a face mask. Rectal temperature was monitored throughout the surgery and maintained at  $37 \pm 0.5^{\circ}\text{C}$ . (Homeothermic control unit, Harvard instruments). A 1 cm long incision was made on the chest and the vena jugularis exposed. 0.2 ml HEt solution was injected 5 min before CIBT into the jugular vein through the overlying muscle to avoid bleeding. Administration of HEt before the induction of the CIBT was necessary to achieve a good distribution of the HEt throughout the brain. The skin wound on the chest was closed by a silk suture. After the injection HEt the animals were kept anesthetized and the CIBT was performed, as described previously (chapter 2.3.4.). Two hours after CIBT animals were sacrificed with an overdose of isoflurane. Immediately after the respiration stopped, the thorax was opened to access the heart which was still beating. The right heart chamber was opened and the mice were transcardially perfused through the left ventricle of the heart with 50 ml heparinized saline to clear the vessels from blood. Afterwards the mice were decapitated, their scalps incised on

the midline, the skin removed, the skull opened and the brain removed with a spatula. The brains were frozen on dry ice and tissue of lesion area and contralateral side was dissected by a sharp scalpel. Tissue of two animals (approximately 50 mg) was pooled, supplemented with dimethylformamide (DMF) (three times the volume of the tissue) and sonicated. After 20 min rest in darkness at room temperature the samples were centrifuged at 20,000 x g for 20 min at 4°C, 100 µl of the supernatant transferred to a multiplate and fluorometrically measured by multiplate reader (Fmax fluorometer) at an excitation of 544 nm and emission of 590 nm.

*Heparinized saline 10 U/ml*

Heparine 1000 U/ml	10 ml
NaCl	9 g
Demineralized water	ad 1000 ml

*HEt stock solution*

Dihydroethidium (Hydroethidine)	100 mg
DMSO	1 ml

**2.3.8. Perl's iron staining**

To examine hemorrhagic transformations in the damaged tissue, Perl's iron staining was performed on brain sections following the protocol of Koeppen (Koeppen, 1995). Perl's iron staining is the classic method to demonstrate intracellular iron in tissues e.g. in hemoglobin or hemosiderin. Paraffin sections of 6 µM thickness on slides (->2.3.5.) were deparaffinized and hydrated by the following process:

- 3 min resting in 100 % xylene
- 3 min washing in 100 % xylene
- 3 min washing in 100 % xylene /100 % ethanol (1:1)
- 3 min washing in 100 % ethanol
- 3 min washing in 100 % ethanol
- 3 min washing in 95 % ethanol
- 3 min washing in 70 % ethanol
- 1 min washing in demineralized water

Afterwards sections were incubated in Perl's iron solution for 15 min on a shaker at room temperature. After 3 times washing with PBS they were incubated with DAB-solution for 15 min at RT in the dark, washed 3 x 5 min with PBS, and counterstained with methyl green solution for 15 min. They were washed 3 x for 20-30 sec in demineralized water and dehydrated by immersing 3 x 20-30 sec in butanol 100 % and 3 x 5 min in xylene 100 %. Slides were sealed with Permount using a glass coverslip (Premium Cover Glass, Fisher Scientific). Digital pictures of the lesion area were taken with a light microscope (Axioplan 2 Imaging microscope, Axiovision software), printed out and the hemorrhagic transformations graded by a "blinded" examiner (grade 0: no bleeding at all, grade 1: virtually no bleeding/restricted to some spot in < 25 % of sections of each animal, grade 2: some bleeding, restricted to traumatic region in 25-50 % of sections, grade 3: extensive bleeding encompassing entire traumatic region in 50-75 % of sections, grade 4: extensive bleeding/staining in core, penumbra and beyond in all sections).

*Perl's iron solution*

Potassium ferrocyanide	1 g
HCl, concentrated	1 ml
Demineralized water	ad 100 ml

*DAB solution*

DAB-tablet	10 mg
PBS	50 ml
Tween 20	50 µl
H <sub>2</sub> O <sub>2</sub> 30 %	50 µl

*PBS*

PBS tabs	5 pieces
Demineralized water	1000 ml

### **2.3.9. MPO immunohistochemistry**

To assess the anatomical distribution of myeloperoxidase (MPO)-positive neutrophils taking part in the inflammatory process, immunohistochemistry was performed on paraffin sections of 6 µm thickness (-> 2.3.5.). Three sections of representative animals of each group were



stained. After deparaffinizing and hydration (as described in chapter 2.3.8.), paraffin sections were heated up in a microwave oven in 0.01 M citric acid in demineralized water at high power for 2 min and 50 % power for 20 min. Every 5 min the evaporated solution was replaced to prevent the slides from drying. The sections cooled down for 20 min and were washed 2 x 5 min with demineralized water. They were dried on a slide heater at 30°C for 5 min and the sections circled with a PAP-pen. After blocking endogenous peroxidases with blocking solution for 30 min, sections were washed 3 x 5 min with PBS and incubated with 5 % fat-free milk powder solution for 1 h. After removal of the milk solution each section was incubated with 50 µl 1:500 MPO-antibody (rabbit, polyclonal, in PBS) solution overnight at 4°C in a humid chamber to prevent the sections from drying out. The next day, sections were washed 3 x 10 min with PBS and the secondary antibody solution (biotinylated anti-rabbit IgG, 1:200 in PBS) was applied for 30 min at room temperature. Sections were washed again 3 x 10 min with PBS and incubated with ABC solution (Vectastain ABC- Kit) for 30 min at room temperature to enhance the signal of the secondary antibody. After washing 2 x 5 min with PBS, visualisation was accomplished by incubation with Vector Vip solution for 15 min. Afterwards they were washed 3 x 5 min with PBS and counterstained with methyl green solution for 15 min.

Sections were dehydrated (washed 3 x for 20-30 sec in demineralized water, 3 x for 20-30 sec in butanol 100 % and 3 x for 5 min xylene 100 %) and sealed with Permount using a glass coverslip (Premium Cover Glass, Fisher Scientific). MPO-positive cells were counted in four different areas of the lesion in two sections of each animal under high power magnification (x 400).

*ABC solution*

Solution A	1 drop
Solution B	1 drop
PBS	5 ml

(Vortex solution A with PBS, add solution B, vortex, let it rest 30 min at R/T)

*Blocking solution*

Sodium azide	0.33 g
Triton-X 100	0.1 ml
PBS	100 ml
Hydrogen peroxide, 30 %	0.33 ml

*PBS*

PBS tabs	5 pieces
Demineralized water	1000 ml

*Vector Vip solution*

PBS	5 ml
Reagent 1	3 drops
Reagent 2	3 drops
Reagent 3	3 drops
Hydrogen peroxide solution	3 drops

(Mix PBS and reagent 1, add reagent 2, mix well, add reagent 3, mix well, add hydrogen peroxide solution, mix well, use within 15 min)

**2.3.10. Transferase-dUTP-Nick-End-Labeling (TUNEL-staining)**

DNA-fragmentation was examined by *in-situ*-labelling of fragmented DNA in the nucleus. DNA strand breaks are a typical feature of apoptosis and strong labelling of cells with condensed nuclei or fragmented allows detection of apoptotic cells and their distribution in brain tissue. Paraffin sections (6  $\mu$ M thickness) were deparaffinized first using a protocol described previously (-> chapter 2.3.6.). Afterwards, the sections were circled by a Pap pen and dried on a 30 °C warm plate. Freshly diluted proteinase K (20  $\mu$ g/ml in demineralized water) solution was applied for 15 min and later sections were washed two times with PBS. Endogenous peroxidases were quenched in 1.5 % H<sub>2</sub>O<sub>2</sub> in PBS for 5 min at room temperature. After washing again 3 times with PBS, sections were incubated in TdT buffer for 15 min at room temperature.

Afterwards, they were incubated with TdT/dUTP solution for 60 min at 37°C, followed by 3 times 10 min washing with 2xTB buffer and 2 times for 15 min washing with 2 % BSA in PBS.

They were washed 3 x 5 min with PBS and incubated with ABC solution (Vectastain ABC-Kit) for 30 min at room temperature. After washing with PBS once, sections were washed twice with 0.175 M sodium acetate solution for 10 min. The visualisation of the fragmented DNA was achieved by incubation with Ni-DAB for 10 min. Afterwards sections were washed 3 x 5 min with PBS and stained with methyl green solution for 15 min. They were washed 3 x

20-30 sec in demineralized water, 3 x 20-30 sec in butanol and 3 x 5 min in xylene. Afterwards they were sealed with Permount using a glass coverslip (Premium Cover Glass, Fisher Scientific).

*ABC solution*

Solution A	1 drop
Solution B	1 drop
PBS	5 ml

(Vortex solution A with PBS, add solution B, vortex, let rest 30 min at room temperature)

*Ni-DAB solution*

DAB tablet	10 mg
NiSO <sub>4</sub>	0.4 g
0.175 M Sodium acetate	40 ml
Hydrogen peroxide, 30 %	100 µl

(Dissolve DAB and 0.4 g Ni-sulfate in sodium acetate solution under stirring, filtrate solution, store in darkness, add H<sub>2</sub>O<sub>2</sub> freshly before use)

*PBS*

PBS tablet	5 pieces
Demineralized water	ad 1000 ml

*2xTB buffer*

NaCl	1.7646 g
Sodium citrate	3.5064 g
Demineralized water	200 ml

*TdT/dUTP buffer (for 8 sections)*

TdT, 25 µl/ml	7.5 µl
Biotinylated 16-dUTP (60 µl/ml)	18 µl
TdT buffer (1 x)	ad 300 µl

## **2.4. Experiments of intrastriatal 3-NP injection**

### **2.4.1. Animals**

Heterozygous SOD1 transgenic mice 1), their wild-type littermates and homozygous SOD1 knock-out mice 2) were used to study neurodegeneration induced by intrastriatal injection of 3-nitropropionic acid (3-NP)- model. They were obtained from local stocks, kept under controlled conditions (12 h light/dark cycle,  $23 \pm 1^\circ\text{C}$ ,  $55 \pm 5\%$  humidity) and had free access to food and water.

*Ad 1)* Heterozygous SOD1 transgenic mice (SOD1-TG) of the strain TgHS/SF-218, carrying the human CuZn-SOD (h-SOD1) gene in addition to their endogenous m-SOD1 genes, were bred on a CD-1 background. They had been created by Epstein and colleagues (Epstein et al., 1987) and showed a ~3-fold increase in endogenous SOD1 activity (Chan et al., 1991).

*Ad 2)* Homozygous SOD1 knock-out mice (SOD1 KO) of the strain 129/CD-1SOD1<sup><tm1></sup> were originally produced by Reaume and colleagues at Cephalon, Inc. (West Chester, PA, USA) (Reaume et al., 1996). These animals were bred on a CD-1 background. There were no differences in phenotypes between these mutants and their wild-type littermates. The knock-out mice showed no SOD1 activity.

### **2.4.2. Genotyping of SOD1 transgenic and knock-out mice**

The animals were typed by detecting SOD activity photochemically via its inhibition of nitroblue tetrazolium (NBT) reduction by superoxide anion radicals. When reactive oxygen species are formed, NBT is converted to a blue-colored formazan which shows an increased absorbance at 560 nm. In the presence of SOD which scavenges superoxide anion radicals, reduction of NBT is blocked. For phenotyping, soluble cellular protein samples are separated by gel electrophoresis and tested for SOD1 activity. SOD1 can be observed as unstained bands on the gel. SOD1 transgenic mice have an additional gene coding for human SOD and show one strong (homodimer of human SOD1) and one weak band (heterodimer of human SOD1 and mouse SOD1), homozygous SOD1-KO mice do not show any signal for SOD1 at all and can therefore be easily distinguished from wild type littermates which show one band (homodimer of mouse SOD1) (Fig. 6).

For phenotyping, animals were labelled with a numbered earring clip to allow identification. A short piece of tail was cut off and a drop of blood from the wound transferred into a 1.5 ml Eppendorf tube containing 50  $\mu\text{l}$  of lysis buffer. A XCELL Surelock Electrophoresis Cell

was set up with a 10 % Tris-Glycine gel (Novex precast gel), the electrophoresis apparatus filled with 1x running buffer. On a Parafilm strip 10 µl of 2x loading buffer and 10 µl lysated blood samples were mixed, and the samples loaded on the gel. Electrophoresis was performed for 45 min at 20 mA /gel. The gel was stained on a shaker with staining solution for 15 min and afterwards exposed to UV-light. After the reaction of NBT, the gel appeared blue, the areas of SOD activity remained white (Fig. 6). The results were recorded as photographic images.

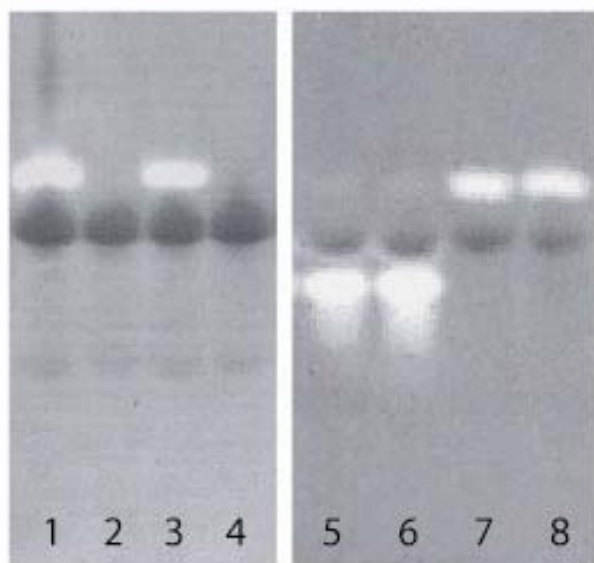


**Figure 6: Detection of SOD1 after nitro-blue tetrazolium/ staining.**

Lanes **1, 3, 7, and 8** show samples from wild-type animals, lanes **2+4** are samples from SOD1-KO mice, lanes **5+6** are samples from SOD1-TG mice. Active SOD1 can be detected as bright spots on the gel.

*2x Loading buffer*

Glycerol	1 ml
Bromophenol blue	1 mg
Upper gel buffer	1.25 ml
Demineralized water	6.75 ml

*Lysis buffer*

EDTA	1 mM
NP-40	50 µg
Demineralized water	ad 10 ml

*1x Phosphate buffer*

Potassium phosphate	62.6 g
Demineralized water	1000 ml

Adjust to pH 7.8

*1x Running buffer*

Glycine	14.4 g
Tris	3.02 g
Demineralized water	1000 ml

*Staining solution*

Riboflavin	2 mg
0.5 M EDTA in demineralized water	20 µl
Nitro-blue tetrazolium (NBT)	16.4 g
TEMED	175 µl
Demineralized water	100 ml

*Upper gel buffer*

Tris	6.05 g
Demineralized water	100 ml
Adjust to pH 6.8 with 1 N HCl	

### **2.4.3. Intrastratial 3-NP injection**

3-NP was freshly dissolved in saline (1 g in 28 ml) and the pH adjusted to 7.4 with 1 N NaOH. The solution was sterile-filtered and stored under argon until use. Throughout the surgery, maximal asepsis was achieved by using autoclaved instruments and disinfecting the surgery place with 70 % ethanol before each use.

Mice (3 months, male, 35-40 g) were anesthetized with an initial dose of 5 % isoflurane/ 30 % oxygen /70 % nitric dioxide and the anaesthesia was maintained with 2 % isoflurane/30 % oxygen/70 % nitric dioxide. After shaving their heads with an electric shaver and disinfection with iodine, the mice were placed in a small stereotactic frame and kept under anaesthesia using a face mask. They rested on a heating pad throughout the surgery and were covered with a blanket to avoid dropping of body temperature. Rectal temperature was monitored throughout the surgery and maintained at  $37 \pm 0.5^{\circ}\text{C}$ . After scalp incision on the midline, the skull was exposed and cleaned from tissue. Afterwards, a small piece of skull ( $\varnothing$  1.5 mm) was removed by means of a hand-held drill and 3-NP was injected in the striatum (3.3 mm

deep, 2 mm lateral left, 0.5 mm anterior to the bregma) with a volume of 0.4  $\mu$ l over a time of 4 min using a 5  $\mu$ l Hamilton syringe fitted with a 30 gauge blunt-tipped needle which was held by a microinjection unit (Model 5000 Microinjection Unit, David Kopf Instruments). The needle was left in place for another 4 min before being removed. After the injection the drilled piece of skull bone was moved back into place, the skin wound was closed by a silk suture (6-0) and the animals kept on the heating pad until regaining consciousness. After surgery the animals were kept in a clean cage under controlled conditions (12 h light/dark cycle,  $23 \pm 1^\circ\text{C}$ ,  $55 \pm 5\%$  humidity) and had free access to food and water.

#### **2.4.4. Removal of brains and subsequent paraffin-embedding**

3-NP treated animals were sacrificed with an overdose of isoflurane. Immediately after the respiration stopped, the thorax was opened allowing free access to the still beating heart. After opening the right atrium, the mice were transcordially perfused through the left ventricle of the heart with 50 ml heparinized saline (10 Units/ml) to clear the vessels from blood. For “floating” sections and paraffin-embedded tissue, animals were additionally perfused with 50 ml 3.7 % formalin in PBS. Animals were not perfused with formalin for preparation of frozen brain sections. Afterwards, the mice were decapitated with scissors, the skull opened and the brain removed with a spatula. Brains were differently processed afterwards for preparation of paraffin sections, frozen section or floating sections.

For paraffin-embedding the brains were further processed as described in chapter 2.3.5., and 6  $\mu$ m sections in 150  $\mu$ m intervals were prepared. Adjacent sections were used for myeloperoxidase (MPO)-immunohistochemistry and TUNEL staining.

For immunohistochemistry brains were postfixed in 3.7 % formalin/PBS solution for 1 day, cut into 50  $\mu$ m sections by vibratome (Vibratome 1000 Series, Technical Products International) and stored in PBS as “floating” sections. They were used for caspase-3 and caspase-9 immunohistochemistry.

For frozen sections brains were rapidly frozen in  $-18^\circ\text{C}$  methylbutane. By cryostat (Leica CM 1800) they were cut into sections of 20  $\mu$ m thickness in 300  $\mu$ m intervals and transferred onto glass slides and used for assessment of the lesion after cresyl violet staining.

#### 2.4.5. Cresyl violet staining of frozen sections and measurement of lesion size and edema

Frozen sections were defrozen, air-dried at room temperature for 1 h, afterwards Nissl-stained with cresyl violet. The striatal lesions could be seen as pale, unstained area. For cresyl violet staining, sections were subjected to the following staining steps:

Xylene 100 %	2 x 2 min
Ethanol 100 %	2 x 1 min
Ethanol 95 %	1 min
Ethanol 70 %	1 min
Demineralized water	2 x 3 min
Cresyl violet solution	15 min
Demineralized water	2 x 3 min
Ethanol 70 %	30 sec
Ethanol 90 %	1 min
Ethanol 100 %	1 min
Xylene 100 %	3 x 3 min

After staining the sections were sealed with Permount and covered with coverslips. The area of injury was defined examining the stained sections under a light microscope and outlined on printouts. Ipsilateral hemisphere, contralateral hemisphere and area of striatal injury were measured on the printouts using an image analysis system (MCID). Lesion size was calculated as average % damage of ipsilateral hemisphere of 12 consecutive sections. The size of the edema was evaluated as average hemisphere enlargement in 4 defined core sections.

##### *Cresyl violet solution:*

Solution A:	Cresyl violet	0.15 g
	Demineralized water	25 ml
Solution B:	Glacial acetic acid	1.69 ml
	Demineralized water	150 ml
Solution C:	Sodium acetate	2.72 g
	Demineralized water	100 ml

(Combine solutions A, B and C)



#### **2.4.6. Transferase-dUTP-Nick-End-Labeling (TUNEL-staining)**

The same protocol, as described in chapter 2.3.10., was used.

#### **2.4.7. Immunohistochemistry of caspase-3 and caspase-9 in floating sections**

Additionally to TUNEL-staining, immunohistochemistry of active caspase-3/9 enzymes was performed to detect apoptosis after 3-NP injection. Caspases are cystein proteases synthesized as inactive proforms and processed in cells undergoing apoptosis by self proteolysis or cleavage by another protease. The antibodies against active caspase-3 and caspase-9 used in this study had a 50-fold higher affinity towards the active forms than to the proforms. Formalin-fixed floating brain sections from 4 h, 24 h and 72 h time points were used for this staining. They were incubated with peroxidase block solution for 60 min and, afterwards, washed with PBS/0.1 % Triton-X -100 solution (PBS-TrX) 3 x 5 min, blocked with 20 % normal goat serum in PBS-TrX for 90 min and washed again 3 x 5 min with PBS-TrX. Brain sections were incubated with the primary antibody solution (1:100, polyclonal anti-caspase-3, active form, polyclonal anti-caspase-9, active form) in 0.5 % normal goat serum in PBS-TrX for 48 h at 4°C. Afterwards, the sections were washed 3 x 10 min with 1 % BSA /PBS-TrX and then incubated with the secondary antibody solution (1:300, biotinylated anti-rabbit IgG in 1 % BSA/ PBS-TrX) for 1 h. After washing 3 x 10 min with 1 % BSA/PBS-TrX sections were incubated with ABC-AP solution (Vectastain ABC-AP Kit) for 30 min, washed 2 x 10 min with PBS and the labelling was visualized with Vector Red solution. The sections were washed twice with PBS, mounted on glass slides (Fisherbrand superfrost/Plus microscope slides, precleaned) and dried over night at room temperature.

The next day, they were counterstained with methyl green for 5 min, dehydrated (washed 3 x 20-30 sec in demineralized water, 3 x 20-30 sec in butanol 100 % and 3 x 5 min in xylene 100 %) and sealed with Permount using glass coverslips. Sections were examined under light and fluorescence microscopy using a rhodamine filter (Axioplan 2 Imaging microscope, Axiovision software). Digital pictures of the lesion were taken.

#### *ABC-AP solution*

Solution A	2 drops
Solution B	2 drops

PBS 10 ml

(Combine solution A and PBS, mix well, add solution B, mix well, incubate 30 min before use)

*Peroxidase block solution*

Sodium azide	0.33 g
H <sub>2</sub> O <sub>2</sub> 30 % (freshly added)	0.33 ml
Triton-X 100	0.1 ml
PBS	ad 100 ml

*Vector Red solution*

Reagent 1	2 drops
Reagent 2	2 drops
Reagent 3	2 drops
100 mM Tris-HCl in demineralized water, pH 8.2-8.5	5 ml

(Add reagent 1-3 to 5 ml of 100 mM Tris-HCl, pH 8.2 - 8.5 buffer and mix well after each step)

## **2.5. PP2C/Oleic acid experiments**

### **2.5.1. Animals**

Fischer-344-rats from domestic breeding were used for primary mixed hippocampal cultures from neonatal rats (day 1). Animals were held under controlled conditions (12 h light/dark cycle,  $23 \pm 1^\circ\text{C}$ ,  $55 \pm 5\%$  humidity) and had free access to food (Altromin, Germany) and water.

For establishment of primary embryonic cortical cultures, pregnant G18 Sprague-Dawley rats were obtained from Charles River (Charles River Wiga, Sulzfeld, Germany). Embryonic cortices were prepared from 18 days old embryos.

### **2.5.2. Preparation and cultivation of embryonic cortical neurons**

All procedures were performed under sterile conditions. All instruments, trypsin and trypsin inhibitor were UV-sterilized; solutions were sterile-filtrated before use. All preparations were performed in a laminar flow hood.

Pregnant rats were deeply-anesthetized with halothane and killed by dislocation of the neck. They were disinfected with 70 % ethanol, their abdomen opened with scissors and the uterus containing the embryos removed. The embryos' skulls were opened with scissors, the brains gently removed with tweezers and kept in cold 1x HBSS. The cortices were dissected under a stereomicroscope and afterwards incubated in 1xHBSS supplemented with 1mg/ml trypsin for 15 min. Afterwards the supernatant was removed, the cortices incubated with 1mg/ml trypsin-inhibitor/HBSS 1x for 2 min. Then they were washed with 10 ml HBSS 1x and gently triturated 20 x in 4 ml HBSS 1x with a 10 ml glass pipette. After trituration, the cell suspension was diluted to 10 ml and transferred into a 50 ml falcon tube excluding bigger tissue fragments. The suspension was diluted 1:2 with HBSS 1x, centrifuged at 1000 rounds/min for 5 min and the pellet dissolved in 20 ml HBSS medium. For preparation of 60 mm dishes, this suspension was seeded at  $4 * 10^4$  cells/cm<sup>2</sup> density in PEI-coated Petri dishes filled with 2 ml MEM+. For 35 mm diameter Petri dishes the suspension was diluted 1:2 with MEM+ and seeded at a  $4 * 10^4$  cells/cm<sup>2</sup> density in PEI-coated Petri dishes filled with 2 ml MEM+. After 5 hours the medium was changed from MEM+ to Neurobasal medium pH 7.2 washing the cells once with Neurobasal medium pH 7.2. At day 5 after seeding the medium was changed to fresh medium. Cultures from this preparation contained should contain over 95 % neurons and less than 5 % astrocytes according to Mattson et al., 1993.

*HBSS stock*

KCl	4 g
KH <sub>2</sub> PO <sub>4</sub>	0.06 g
NaCl	80 g
NaH <sub>2</sub> PO <sub>3</sub>	3.5 g
Na <sub>2</sub> HPO <sub>4</sub>	0.6 g
D-Glucose	10 g
Phenol red	0.1 g
Demineralized water	ad 1 l

*HBSS, pH 7.2*

HBSS stock	50 ml
HEPES	1.2 g
B-27 supplement, 50x	10 ml
Gentamicin	5 mg
Demineralized water	ad 500 ml

*Minimal Essential Medium pH 7.2 (MEM+)*

MEM	4.695 g
HEPES	0.119 g
NaHCO <sub>3</sub>	1.1 g
Glucose	5.0 g
Fetal calf serum	50 ml
KCL	0.605 g
Pyruvate	0.06 g
L-Glutamine	0.088 g
Gentamicin	5 mg
Demineralized water	ad 500 ml

*Neurobasalmedium pH 7.2 (for embryonic cortical neuronal culture)*

Neurobasal	500 ml
HEPES	0.573 g
L-Glutamine	0.088 g
Gentamicin	5 mg

B-27 supplement

10 ml

*PEI coating of Petri dishes*

Petri dishes were coated with PEI solution for 2 h at room temperature (Ø 35 mm: 1 ml; Ø 60 mm: 2 ml). Afterwards they were washed thrice with 1.5-2 ml sterile, demineralized water. Dishes were opened and allowed to dry under UV light for 30 min in the laminar flow hood. They were filled with MEM+ (Ø 35 mm: 1 ml; Ø 60 mm: 2 ml) and incubated at 5 % CO<sub>2</sub>/37°C over night.

*Borate buffer*

Boric acid	1.24 g
Sodium tetraborate	1.9 g
Demineralized water	ad 400 ml
Adjust to pH 8.4	

*PEI solution*

PEI 5 %	0.4 ml
Borate buffer	400 ml

*PEI 5 %*

PEI 50 %	1:10 in demineralized water
----------	-----------------------------

**2.5.3. Primary mixed hippocampal cultures from neonatal rats**

Cultured hippocampal cells were prepared from neonatal (day 1) Fischer 344 rats as described previously (Sengpiel et al., 1998). Pups were disinfected with 70 % ethanol and decapitated with scissors. After opening the skull with small scissors, the brains were removed with a spatula and immediately placed into a Petri dish containing 37°C solution 1. Brains were dissected in a Petri dish coated with solid paraffin, the hippocampi were removed, cleaned from blood vessels and transferred into solution 2. They were incubated at 37°C in a water bath for 20 minutes and gently shaken. Afterwards, solution 2 was removed, the hippocampi were washed with cell culture medium and gently triturated 3 times with a fire-polished Pasteur pipette in 2 ml cell culture medium. After each trituration the triturated tissue was

allowed to sediment until the supernatant became free of visible pieces of tissue. The clear supernatants were combined by transferring them into solution 3.

Solution 3 containing the cells was centrifuged at 1000 x g for 10 minutes and the pellet gently resuspended in cell culture medium. Cells were seeded in poly-L-lysine-coated Petri dishes with 35 mm diameter or 24-multiwell plates containing Neurobasal cell culture medium pH 7.2 to an approximate density of  $2 \times 10^4$  cells/cm<sup>2</sup>. Cultures were incubated in a humidified 5 % CO<sub>2</sub>/95 % air atmosphere for one week, medium was changed to fresh Neurobasal cell culture medium at day 4 and cultures treated on day 7 or 8. The culture prepared after this protocol is expected to contain approximately 40 % astrocytes and 60 % neurons (Ravati, thesis, 2001).

*Media for preparation of neonatal hippocampal mixed culture:*

*Neurobasal medium pH 7.2 (for primary hippocampal mixed culture)*

Neurobasal	100 ml
B27 supplement	2 ml
L-Glutamine (50 mM)	1 ml
Penicillin-streptomycin solution	5 ml

*Solution 1*

Bovine serum albumin	30 mg
Neurobasal medium pH 7.2	150 ml

*Solution 2*

Papain	30 mg
Bovine serum albumin	30 mg
Neurobasal medium pH 7.2	150 ml

*Solution 3*

Bovine serum albumin	500 mg
Trypsin inhibitor	500 mg

### *Poly-L-lysine coating of Petri dishes*

The poly-L-lysine solution was sterile-filtrated, each Petri dish (35 mm diameter) filled with 2 ml (1 ml for each well in 24-multiwell) solution and incubated over night at RT. The following day the dishes were washed 4 times with sterile demineralized water over a period of at least 5 hours and dried afterwards. Shortly before preparation the Petri dishes were loaded with 2 ml Neurobasal medium (1 ml Neurobasal cell culture medium for each of 24-multiwell) and stored in an incubator at 37°C at 5 % CO<sub>2</sub>/95 % air atmosphere to let pH and temperature adjust.

### *Poly-L-lysine solution*

Poly-L-lysine (MG 300,000-700,000)	1 mg
Boric acid solution in demineralized water (1.25 %)	5 ml
Sodium tetraborate solution in demineralized water (1.91 %)	5 ml

### **2.5.4. Trypan blue staining**

Viability of the cultured neurons was determined by Trypan blue staining. Trypan blue, a hydrophilic azo-dye can permeate cellular membranes; however, intact cells export the dye actively and remain unstained. Under damaging conditions cell membranes as protective barriers can become more permeable while the cells are not able to maintain the active removal of the dye which results in blue staining of the cytosol. Intact, unstained cells can be easily distinguished from damaged, blue-stained cells.

The medium of the cell cultures was removed and replaced by 50 %/50 % Trypan blue solution/ Neurobasal medium pH 7.2 which had been warmed up to 37°C. They were kept in the incubator at 37°C/5 % CO<sub>2</sub> for 20 minutes, washed 3 times with PBS and fixed with formaldehyde-phosphate-buffer 4 % for 30 min. Afterwards they were washed with PBS twice and blue-stained/all cells were counted in 5 representative subregions per dish in at least 4 dishes per group. Cell damage was expressed as percentage of Trypan blue-positive cells. The groups were compared statistically, ANOVA and Scheffé tests were performed, P-values ≤ 0.05 were considered to be significant.

*Formaldehyde-phosphate-buffer 4 %*

NaH <sub>2</sub> PO <sub>4</sub>	9.39 g
Na <sub>2</sub> HPO <sub>4</sub>	71.2 g
Formaldehyde 37 %	500 ml
Demineralized water	ad 5000 ml

*PBS (Phosphate buffered saline) solution*

NaH <sub>2</sub> PO <sub>4</sub>	9.39 g
Na <sub>2</sub> HPO <sub>4</sub>	71.2 g
Demineralized water	ad 5000 ml

*Trypan blue solution*

Trypan blue	400 mg
NaCl	810 mg
K <sub>2</sub> HPO <sub>4</sub>	60 mg
Demineralized water	100 ml

### **2.5.5. Quantification of apoptosis in neuronal culture**

Hoechst-33258, a lipophilic, cationic dye permeates the cell membranes of intact and degenerated cells and stains nuclear DNA by binding to the minor groove of DNA at AT-rich sequences. This staining allows distinction between cells with intact nuclei and apoptotic cells with nuclei showing a clearly reduced size, chromatin condensation (visible as intensified fluorescence), and fragmentation. After washing the cells with ice-cold PBS once to remove the medium, they were fixed with ice cold 4 % formalin in PBS for 30 min at RT. Cells were observed under a light microscope to examine the cell morphology and representative photographs were taken. Afterwards, cells were incubated with a methanolic solution of Hoechst-33258 (10 µg/ml) for 30 minutes in darkness. They were washed with PBS once and stored in darkness until cell counting. Nuclear morphology of neurons was observed under a fluorescence microscope (Axiovert 100, Zeiss) or confocal laser scanning microscope (LSM, 510, Zeiss) at an excitation wave length of 350 nm and an emission wavelength of 450 nm. Cells with shrunken nuclei, chromatin condensation (visible as intense blue fluorescence) and nuclear fragmentation were considered apoptotic. In each Petri dish 5 different representative subregions were chosen and in each field the number of neurons with apoptotic features as



well as the total number of neurons were recorded. Apoptosis was expressed as percentage of apoptotic cells. Statistical analysis was performed by using ANOVA followed by Scheffé's post-hoc test. A P-value < 0.05 was considered significant.

*PBS (Phosphate buffered saline) solution -> as in 2.5.4.*

### **2.5.6. Nile blue-staining of lipid droplets in neuronal culture**

Nile blue is a dye comprising two components: a red oxazone which dissolves in neutral lipids and a blue oxazine which is basic and reacts with phospholipids and free fatty acids. When dissolved in phospholipids/free fatty acids, the blue dye shows orange fluorescence at 488/525 nm. After fixation of the cell cultures with formalin for 30 min, they were washed with PBS and stained with 10 µg/ml solution Nile red solution/PBS for 2 h. After washing the cells 3 times with PBS, they were counterstained with water-based fluorochrome Hoechst 33258 (10 µg/ml) solution for 30 min, washed 3 times with PBS and observed under laser scanning-microscope. (LSM, Zeiss). Representative pictures were taken.

*Formaldehyde-phosphate-buffer 4% -> as in 2.5.4.*

*PBS (Phosphate buffered saline) solution -> as in 2.5.4*

### **2.5.7. Protein quantification**

Protein concentration of Western blotting samples was measured by the BCA kit (Micro BCA Protein Assay Reagents) for equal loading of gels. The principle of this protein quantification is the measurement of the absorption of the purple polypeptide-bichinonic acid-Cu<sup>1+</sup> complex. BSA standard solutions were prepared from a BSA stock (2 mg/ml) at concentrations of 1, 2, 3, 4, 5, 10, 20, and 40 µg/µl. Standards (5 µl) and samples (5 µl) and PBS were mixed with working solution of the BCA kit containing a mixture of 10 ml reagent A, 10 ml reagent B and 200 µl reagent C. After incubation for 1 hour at 60°C, 200 µl of each sample or standard was transferred onto a microtiter plate and the absorbance was measured at 562 nm using a photometric multiplate reader. The protein concentrations of the samples were calculated from the BSA standard curve.

*Reagent A*®

Sodium carbonate	
Sodium bicarbonate	
Sodium tartrate	
Sodium hydroxide	0.2 N

*Reagent B*®

Aqueous solution of Bichinchonic acid	0.4 %
---------------------------------------	-------

*Reagent C*®

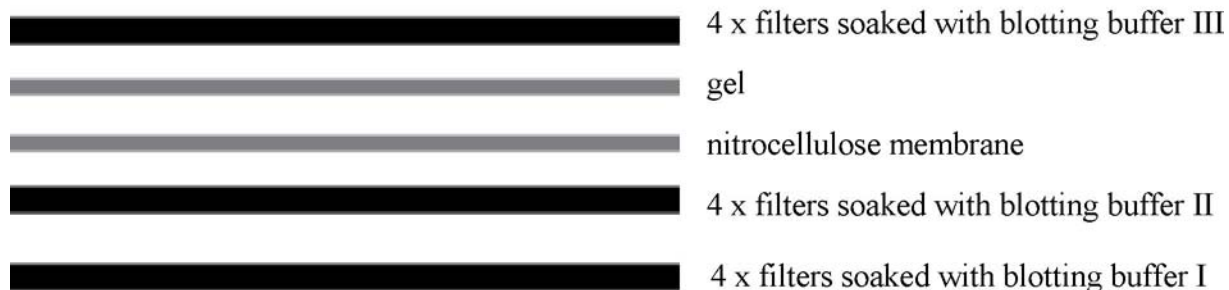
Copper sulfate	4 %
----------------	-----

*Albumin standard*

Bovine serum albumin (BSA)	2 mg/ml
Sodium chloride	0.9 %
Sodium azide	0.05 %

### **2.5.8. Western blotting analysis**

Cultured cells were washed with ice-cold PBS and collected with extraction buffer on ice. They were gently triturated through a 25G needle and kept on ice for 30 min before being stored at -80°C. By the high SDS concentration of the lysis buffer and the trituration through a needle the cells were lysed. The protein concentration of the lysates was measured using the BCA protein assay kit. Equally protein amounts of samples of lysates (ranging from 15-50 µg/lane) were first incubated in sample buffer for 5 min at 95°C and, then, loaded and separated on a 15 % SDS-polyacrylamide gel. After electrophoresis, the gel as well as 4 filters and a nitrocellulose membrane were soaked in blotting buffer II for 5 min, 4 sheets of filter paper each in blotting buffer I and III. The filter papers, the gel, and the membrane were stacked on the blotter in the following order:



The proteins were blotted onto nitrocellulose membranes for 30 minutes at 250 mA. Uniform and complete protein transfer was monitored by staining of the membranes with Ponceau S solution for 5 min on a shaker. Afterwards, the membranes were washed with washing buffer until total removal of Ponceau S staining and blocked with blocking buffer for 1 hour at room temperature. After 3 times washing for 5 min with washing buffer, the membranes were incubated with primary antibody solutions overnight at 4°C. The next day, blots were washed three times for 5 min with washing buffer and incubated with secondary antibody solutions for 1 h at room temperature. Before the detection, the membranes were washed 3 times 15 minutes with washing buffer, afterwards they were incubated in enhanced chemiluminescence solution for 1 min, put on a glass plate and covered with saran wrap. The blots were then exposed to a film. Exposure time varied depending on the intensity of the signals. The films were developed in developer solution until signals were visible. Afterwards, they were washed in tap water for 10 seconds, fixed in fixative solutions, washed in tap water, and dried. For detection of several proteins on the same blot, membranes were stripped, as follows, before incubation with a new primary antibody: Membranes were washed 3 x 10 min with washing buffer and incubated in stripping buffer for 30 min at 60 °C on a shaker and washed again 3 x 15 min. Then the stripped membrane could be used for a second detection starting with the blocking of the membrane.

*Blocking buffer*

BSA	2 g
Dry milk powder	5 g
Washing buffer pH 7.6	ad 100 ml

*Blotting buffer I*

Tris	18.17 g
Methanol	100 ml

Demineralized water	ad 500 ml
<i>Blotting buffer II</i>	
Tris	1.82 g
Methanol	100 ml
Demineralized water	ad 500 ml
<i>Blotting buffer III</i>	
Tris	1.51 g
Methanol	100 ml
Amino-n-caproic acid	2.62 g
Demineralized water	ad 500 ml
<i>Collecting gel</i>	
Gel buffer 2	8 ml
Demineralized water	5 ml
Acrylamide/Bisacrylamide	3 ml
Ammonium persulfate 10 % in demineralized water	30 $\mu$ l
TEMED	60 $\mu$ l
<i>Electrophoresis buffer</i>	
Tris	3 g
Glycine	14.4 g
SDS	1 g
Demineralized water	ad 1 l
<i>Extraction buffer</i>	
Glycerol	1 ml
SDS 10 % in demineralized water	3 ml
Tris 0.5 M, pH 6.8 in demineralized water	2.5 ml
PMSF	1 mM
Calpain inhibitor	1 $\mu$ M

Trypsin inhibitor	7 µg/ml
Demineralized water	ad 10 ml

*Gel buffer 1*

Tris	72.8 g
SDS	1.6 g
Sodium azide 5 %	4 ml
Demineralized water	ad 400 ml
(adjust to pH 8.8 with 1 N HCl)	

*Gel buffer 2*

Tris	12.1 g
SDS	0.8 g
Sodium azide 5 %	2 ml
Demineralized water	ad 200 ml
adjust to pH 6.8 with 1 N HCl	

*Loading buffer*

Glycerol	1 ml
SDS 10 % in demineralized water	3 ml
2-Mercaptoethanol	2.5 ml
Bromophenol blue 0.05 % in demineralized water	2.5 ml
Tris 0.5 M, pH 6.8, in demineralized water	2.5 ml

*PBS (Phosphate buffered saline) solution -> as in 2.5.4.*

*Ponceau red solution*

Ponceau S	0.4 g
Trichloroacetic acid	3 g
Demineralized water	ad 200 ml

### *Primary antibody solutions*

- 1) Anti-Bad-155P (rabbit, polyclonal, Cell Signaling), 1:400 in 5 % BSA/washing buffer
- 2) Anti-Bad (rabbit, polyclonal, Cell Signaling), 1:400 in 5 % BSA/washing buffer
- 3) Anti-PP2C $\beta$  (rabbit, polyclonal, Klumpp lab), 1:1000 in 0.1 % BSA/washing buffer
- 4) Anti- $\alpha$ -tubulin (mouse, monoclonal, Sigma), 1:10, 000 in blocking buffer
- 5) Anti-caspase-3 (rabbit, polyclonal, Promega), 1:400 in blocking buffer

### *15 % SDS-polyacrylamide gels (10 pieces)*

Gel-buffer 1	15 ml
Demineralized water	15 ml
Acrylamide /Bisacrylamide	30 ml
Ammonium persulfate 10 % in demineralized water	50 $\mu$ l
TEMED	100 $\mu$ l

### *Secondary antibody solutions*

- 1) When using rabbit primary antibody solutions: horseradish-peroxidase-conjugated anti-rabbit IgG (Amersham or Promega), 1:2000 in blocking buffer
- 2) When using mouse antibody solutions: horseradish-peroxidase-conjugated anti-mouse IgG (Amersham or Promega), 1:2000 in blocking buffer

### *Stripping buffer*

SDS	8 g
Tris HCl	3.958 g
2-Mercaptoethanol	2.8 ml
Demineralized water	ad 400 ml

### *Washing buffer (pH 7.6)*

Tween 20	1 ml
PBS	ad 1 l

### 2.5.9. Phosphorylation of Bad by cA-PK

As a positive control for Bad-155P in Western blots and in order to facilitate the detection of Bad-155P bands in protein extracts of primary cultures, recombinant Bad-GST and samples of embryonic cortical neuronal cultures were phosphorylated in vitro.

Bad-GST or samples were incubated with the phosphorylation solution for 30 min at 30 °C and stored at -20°C until use.

#### *Phosphorylation solution added to 1 µl Bad-GST (3.4 µg/µl)*

Buffer 1	1 µl
1 mM ATP	1 µl
150 mM MgCl <sub>2</sub> in demineralized water	1 µl
cA-PK (1 µg/µl)	1 µl
Demineralized water	5 µl

#### *Phosphorylation solution added to 9 µl sample (4 µg/µl)*

Buffer 1	1 µl
1 mM ATP	2 µl
150 mM MgCl <sub>2</sub> in demineralized water	1 µl
cA-PK (1 µg/µl)	2 µl

#### *Buffer 1*

1 M MOPS in demineralized water, pH 7.2	80 µl
1M β-Glycerophosphate in demineralized water	100 µl
500 mM EGTA in demineralized water	40 µl
Mercaptoethanol	4 µl
Demineralized water	ad 1000 µl

### 2.5.10. Immunohistochemistry of PP2Cβ in embryonic cortical neurons

To explore the intracellular distribution of PP2Cβ in neurons, embryonic cortical neurons were immunocytochemically stained for PP2Cβ after counterstaining with Hoechst-33258 for nuclear localisation. Embryonic cortical neurons, cultured on 25 mm glass coverslips, were washed with ice-cold PBS once to remove the medium and then fixed with ice-cold 100 %

methanol for 30 min at RT. Afterwards, they were incubated with a methanolic solution of Hoechst-33258 (10 µg/ml) for another 30 minutes in darkness, washed 3 x 5 min with PBS and dried for 1 h at 60°C. The coverslips were circled by a Pap pen and the cells blocked with blocking buffer for 30 min to avoid unspecific binding. Over night the cells were incubated with the primary antibody solution at 4°C. The next day, they were washed 3 x 5 min with PBS and exposed to the secondary solution for 30 min at room temperature in the dark. Then they were washed again 3 x 5 min with PBS and Oregon green solution was applied for 1 h in darkness at RT. Coverslips were washed 3 x 5 min with PBS, removed from the Petri dishes, turned over on a glass slide which was moistured with PBS and fixed with varnish. Immunostaining was evaluated using confocal laser scanning microscopy which allowed precise localisation of intracellular immunostaining. Cells were excited at 350 nm by an UV laser to detect Hoechst 33258 staining and an Argon laser to detect the Oregon green dye used for PP2C $\beta$  immunohistochemistry. Data and images of stained neurons were analyzed by Zeiss Image Browser software. Negative controls without incubation with the primary antibody were used to evaluate the intensity of the staining.

*Blocking Buffer*

Goat serum	5 ml
PBS	ad 100 ml

*Oregon green solution (90 µl per coverslip)*

Streptavidin-Oregon green dye	6 µl
PBS	ad 1 ml

*PBS (Phosphate buffered saline) solution -> as in 2.5.4*

*Primary antibody solution (70 µl per coverslip)*

PP2C $\beta$ antibody	1 µl
Goat serum	8 µl
PBS	ad 200 µl

*Secondary antibody solution (70 µl per coverslip)*

Biotinylated anti-rabbit IgG	1 µl
Goat serum	8 µl



PBS

ad 200 µl

### 2.5.11. Drug treatment of rat primary cultures

The damaging effect of oleic acid, elaidic acid (“*trans*-oleic acid”), and ginkgolic acids was examined in primary cultures of embryonic cortical and neonatal hippocampal neurons. Since the damaging properties of oleic acid varied depending on the composition of the culture medium, three different culture media were tested:

- a) Neurobasal without B27 supplement (NB-B27)
- b) Neurobasal with B27 supplement (NB+B27)
- c) Neurobasal with B27 without antioxidants (AO) supplement (NB+B27 –AO)

#### *Neurobasal (NB) culture medium for embryonic cortical culture*

Neurobasal®	500 ml
HEPES	0.5725 g
Glutamine	0.088 g
Gentamicin sulfate	0.0125 g

.....  
alternatively added:

- <u>in NB-B27:</u>	none	0 ml
- <u>in NB+B27:</u>	+B27 supplement	10 ml
- <u>in NB +B27-AO:</u>	+B27-AO supplement	10 ml

#### *Neurobasal culture medium for neonatal hippocampal culture*

Neurobasal®	100 ml
L-Glutamine (50 mM)	1 ml
Penicillin-Streptomycin	5 ml

.....  
alternately added:

<u>in NB-B27:</u>	none	0 ml
<u>in NB+B27:</u>	+B27 supplement	2 ml
<u>in NB +B27-AO:</u>	+B27-AO supplement	2 ml

*B27 supplement*

Biotin  
BSA fraction V  
Catalase  
L-carnithine  
Corticosterone  
Ethanolamine  
D-Galactose  
Insulin, recombinant, human  
Linolic acid  
Linolenic acid  
Progesterone  
Putrescine  
Sodium selenite  
Superoxide dismutase  
T-3 albumin  
DL-Tocopherol  
DL-Tocopherol acetate  
Transferrin  
Vitamin-A acetate

*B27-AO supplement*

Biotin  
BSA fraction V  
L-carnithine  
Corticosterone  
Ethanolamine  
D-Galactose  
Insulin, recombinant, human  
Progesterone  
Putrescine  
T-3 Albumin  
Transferrin

*1) Treatment of primary cultures with oleic acid/DMSO*

Oleic acid, an unsaturated C-18 fatty acid (18:1 cis- $\Delta^9$ ), is a light- and oxygen-sensitive oily liquid. It was stored in frozen aliquots at  $-70^{\circ}\text{C}$  under a mixture of nitrogen/ $\text{CO}_2$  to avoid oxidation of the substance during storage. For each treatment a fresh aliquot was thawed. Since oleic acid is highly lipophilic, almost insoluble in water, it had to be dissolved in DMSO to increase solubility before adding it to the culture medium. The amount of DMSO in the culture medium was kept constant at a final concentration of 0.1 % (V/V) to avoid effects caused by DMSO which is known to have radical scavenging properties while the concentration of oleic acid varied from 1  $\mu\text{M}$  to 150  $\mu\text{M}$ .

In all experiments d7/8 primary embryonic cultures of cortical neurons or d7/8 primary hippocampal mixed cultures were used. They were washed with 37°C Neurobasal culture medium (either NB+ B27, NB-B27 or NB+B27-AO).

Oleic acid was dissolved in DMSO, vortexed thoroughly, and immediately diluted in 37°C Neurobasal culture medium to a final concentration of 0.1 % DMSO. Despite the use of DMSO as a detergent and vortexing for 1 min, oleic acid was not fully soluble in culture media at concentrations higher than 100  $\mu$ M (Neurobasal with B27) or 50  $\mu$ M (Neurobasal without B27, with B27 without AO). The medium was removed from the cultures and the oleic acid/medium solution put on the cells. At different time points ranging from 1 h to 72 h the incubation was stopped either to stain the cells (-> Hoechst-33258 staining, Trypan blue staining, Nile blue staining) or to harvest the cells for protein extraction.

## *2) Treatment of cell cultures with oleic acid/ $\beta$ -cyclodextrin*

Since oleic acid was not entirely soluble in cell culture media at 100  $\mu$ M/0.1 % DMSO and known to be light- and oxygen-sensitive,  $\beta$ -cyclodextrin was employed overcome problems of stability and solubility.  $\beta$ -Cyclodextrin is a cyclic oligosaccharide consisting of 7 glucopyranose units. It is doughnut-shaped and contains an electron-rich, hydrophobic cavity (Fig. 7). Hydrophobic molecules, like oleic acid, are incorporated into the cavity of cyclodextrins by displacing water. This reaction is favored by the repulsion of the hydrophobic molecule by water. This effectively encapsulates the molecule within  $\beta$ -cyclodextrin, rendering it water-soluble. When the water soluble complex is diluted in a much larger volume of aqueous solvent, like the cell culture medium, the process is reversed, thereby releasing oleic acid. Incorporated in  $\beta$ -cyclodextrin, oleic acid is stable against oxidation when stored at 4°C.

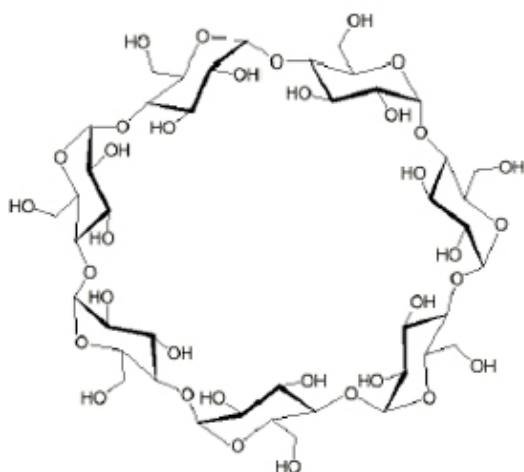


**Figure 7: Structure of  $\beta$ -cyclodextrin**

Sterile-filtered stock solution of 0.1 M oleic acid/ 9.3 %  $\beta$ -cyclodextrin in demineralized water was diluted in Neurobasal culture medium with B27 to working concentrations ranging from 10  $\mu$ M to 200  $\mu$ M oleic acid.  $\beta$ -cyclodextrin stock solution (9.3 %) was used as a control. The culture medium replaced by this solution, and at different time points the incubation was stopped either to stain the cells (with Hoechst 33258) or for protein extraction.

### 3) Treatment with elaidic acid (“*trans*-oleic acid”)

Elaidic acid, an unsaturated C-18 fatty acid (18:1 *trans*- $\Delta^9$ ) and, therefore, the *trans*-isomer of oleic acid, is a solid substance known to be light- and air-sensitive. It was stored in the dark at  $-20^\circ\text{C}$ . This substance was applied to primary cultures of embryonic cortical neurons at a working concentration of 150  $\mu$ M elaidic acid/0.1 % DMSO. Almost insoluble in water like oleic acid, it was freshly dissolved in pure DMSO to a 0.15 M stock solution this stock later dissolved 1:1000 in Neurobasal culture medium without B27 (NB-B27). Like oleic acid, it was not fully soluble in NB-B27 at this concentration. The cells were washed with NB-B27 once before treatment with elaidic acid. After treatment for twenty-four hours the cells were stained with Hoechst 33258 to detect neuronal apoptosis and, in addition, morphologically examined using a light microscope.

### 4) Treatment with ginkgolic acids

Ginkgolic acids, isolated from *Ginkgo biloba* leaves and seeds, are long-chain benzoic derivatives. We used ginkgolic acids composed of 4 different salicylic acid derivatives which had the following alkyl residues: C13:0 (11 %), C15:0 (4 %), C15:1 (43 %), C17:1 (39 %). These ginkgolic acids had a mean molecular weight of 347 g/mol. Before treatment, fresh stock solutions of ginkgolic acids in pure DMSO were prepared and dissolved 1:1000 in Neurobasal medium with B27. The end concentration of DMSO was 0.1 % while ginkgolic acids ranged from 10  $\mu$ M - 250  $\mu$ M. After removal of the old medium the cultures were treated with the cell culture medium containing ginkgolic acids. At different time points the treatment was stopped, either to extract proteins for Western blots, or to perform Hoechst-33258 or Trypan blue staining.

##### *5) Treatment with Staurosporine*

As a control for induction of neuronal apoptosis, we used staurosporine, a non-selective protein kinase inhibitor that has been shown to induce apoptosis in cultured neurons.

We treated primary cultures with 200 nM staurosporine/0.1 % DMSO in Neurobasal medium with B27 or in Neurobasal medium without B27. Staurosporine was stored as a 1 mM stock solution in DMSO at -20°C; aliquots were diluted to 1:5 in DMSO to a concentration of 200 mM staurosporine and this solution dissolved 1:1000 in culture medium to an end concentration of 200 nM staurosporine/0.1 % DMSO. Eight or twenty-four hours later the treatment was stopped and Nile blue staining or Hoechst-33258 staining performed on the cells.

## 2.6. Statistics

Statistically analyses of the results were performed as follows:

### 1) *CIBT experiments:*

Infarct areas, edema levels and  $O_2^-$  production were analysed using one way analysis of variance (ANOVA) followed by Student t-test. All data were expressed as mean  $\pm$  standard error of the mean (SEM); a P value  $< 0.05$  was considered significant. Three stars (\*\*\*) in graphs indicate a significance level of  $P < 0.001$ , two stars (\*\*) a significance of  $P < 0.01$ , one star (\*) a significance of  $P < 0.05$ . The TUNEL and MPO data were analysed using generalized linear models for nested factorial design. The analysis was run using SAS software (v 8., SAS Institute, Cary, NC, USA). Model main effects were animal type, time and area. The hemorrhage data were analysed using a non-parametric method for ranked data.

### 2) *3-NP experiments and PP2C experiments*

For all data of lesion areas and edema levels in 3-NP experiments and data of cell damage and apoptotic cell counts in PP2C experiments one way analysis of variance (ANOVA) with subsequent Scheffé (\*) or Duncan (+) test was employed. Statistics were performed using Microsoft Excel and WinSTAT. All results are expressed as mean  $\pm$  standard error of the mean (SEM) (3-NP experiments) or  $\pm$  standard deviation (SD) (PP2C/oleic acid experiments). Significant differences between groups were considered significant at values  $P < 0.05$  (indicated as \* or +),  $P < 0.01$  (\*\* or ++) and  $P < 0.001$  (\*\*\*) or +++).

### **3. Results**

#### **3.1. Effect of SOD2-reduction on cold injury-induced brain trauma**

##### **3.1.1. Lesion size and edema development in SOD2-KO mice and wild-type animals**

Edema formation correlating with blood brain barrier (BBB) breakdown in the lesion and lesion size indicating the expansion of the lesion into the cortex are two parameters which reflect the degree of tissue damage after induction of cold injury brain trauma. To detect possible differences in these parameters, brain sections of SOD2-KO animals and their wild-type littermates following CIBT (as described in chapter 2.3.4.) were stained with hematoxylin & eosin (H&E) which allowed detection of damaged tissue as a pale area when compared to undamaged tissue. The lesion area was determined on printouts of recorded photomicrographs. Percentage hemisphere enlargement (= edema formation) and percentage damage ipsilateral hemisphere were calculated (lesion size). A total number of 8-11 animals per group were analyzed. There was no difference in lesion size between SOD2 KO animals and wild-type (WT) mice at any of the time points 24 h, 72 h and 7 days (Fig. 8A). Lesion size remained constant between 1 and 3 days post-CIBT followed by a significant decrease at 7 days due to tissue loss. There were also no significant differences in edema formation between WT and SOD2-KO mice at the time points examined. In both groups edema gradually decreased from 1 day to 7 days (Fig. 8B).

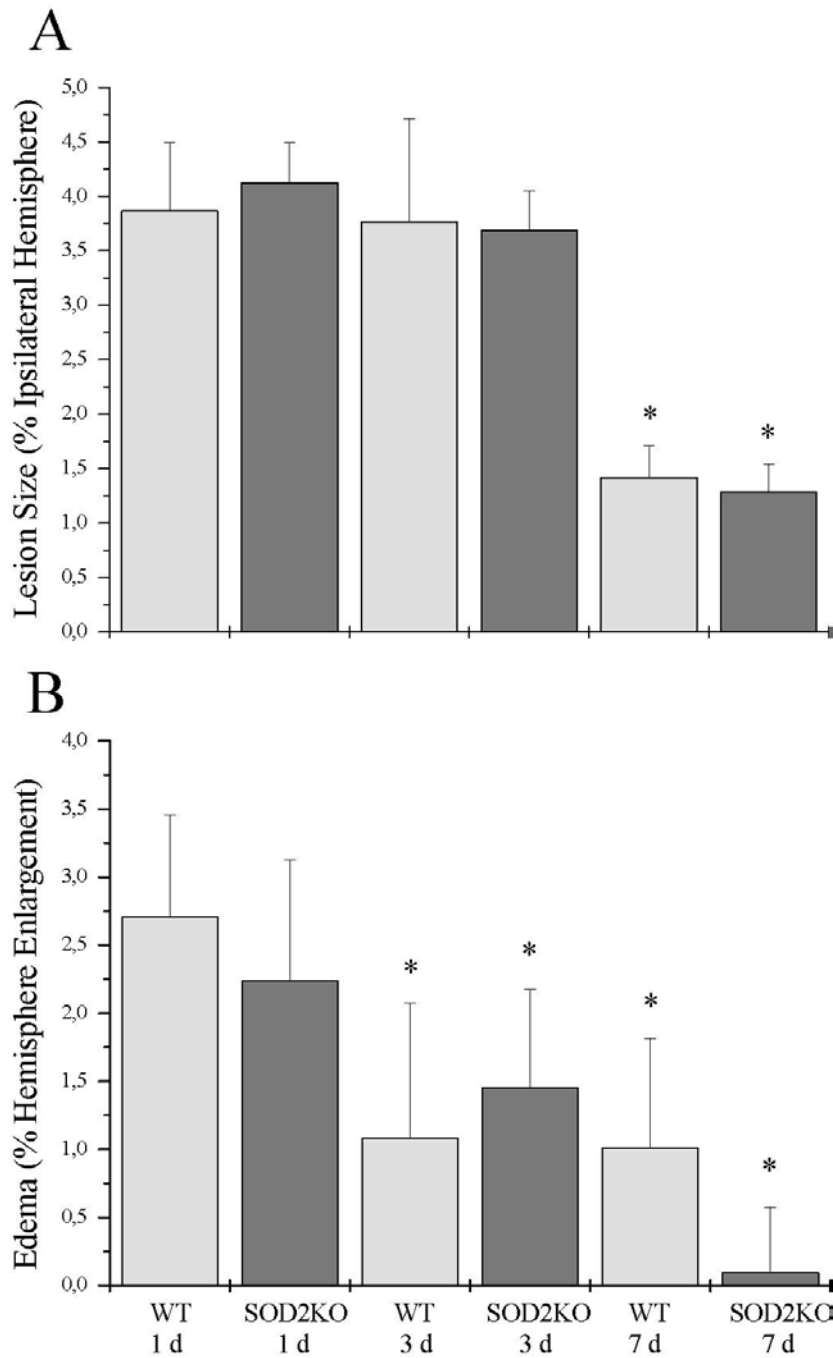


**Figure 8A+B: Lesion size and edema formation in SOD2-KO mice and WT animals**

A) Percentage area of damage (lesion size) for the affected hemisphere in wildtype (WT) and Mn-superoxide dismutase knockout mice (SOD2-KO) was calculated at 1, 3 and 7 days following cold injury-induced brain trauma (CIBT). By 7 days post-CIBT, both WT and SOD2-KO showed a significant reduction in lesion size compared to 1 and 3 days.

B) Edema formation was significantly reduced in both animal groups by 3 and 7 days compared with 1 day.



### 3.1.2. Hemorrhagic transformations followed the same pattern in WT and SOD2-KO mice

Hemorrhagic transformations were used as an indicator for alterations of the blood brain barrier which have been described to appear after CIBT. Both grade and distribution of hemorrhagic transformation were examined at 24 h, 72 h and 7 days in CIBT-treated SOD2-KO mice and WT littermates using Perl's Iron staining (-> 2.3.8.).

#### A) Comparison of grade of hemorrhagic transformation in WT and SOD2-KO mice

Hemorrhagic transformations in the cold injury-induced lesions were detected by Perl's Iron staining in SOD2-KO and WT animals and degree of hemorrhagic transformations graded (Table 1).

Score	0	1	2	3	4	
Number of animals						
WT	1 d	3	4	1	0	0
	3 d	0	0	0	5	3
	7 d	0	0	0	5	4
SOD2-KO	1 d	5	3	1	2	0
	3 d	0	0	0	5	6
	7 d	0	0	0	4	4

**Table 1. Hemorrhage scores in SOD2-KO and WT mice after CIBT**

*Scores: Grade 0, no bleeding; grade 1, very minor Perl iron staining restricted to a small area in <25 % of all sections examined; grade 2, some staining restricted to the injured area in 26-50 % of sections; grade 3, extensive staining encompassing entire injured region in 51-75 % of sections; grade 4, extensive staining within and outside of the injured area in more than 76 % of sections.*

A non-parametric method for ranked data was used for statistical analysis of the score results. The statistical analysis revealed that there was no significant difference in hemorrhagic transformation between the two groups, WT and SOD2-KO mice, however, significant ( $p < 0.0001$ ) changes were found when comparing different time points; the interaction of animal type and time was not significant. Pair wise comparisons of the ranks then showed that hemorrhage score for one day was different (lower) compared to days 3 and 7 which were not

different from each other ( $p < 0.0001$  for 1 day vs. 3 days and for 1 day vs. 7 days). Results were consistent using Kruskal Wallis non-parametric tests for time stratified by type as well as for type stratified by time.

### **B) Distribution of hemorrhagic transformation in WT and SOD2-KO mice**

In both SOD2-KO and WT mice hemorrhagic transformations followed a characteristic temporal pattern (Fig. 9)

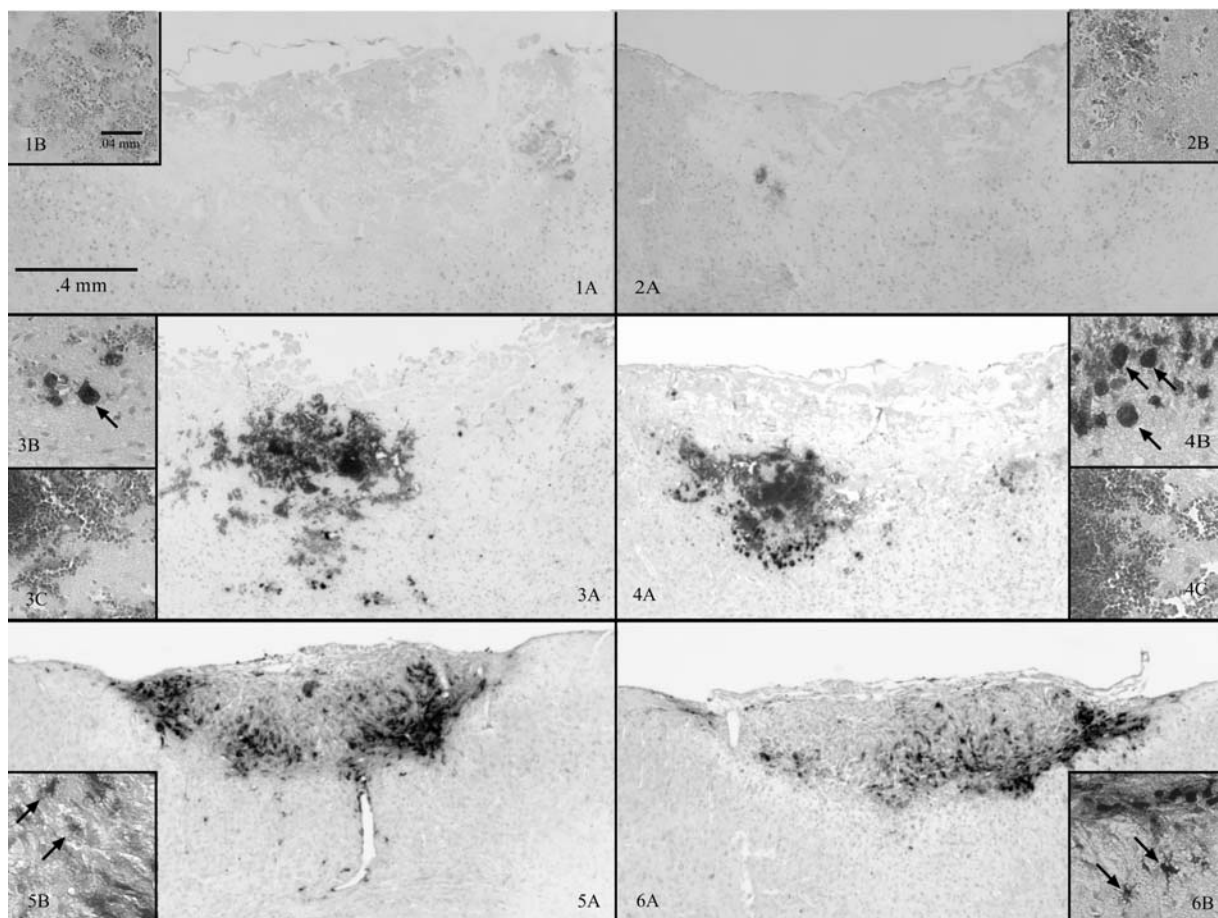


**Figure 9: Hemorrhagic transformations in SOD2-KO and WT mice**

*Representative photomicrographs of Perl's Iron-stained sections show hemorrhagic transformations at 1 day (1, 2), 3 days (3, 4) and 7 days (5, 6) after CIBT. There were no differences in the rate of hemorrhagic transformations between WT (1, 3, 5) and SOD2-KO animals (2, 4, 6). Insets show iron-positive red blood cells (1-4C) and inflammatory cells (3B, 4B, 5B, 6B) in the affected tissue.*

One day after CIBT (Fig 9.1A, 9.2A) little or no red blood cells could be observed in the lesion area (Fig: 9.1B, 9.2B). At this early time point bleeding was caused by mechanical destruction of vessels due to freezing. At 3 days (Fig. 9.3A, 9.4A) extensive bleeding could be observed in both SOD2-KO and WT mice. Both red blood cells (Fig. 9.3C, 9.4C) and inflammatory cells (Fig. 9.3B, 9.4B) could be easily discerned. Since these hemorrhagic transformations were not observed at earlier time points, one can assume that they were caused by secondary damage including gradual damage of the blood brain barrier by free oxygen radicals or digestion of the vessels basal laminar matrix by MMPs (matrix metalloproteinases) which have been described to be activated after induction of CIBT (Morita-Fujimura et al., 2000). Iron-uptake by inflammatory cells had already started and was increased at 7 days. At 7 days (Fig. 9.5A, 9.6A) only a few RBCs could be observed whereas iron-positive inflammatory cells were detected throughout the lesion core and perimeter (Fig. 9.5B, 9.6B).

### **3.1.3. Inflammatory response after CIBT in WT and SOD2-KO mice**

To detect inflammatory response after CIBT, brain sections were stained for myeloperoxidase (MPO) to detect MPO-positive neutrophils. Neutrophil invasion was used as a parameter to quantify the inflammatory response by comparing the amount of MPO-positive cells in the lesion in WT and SOD2-KO mice. To elucidate the pattern of inflammatory response in the lesion the local distribution of MPO-positive cells was observed in both groups.

#### **A) MPO cell count after CIBT in WT and SOD2-KO mice**

In 4 different areas of the lesion (A = left corner lesion, B = right corner lesion, C = penumbra under lesion, D = middle core lesion) cell counts of MPO-positive cells were performed. They showed no differences between WT and SOD2-KO animals at any time point examined (Table 2).

The only factor for which MPO counts differed was time ( $p > 0.001$ ). MPO counts did not differ by animal type, by type crossed by (X) time, by type X area, by time X area or by type time X area. Pair-wise comparison of adjusted least square means is valid only for those factors that are significant in the model and was based on a-priory hypothesis. Adjusted mean MPO counts were significantly different between all times ( $p > 0.0001$  for all comparisons) with 3 days > 1 day > 7 day.

Factors	LSM	SE
Animal type		
Wild type (WT)	12.6	.65
SOD2-KO (KO)	11.7	.65
Time in days*		
1	11.5	.74
3	20.2	.83
7	4.8	.83
Area		
A	12.6	.92
B	11.0	.92
C	11.2	.92
D	13.9	.92
Animal/Time groups		
WT- 1 d	11.7	1.0
WT- 3 d	20.7	1.2
WT- 7 d	5.5	1.2
KO- 1 d	11.2	1.0
KO- 3 d	19.7	1.2
KO- 7 d	4.2	1.2

**Table 2: MPO-positive cell counts**

*Least square mean (LSM) MPO counts and associated standard error (SE) adjusted for the other factors in the model (main factors: animal type, time in days, area). Two measurements were taken from each area for each animal within each time and animal type (5 different animals for the WT/1 day, and KO/1 day groups; 4 different animals for each of the other type/time combinations).*

*\*In the nested analysis mean MPO cell counts were significantly different by time ( $p < 0.0001$ ).*

## B) Distribution of MPO-positive cells after CIBT in WT and SOD2-KO mice

Neutrophil infiltration was evident in animals at 1 day post-insult, peaked at 3 days, and was reduced at 7 days after CIBT (Fig. 10). Hemorrhagic transformations and MPO-positive cells were co-localized.

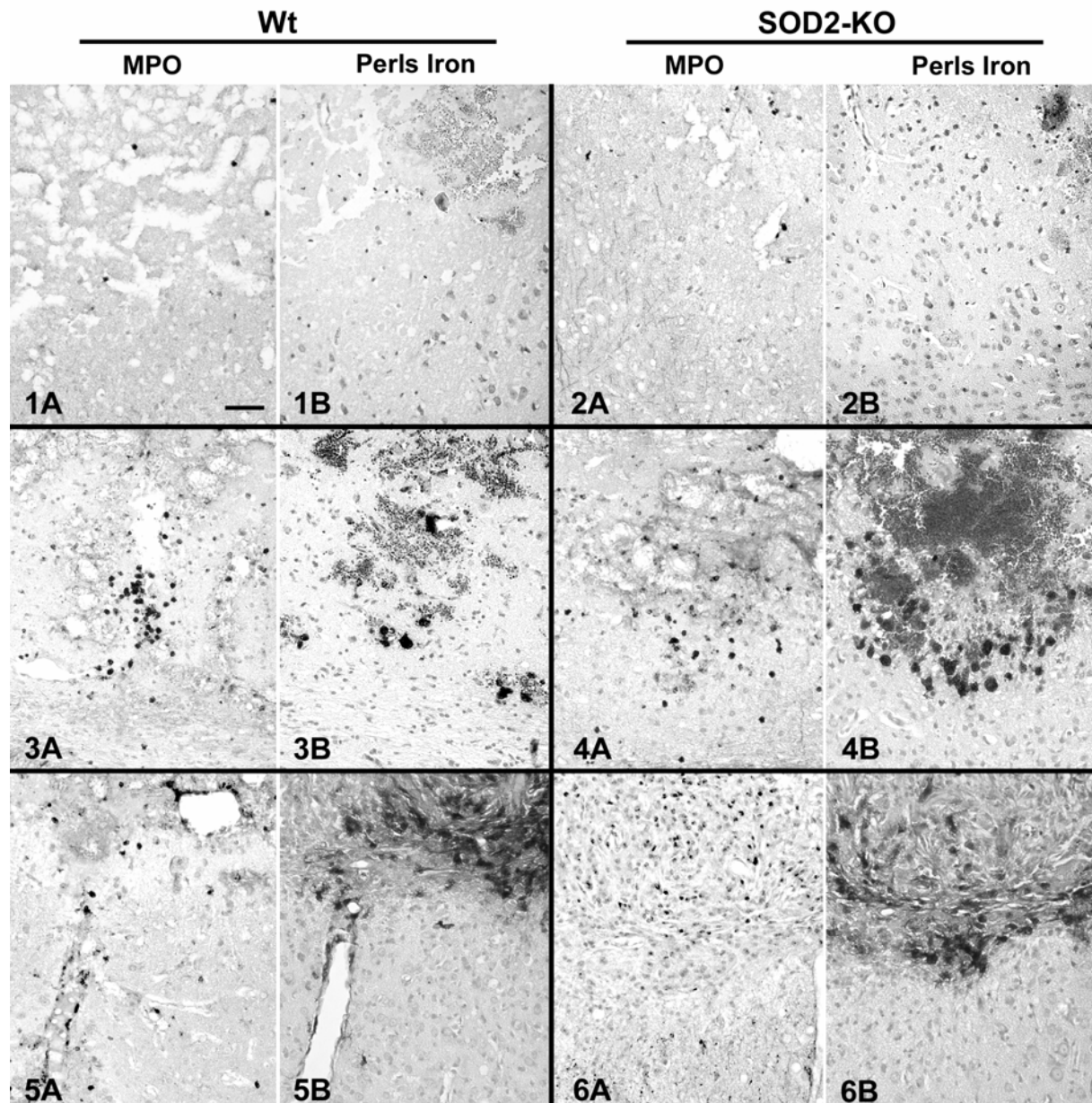


**Figure 10. Co-localisation of MPO-positive cells and hemorrhagic transformations**

Representative photomicrographs show co-localization of hemorrhage (Perl's iron staining) and MPO-positive cells in adjacent sections from the same animals. There were very few MPO-positive cells and little or no hemorrhage at 24 h post-insult in both WT and SOD2-KO animals (1A+B, 2A+B). By 3 days after CIBT there was a significant increase in MPO-positive cells and in Perl's iron staining in both animal groups (3A+B, 4A+B). At 7 days

*post-insult the grade of hemorrhagic transformation was equally high in both WT and SOD2-KO animals while the number of MPO-positive cells was equally reduced in both groups (5A+B, 6A+B). Bar = 50  $\mu$ m.*

#### **3.1.4. TUNEL-labelling in SOD2-KO and WT mice**

DNA-fragmentation as a typical feature of apoptosis was examined by in-situ labelling of fragmented DNA (TUNEL-staining) in the nucleus. Both apoptosis and necrosis have been described in this model (Murakami, Neuroscience, 1997); morphologically, they can be differentiated since apoptotic cells show typical features like condensed or fragmented nuclei which are more intensely labelled. Necrotic cells are fainter labelled and their nuclei appear enlarged. The amount of apoptotic cells as well as their distribution was compared between SOD2-KO mice and WT animals.

##### **A) Similar numbers of apoptotic cells in WT and SOD2-KO animals**

TUNEL-positive cells were counted in 4 different areas of the lesion (A = left corner lesion, B = right corner lesion, C = penumbra under lesion, D = middle core lesion) and the results statistically analyzed. Only strongly labelled cells were counted as positive. The results are shown in Table 3. Comparison of least square means for factors significant in the model showed that adjusted mean cell counts for 1 day and 7 days were significantly different from the value obtained for to 3 days ( $p = 0.04$  and  $p = 0.009$ , respectively), but not different from each other. TUNEL-positive cells could be found predominantly in the corner region of the lesion and less in the core or penumbra under lesion, however, this tendency was not significant due to high variation within the groups.

Factors	LSM	SE
Animal type		
Wild type (WT)	14.6	.57
SOD2-KO (KO)	14.4	.57
Time in days*		
1	15.0	.70
3	12.9	.70
7	15.5	.70
Area		
A	18.5	.80
B	20.0	.80
C	7.9	.80
D	11.5	.80
Animal/Time groups		
WT- 1 d	14.2	.98
WT- 3 d	13.9	.98
WT- 7 d	15.6	.98
KO- 1 d	15.7	.98
KO- 3 d	12.0	.98
KO- 7 d	15.5	.98

**Table 3: TUNEL-Positive Cell Counts**

*Least square mean (LSM) counts of TUNEL-positive cells and associated standard error (SE) adjusted for the other factors in the model (main factors: animal type, time in days, area). Three measurements were taken from each area for each animal within each time and animal type (3 different animals for each type/time combination).*

*\*In the nested analysis mean TUNEL- positive cell counts were significantly different by time ( $p=0.046$ ).*

### **B) Similar distribution of TUNEL-positive cells**

Cells with intensely labeled nuclei could be observed at all time points examined (Fig. 11, 1-6B). Aside from TUNEL-positivity, several cells showed the characteristic morphological features of apoptosis, including cell shrinkage, blebbing of the nucleus and apoptotic bodies

(Fig. 11, 1-6B, arrows). However, a large number of TUNEL-positive cells (with weaker, diffuse brown staining) could not be identified as apoptotic by morphologic criteria, particularly at 7 days post-CIBT. These cells were considered necrotic, and were not included in the cell count.

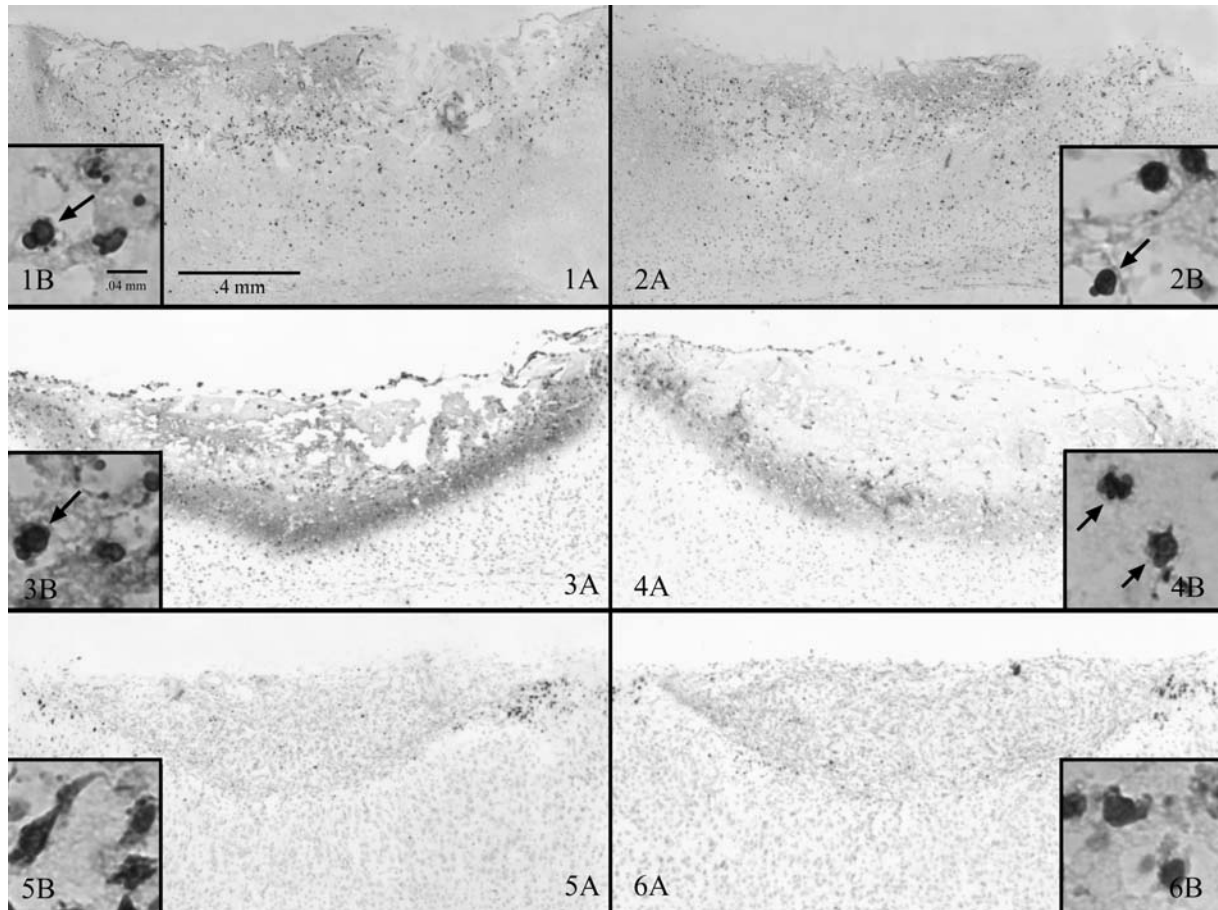


**Figure 11: TUNEL-positive cells after CIBT**

*Representative photomicrographs of TUNEL-stained sections show distribution of TUNEL-positive cells at 1 day (1, 2), 3 days (3, 4) and 7 days after CIBT (5, 6). No differences in spatial distribution or number of TUNEL positive cells could be observed between wild-type (1, 3, 5) and SOD2-KO animals (2, 4, 6). High magnification insets show TUNEL-positive cells (1 - 6B). TUNEL-(+) cells with characteristic apoptotic features are highlighted by arrows.*



### 3.1.5. Hydroethidine oxidation showed no significant difference in superoxide anion production

Measurement of hydroethidine oxidation in the injured hemisphere showed no significant differences in ROS production between SOD2-KO animals and their WT counterparts (WT/SOD2-KO:  $1.3 \pm 0.5/1.2 \pm 0.2$ ) 2 hours following CIBT (Fig. 12).

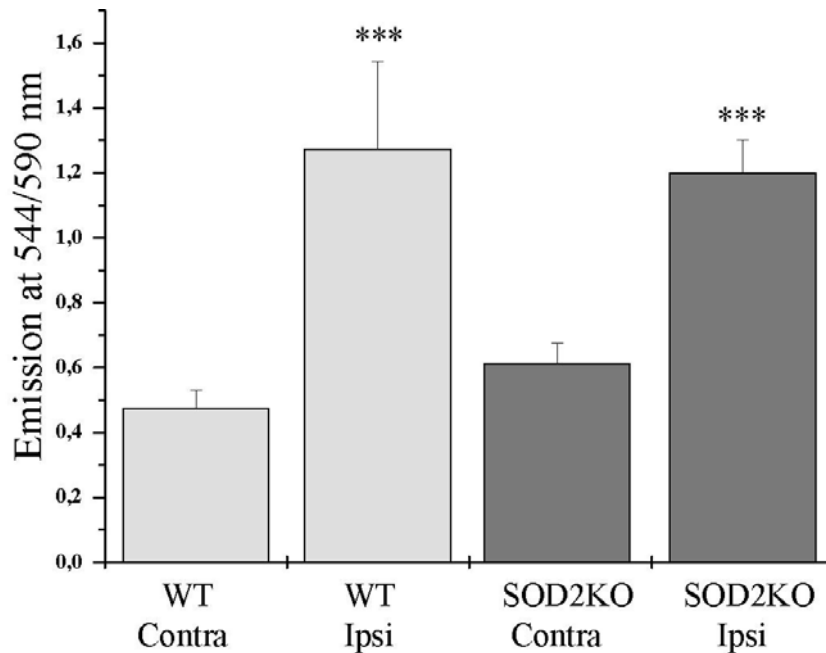


**Figure 12: ROS production measured by hydroethidine assay of SOD2-KO and WT mice after CIBT**

Measurements of oxygen radical generation 2 hours after CIBT in the affected ipsilateral hemisphere (Ipsi) and on the contralateral (Contra) side by recording the emission by ethidium in 8 animals per group showed a significant increase in superoxide anion production in the ipsilateral hemisphere of both WT and SOD2-KO animals compared with the contralateral hemisphere. Data are expressed as mean  $\pm$  SEM

## 3.2. The influence of the SOD1 level on intrastriatal 3-NP lesion

### 3.2.1. Establishment of the model in wildtype animals

Since the aim of this study was to test the influence of SOD1 levels on the outcome of the intrastriatal 3-NP lesion, it was crucial to create a lesion which did not exceed the striatum and allowed to detect an increase as well as decrease of the lesion. Using a protocol of intrastriatal 3-NP injection in mice invented by Kim et al. (Kim, unpublished data) did not seem practicable since the created lesion was too severe for the purpose of this study since the lesion expanded in hippocampus and cortex. Therefore the dose was reduced on 0.4  $\mu$ l 3-NP solution (1 g/14 ml saline) (-> 2.4.3.) to create a reproducible, medium-sized lesion which within the striatum (Fig. 13). Control animals receiving saline injection revealed no lesion as determined after cresyl violet staining.

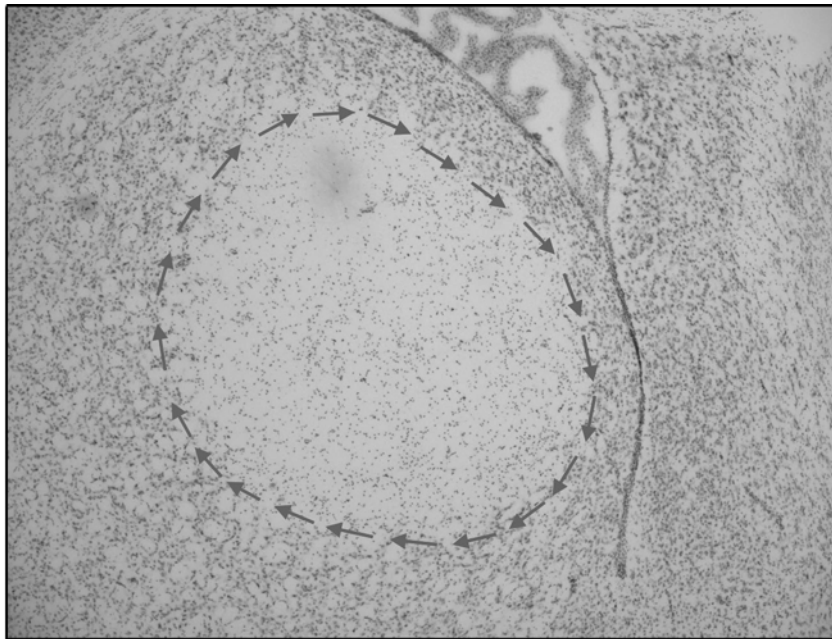


**Figure 13: Striatal damage after 3-NP injection**

*Cresyl violet staining of frozen brain sections the lesion was identified as a pale area (outlined with arrows) within the striatum. The photomicrograph shows a lesion at 24 h after the injection of 0.4  $\mu$ l 3-NP solution (1 g/14 ml saline).*

To define the development of the lesion, lesion size and edema formation were examined after 3-NP injection. Lesion size in CD-1 WT animals (n=5-6) was not significantly different between 4 h, 24 h, 72 h after injection but decreased significantly from 72 h to 7 days. (4 h:  $30.80 \pm 2.67$ , 24 h:  $33.83 \pm 4.60$ , 72 h:  $28.64 \pm 2.88$ , 7 days:  $8.83 \pm 2.61$ ) (Fig.14A): The

edema, measured as hemisphere enlargement, peaked at 24 h after injection and was still evident at 7 days. (4h:  $14.98 \pm 2.77$ , 24h:  $25.72 \pm 4.41$ , 72h:  $14.77 \pm 1.71$ , 7days:  $7.74 \pm 6.53$ ) (Fig.14B).

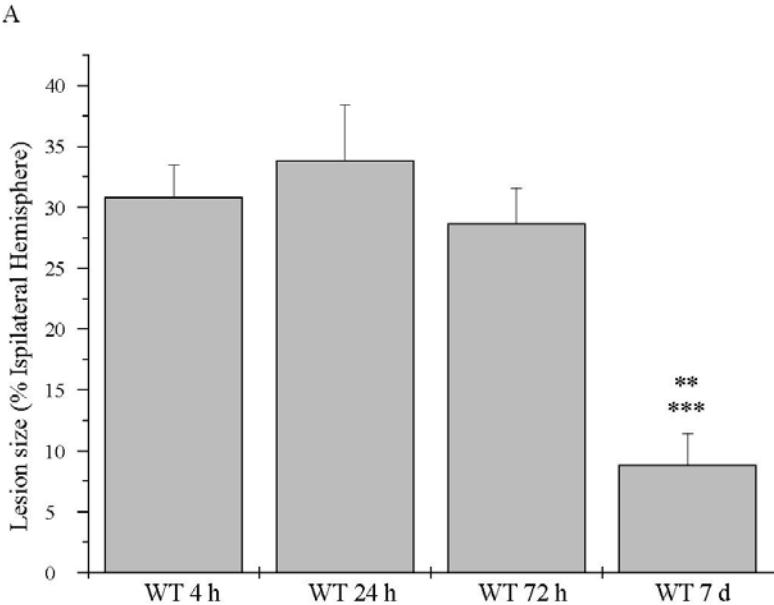


**Figure 14A: Lesion size after 3-NP injection in wild-type animals**

Size of lesion in CD-1 wild-type animals was measured from 4 h to 7 days post injury. At day 7 the size of the lesion was significantly decreased ( $P$ -value  $< 0.001$  compared with 24 h time point,  $P$ -value  $\leq 0.01$  compared with 4 h and 72 h, Scheffé) compared to all other time points.

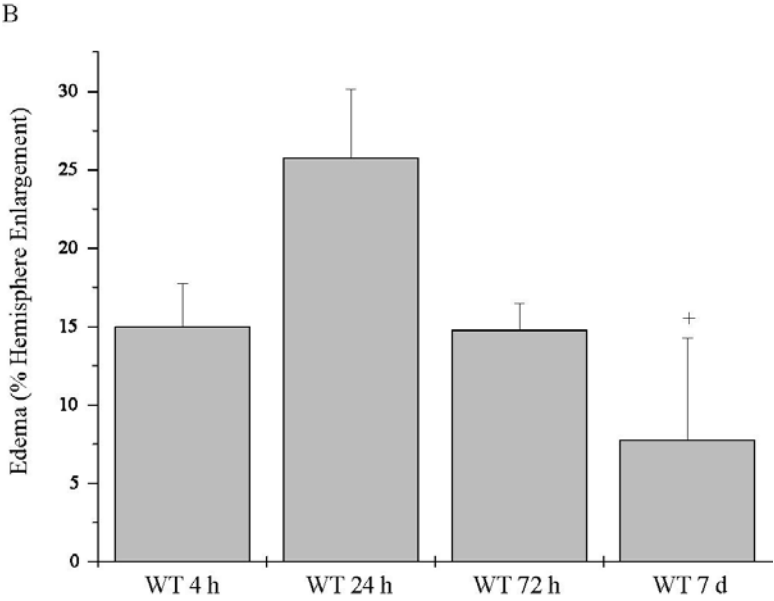


**Figure 14B: Edema development after 3-NP injection in wild-type animals**

*Edema development was measured in CD-1 wild-type animals from 4 h to 7 days post injury. Edema peaked at 24 h after 3-NP injection and was evident from 4 h to 7 days. From 24 h to 7 days edema was significantly reduced ( $P$ -value < 0.05, Duncan).*

**3.2.2. Detection of apoptosis in WT animals**

Since necrosis as well as apoptosis have been found after intrastriatal injection of 3-NP (Ankarcrona et al., 1995) (Sato et al., 1997a; Sato et al., 1998), TUNEL-staining was performed to detect apoptotic cells after intrastriatal 3-NP injection. TUNEL-staining was performed on paraffin sections of CD-1 mice at 4 h, 24 h, 72 h and 7 days after injury. At all time points, TUNEL-stained cells could be detected throughout the lesion (Fig. 15). However, this staining was relatively weak and the majority of stained cells did not reveal typical morphological features of apoptosis such as condensed nuclei, formation of apoptotic bodies. Only in the needle track area positively stained cells with apoptotic morphology could be detected (Fig. 16).

In addition, caspase-3 and caspase-9 immunohistochemistry were performed on floating sections in wild-type animals at 4 h, 24 h and 72 h time points to detect whether caspases as typical markers for the apoptotic pathway were activated. No specific staining could be achieved inside the lesion at any time point. However, at 4 h (but not at 24 h or 72 h after injection) caspase-3- (Fig. 17) and caspase-9-positive cells (Fig. 18) could be detected in the needle track and, thus, served as a positive control for the staining. Control sections without primary antibody remained unstained.

TUNEL-staining sections of SOD1-TG mice at all these points showed the same staining as observed in WT animals. In both groups the cells within the lesion predominantly showed necrotic features.

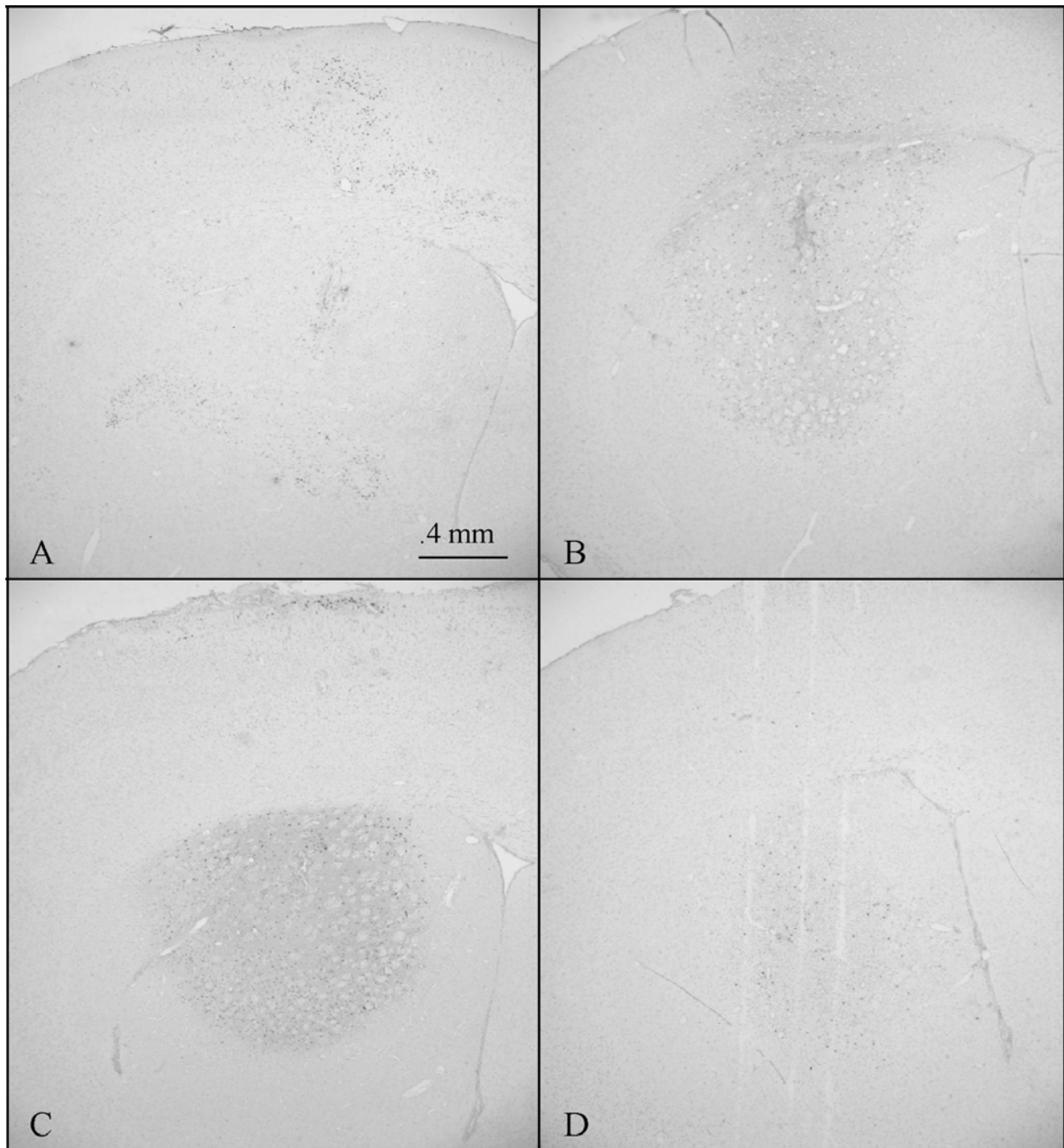


***Figure 15: Representative TUNEL-staining in WT animals***

*At 4 h (A), 24 h (B), 3 days (C) and 7 days (D), unspecific TUNEL-staining could be detected in the lesion area inside the striatum. The staining is weak and indicates the labelled cells to be necrotic since apoptotic cells would reveal intensely labelled nuclei.*

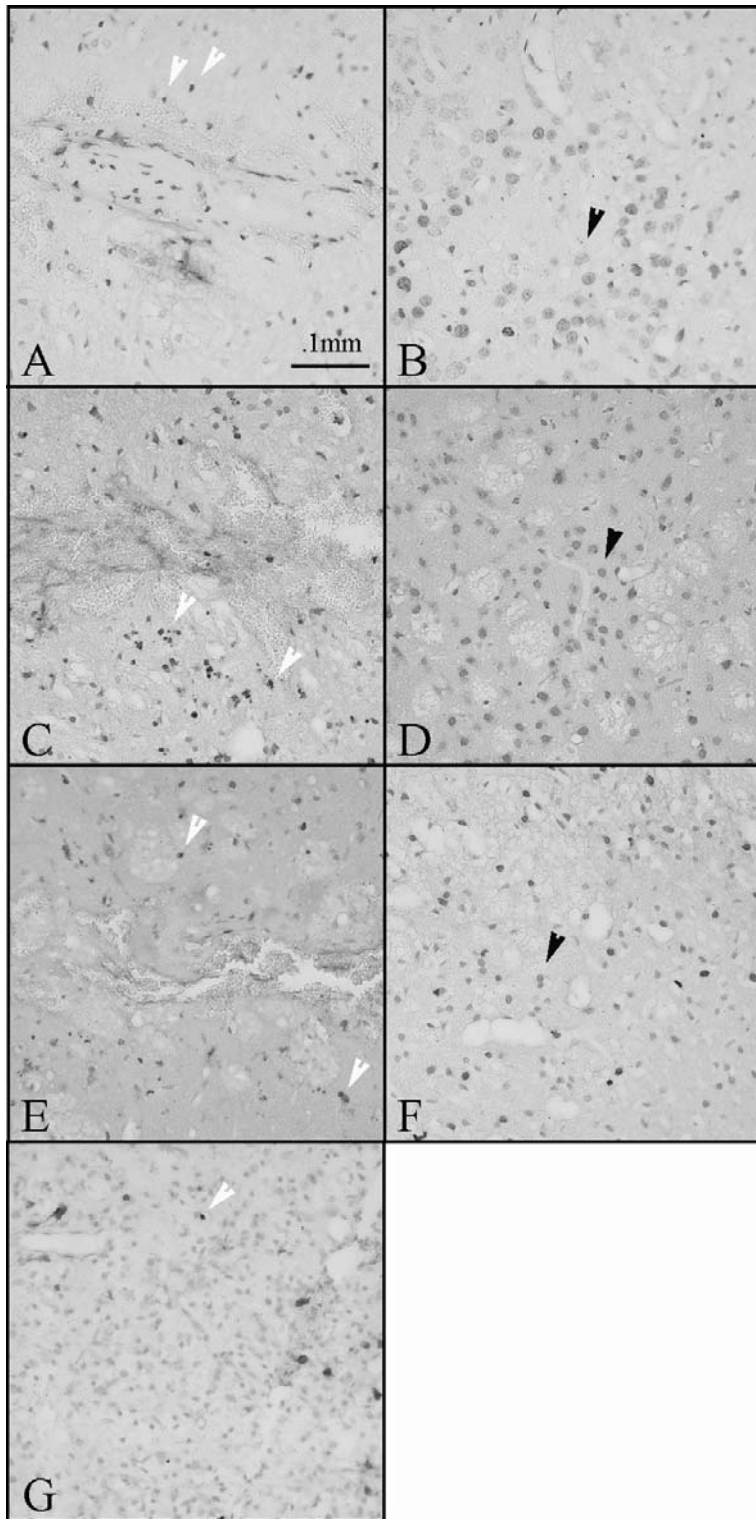


**Figure 16: Difference morphology of TUNEL-labelled cells in needle track area and inside the lesion**

Representative photomicrographs of the needle track area (A, C, E) and striatal lesion area (B, D, F, G) show TUNEL-positive cells with apoptotic morphology only around the needle track. Few intensely labelled, condensed or fragmented nuclei (pointed out by white arrows)

could be observed while the vast majority of stained cell in the lesion area had faintly stained nuclei with increased size (black arrows) suggesting necrosis. This pattern could be observed at all time points 4 h (A+B), 24 h (C+D) and 72 h (E+F). At 7 days post injury the needle track area could not be distinguished from the rest of the lesion. (Scale bar = 0.1 mm)

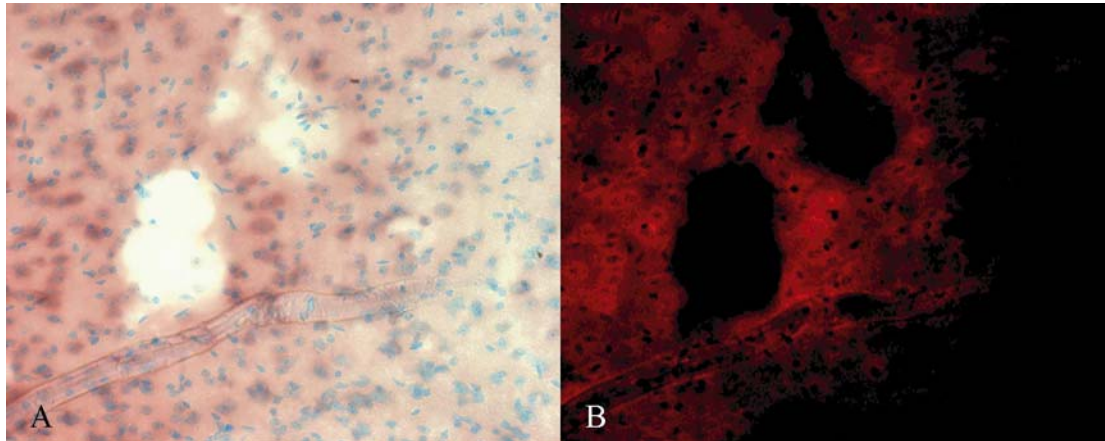


**Figure 17: Caspase-3 immunohistochemistry**

Caspase-3-positive cells could be detected in the damaged cortical needle track area under light microscopy (A) and fluorescence microscopy (B) after caspase-3 immunohistochemistry in floating sections. Nuclei were counter-stained by methyl green.

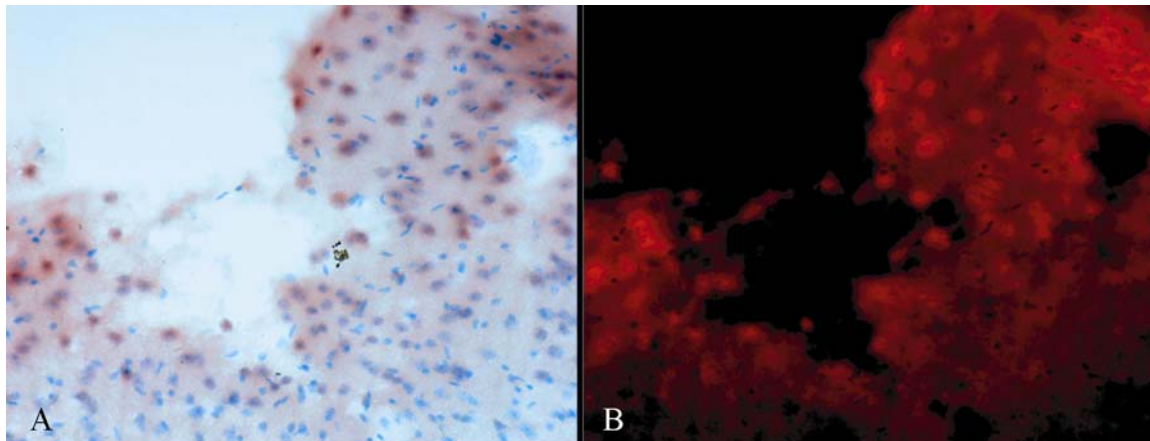


**Figure 18: Caspase-9 immunohistochemistry**

Mechanically damaged cortex shows caspase-9 positive cells by immunohistochemistry under light microscopy (A) and fluorescence microscopy (B) at 4 h after 3-NP injection. Nuclei appear green by methyl green counter-staining.

### **3.2.3 Size of lesion and edema formation in SOD1-TG mice, their wild-type littermates and SOD1-KO mice.**

At 24 h after 3-NP injection, SOD1-TG mice showed a significantly smaller size of lesion and edema formation than wild-type animals. On the other hand, SOD1-KO mice did not have a significantly different lesion size compared with the WT animals (Fig. 19A). At 24 h, the edema was also significantly smaller in SOD1-TG mice compared to wildtype animals. A significant increase in edema was found in SOD1-KO animals compared to wild-type animals and SOD1-TG mice (Fig. 19B). At 72h, the lesion size remained significantly smaller in SOD1-TG animals compared to wild-type animals, edema formation, however, was not significantly different between wild-type animals and SOD1-TG. (Fig. 19A+B)



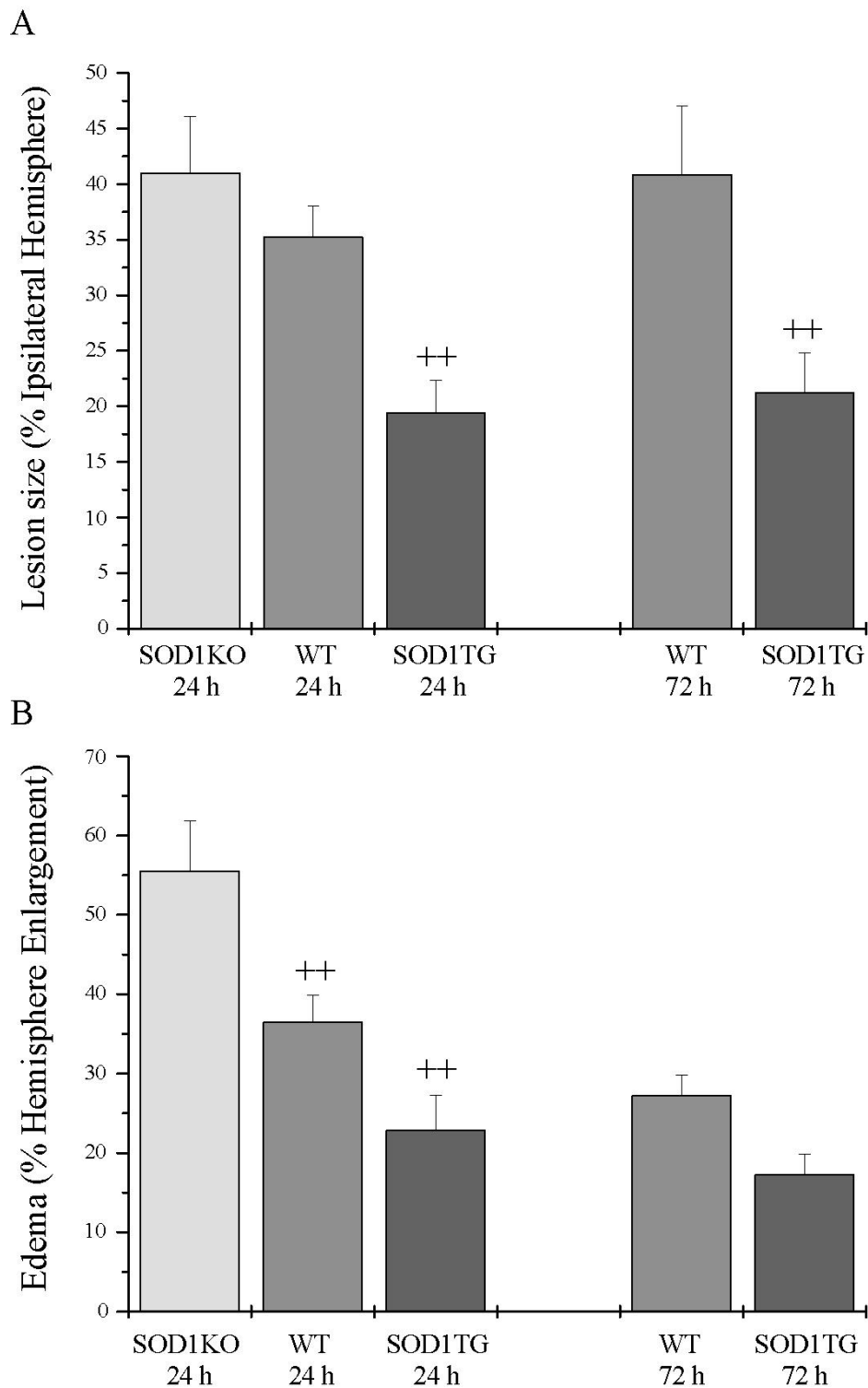


**Figure 19 A+B: Size of lesion and edema formation at 24 h and 72 h after 3-NP injection in SOD1-TG mice, wild-type littermates and SOD1-KO mice**

A) Lesion size as % ipsilateral hemisphere enlargement was significantly reduced in SOD1-TG mice compared to WT or SOD1-KO at 24 h after injection and stayed significantly decreased at 72 h ( $P$ -values  $< 0.01$ ). B) The edema as % hemisphere enlargement was significantly different in SOD1-KO animals compared to wild-type and SOD1-TG animals ( $P$ -

*value < 0.01) and in SOD1-TG animals compared to their wild-type littermates ( P-value < 0.05). At 72 h, edema showed no significant difference between wild-type animals and SOD1-TG animals. (n=7-10).*

### **3.3. Search for PP2C $\beta$ activation after induction of damage in cultured neurons**

#### **3.3.1. Detection of Bad and Bad-155P and PP2C $\beta$ in cultured rat neurons**

In this study, the hypothesis was tested that oleic acid treatment of cultured neurons activates PP2C $\beta$  which contributes to apoptosis by dephosphorylation of Bad especially at Ser<sup>155</sup>. First, it was demonstrated that all enzymes were expressed in the cultured neurons (rat embryonic cortical and rat neonatal hippocampal) and co-localized in the same cellular compartment which is a precondition for their interaction. Western blot protocols for detection of Bad, Bad-155P and PP2C $\beta$  proteins were established, optimized and all proteins detected in both rat primary cultures. PP2C $\beta$ 's cellular distribution in neurons was elucidated by immunocytochemistry. Bad or Bad-155P immunocytochemistry could not be performed since the available primary antibodies were too unspecific.

##### ***3.3.1.1. Detection of Bad/ Bad-155P by Western blotting in embryonic cortical neurons***

To identify specific Bad bands by Western blotting, two polyclonal peptide antibodies were tested which were designed to detect different peptide sequences of Bad. The Bad-antibody produced by Cell Signaling Inc. (CS) detected amino acids of the N-terminal end of Bad, the Bad-antibody by Santa Cruz Inc. (SC) was designed to detect an amino acid sequence at the C-terminal end. The Bad-155P antibody (CS) used in these experiments was designed to detect an amino acid sequence including phospho-Ser<sup>155</sup>. Bad antibodies were used on untreated samples of rat embryonic cortical neuronal cultures (CC) (18  $\mu$ g/lane), for Bad-155P detection CC samples were used, as well. Additionally, CC samples were phosphorylated with the catalytic unit of protein kinase A (cA-PK) before detecting Bad-155P (CC+P, 18  $\mu$ g/lane) in order to increase the intensity of the phospho-Bad band. (Fig. 21A). As controls, 0.1  $\mu$ g purified recombinant Bad-GST (provided by Dr. P.Cohen, Dundee; Scotland) or cA-PK-phosphorylated Bad-GST (Bad-GST+P) were applied. On all blots two bands (23 kDa and 27 kDa) were revealed in CC by the different Bad-antibodies. These observations are compatible with the two protein variants derived from two splicing products of Bad which have been described in rat tissue (Datta et al., 2002) (Datta et al., 2000) (Hamner et al., 2001):

Bad- $\beta$ /BAD<sub>S</sub> and Bad- $\alpha$ /Bad<sub>L</sub>. These isoforms differ in length and amino acid sequence at their carboxy-terminal regions (Bad- $\beta$  is 15 amino acids longer) but both still interact with anti-apoptotic members of the Bcl-2 family and therefore have proapoptotic qualities.

Additionally, “clean” blots without strong background and clear bands showed that the higher band (Bad- $\alpha$  or Bad<sub>L</sub>) was split into two separate bands with ~1 kDa difference (Fig. 20C). It has been argued that hyperphosphorylation of Bad leads to a mobility shift and results in two bands (Zha et al., 1996). The upper one was described as a hyperphosphorylated form of Bad, the lower was thought to be composed of unphosphorylated as well as phosphorylated Bad. In untreated embryonic cortical neuronal culture samples the upper band was very weak.

Bad-GST was detected by all Bad antibodies at 47 kDa, Bad-GST+P by the phospho-Bad-155 antibody at the same molecular weight. Although all Bad antibodies were able to detect Bad, their quality and specificity for Bad varied: Not only did the use of different primary antibodies influence the quality of the Western blots, the choice of secondary antibody (HRP-conjugated anti-rabbit antibody, Promega or Amersham) was of equal importance:

A) The Santa Cruz Bad-antibody combined with any secondary antibody always resulted in blots with many strong unspecific bands indicating a high unspecificity of the primary antibody (Fig. 20 A).

B) The Cell Signaling Bad or Bad-155P-antibodies produced markedly less unspecific bands than the Santa Cruz antibody when combined with the Promega secondary antibody (Fig. 20A+B, 21A), and hardly any unspecific bands with the Amersham 2ndary antibody (Fig. 20C, 21B).

In conclusion, Bad or Bad-155P primary antibodies from Cell Signaling combined with secondary antibodies from Amersham allowed optimal detection of Bad/Bad-155P by Western blot.

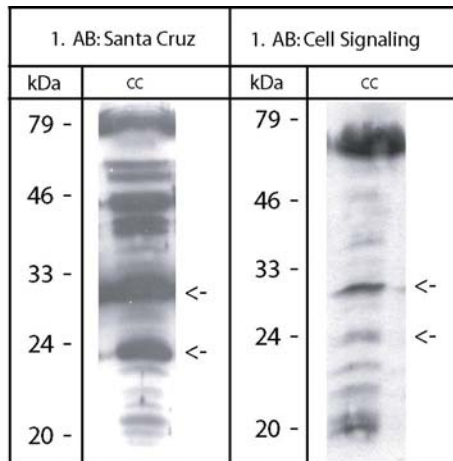


**Figure 20A: Comparison of Bad antibodies for Western blotting**

Proteins extracted from CC were separated electrophoretically (->2.5.8.) and analyzed with primary antibodies from Santa Cruz and Cell Signaling, respectively. Secondary antibodies were from Promega. Arrows indicate the bands expected to represent isoforms of Bad according to their molecular weight.

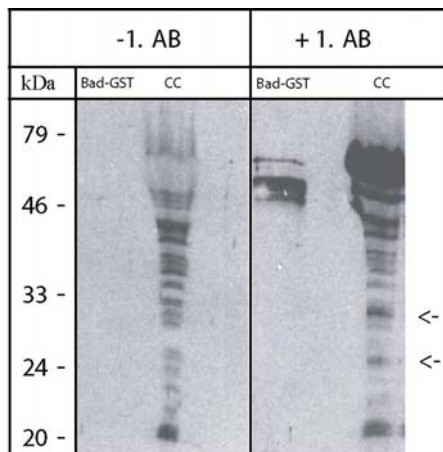


**Figure 20B: Unspecific bands by Promega 2ndary antibody on Bad Western blot**

Proteins from CC or recombinant Bad-GST were analysed by Western blotting with or without primary antibody (1. AB) from Cell Signaling and secondary antibody from Promega. In CC the secondary antibody produced a ladder of unspecific bands. The position of specific bands is indicated by arrows.

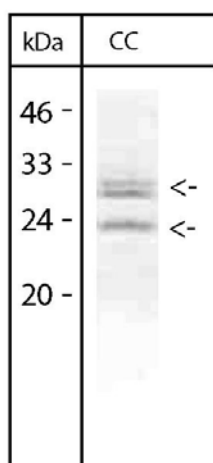


**Figure 20C: Optimized Western blot detecting Bad in cultured embryonic cortical neurons**

The combination of the primary Cell Signaling antibody and the secondary antibody from Amersham allowed detection of Bad without unspecific bands. Bad migrated as 2 bands, potentially representing splicing products at 23/27 kDa (arrows). The larger band was split in two, possibly one hyperphosphorylated and one unphosphorylated/partly-phosphorylated band.

A

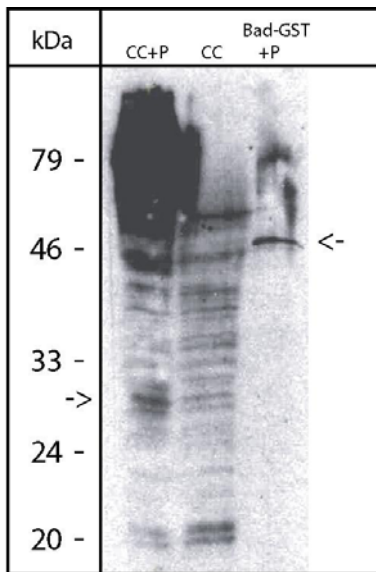
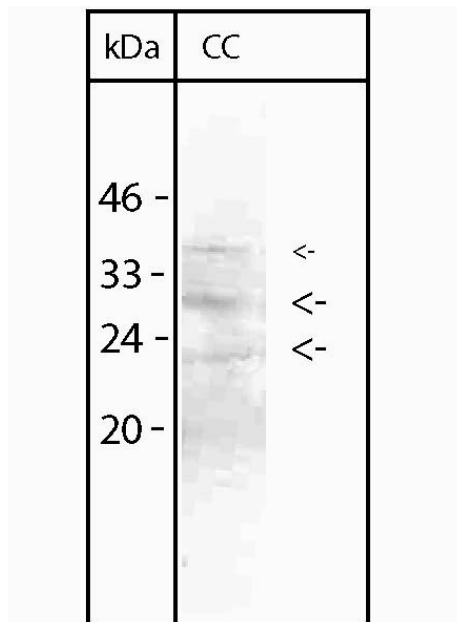


**Figure 21A+B: Detection of Bad-155P by Western blotting in primary cultures of embryonic cortical neurons**

A) *Bad-155P* antibodies indicated an increased band at 27 kDa (arrow, left) in phosphorylated samples of embryonic cortical neurons (CC+P) compared to the unphosphorylated sample (CC). Phosphorylated *Bad-GST* was used as a control and detected a band at 47 kDa (arrow, right). The secondary antibody from Promega resulted in additional unspecific bands.

B



B) Western blot on *Bad-155P* (Cell Signaling antibody in combination with the secondary antibody from Amersham) showed two bands detectable at 23/27 kDa in samples of embryonic cortical neurons (CC) as indicated by large arrows. The combination with the secondary antibody by Amersham did only produce one unspecific band at about 40 kDa (small arrow).

### 3.3.1.2. Detection of PP2C $\beta$ in cultured neurons

PP2C $\beta$  is one isoform of the enzyme protein phosphatase 2C. It is a Mg<sup>2+</sup>-dependent serine phosphatase and can be activated by unsaturated fatty acids like oleic acid. Since the hypothesis was that PP2C activation by oleic acid contributed to apoptosis, it was necessary to show that PP2C, as well as Bad, could be detected in cultured neurons by Western blotting. Since so far PP2C's cellular localization had not been established in cultured neurons,

immunocytochemistry was performed in cultured embryonic cortical neurons using a novel PP2C $\beta$  antibody produced and kindly provided by Prof. S. Klumpp, Münster, which proved to be highly specific and useful for both Western blot detection and immunocytochemistry of PP2C $\beta$ .

*A) Western blotting on PP2C $\beta$  in embryonic cortical neurons*

In combination with the secondary antibody produced by Amersham PP2C $\beta$  could be detected on Western blots of protein extracts from cultured embryonic cortical neurons without additional unspecific bands (Fig. 22). PP2C $\beta$  migrated as a single band of  $\sim$  45 kDa. In contrast, the secondary antibody from Promega produced faint unspecific bands.

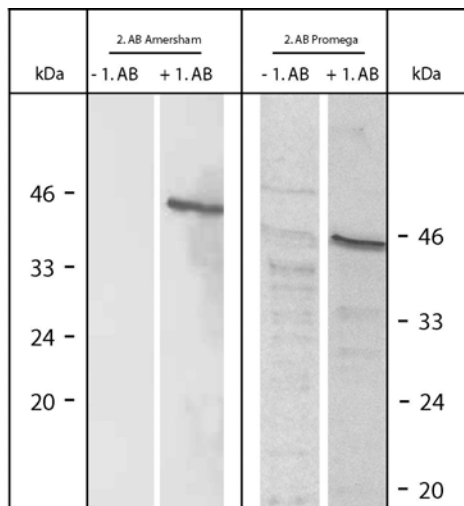


**Figure 22: Western blotting of embryonic cortical neurons to detect PP2C $\beta$**

*In embryonic cortical neuronal culture PP2C $\beta$  was detected as a single band migrating at  $\sim$ 45 kDa molecular weight. Using the 2ndary antibody from Amersham allowed detection of a single specific band without generation of unspecific bands. Respectively, controls without the 1. AB were performed on the same blots as used for incubation with the 1. AB.*

### *B) Immunocytochemistry on PP2C $\beta$ in embryonic cortical neurons*

PP2C $\beta$  immunocytochemistry revealed that PP2C $\beta$  was localized in the cytosol but not in the nucleus (Fig. 23). Since Bad has been described to be localized in the cytosol, as well, these two enzymes could very possibly interact with each other.

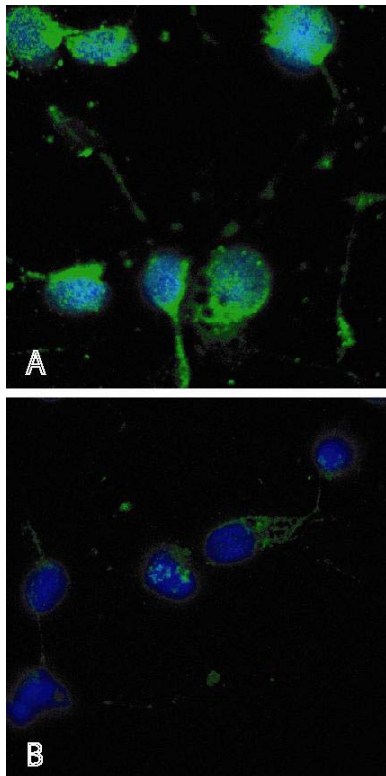


**Figure 23: Detection of PP2C $\beta$  in embryonic cortical neurons by immunocytochemistry**

*Embryonic cortical neurons growing in cell culture were immuno-stained with (A) and without (B) primary antibody. PP2C $\beta$  is localized in the cytosol of neurons and not in the nucleus (stained by Hoechst 33258).*

### **3.3.2. Treatment of cultured rat neurons with oleic acid**

#### **3.3.2.1. Influence of B27 supplement on damaging effects of oleic acid**

Oleic acid has been shown to induce apoptosis in cultured chick neurons in a dose-dependent manner; treating chick neurons with oleic acid in Dulbecco's Eagle medium without serum in concentrations  $\geq 100 \mu\text{M}$  has been shown to significantly increase the number of apoptotic neurons in culture (Klumpp et al., 2002). In this study, when treating either rat embryonic cortical or neonatal hippocampal neurons with oleic acid/0.1 % DMSO in Neurobasal culture medium with B27 in concentrations up to  $200 \mu\text{M}$ , neither could any morphological damage be observed under light microscopy nor a significant increase in apoptotic nuclei of neurons under fluorescence microscopy (Fig. 24, 25 26A). By using fresh aliquots of oleic acid which

had been stored under nitrogen/CO<sub>2</sub> at -70°C, the possibility was excluded that light- and air-sensitive oleic acid was deteriorated before use. Therefore, the lack of damage by oleic acid on cultured rat neurons could not be explained by the instability and oxidizability of oleic acid.

To identify components of the culture medium which might inhibit the damaging effect of oleic acid, three different culture media were tested which had the same basic Neurobasal media composition but differed in the added supplements. The established protocol of culturing neurons suggested growing them in Neurobasal medium enriched with B27 supplement (NB+B27). This supplement contained, among other components, antioxidants and bovine serum albumin (BSA). In a modified protocol cultured neurons were treated with 150 μM oleic acid/0.1 % DMSO in Neurobasal medium without B27 (NB-B27) or Neurobasal medium with B27 without antioxidants supplement (NB+B27-AO) and compared to the NB+B27 group (Fig. 24, 25, 26A+B). Hoechst-33258 staining for apoptotic nuclei revealed that oleic acid in NB-B27 treatment led to a significant dose-dependent increase in apoptotic neurons at 24 h after treatment compared to the untreated control group. The number of apoptotic cells doubled after treatment with 150 μM oleic acid/0.1 % DMSO in NB-B27. Morphologically, all treated cells had damaged dendrites and showed “droplets” in the cytoplasm (Fig. 26B+C). Oleic acid treatment in NB+B27 and NB+B27-AO did neither lead to morphological damage nor increased numbers of apoptotic neurons. These numbers were not significantly different from control levels of ~ 15 % apoptotic cells in neonatal hippocampal and 20 % in embryonic cortical neurons.

In all variations of Neurobasal cell culture medium oleic acid revealed solubility problems. In NB+B27 oleic acid was soluble in concentrations up to 100 μM, in NB-B27 or NB+N27-AO up to 50 μM. However, even if oleic acid was less soluble in NB-B27 compared to NB+B27, it damaged the cell significantly. Increased solubility did not correlate with increase in apoptosis.



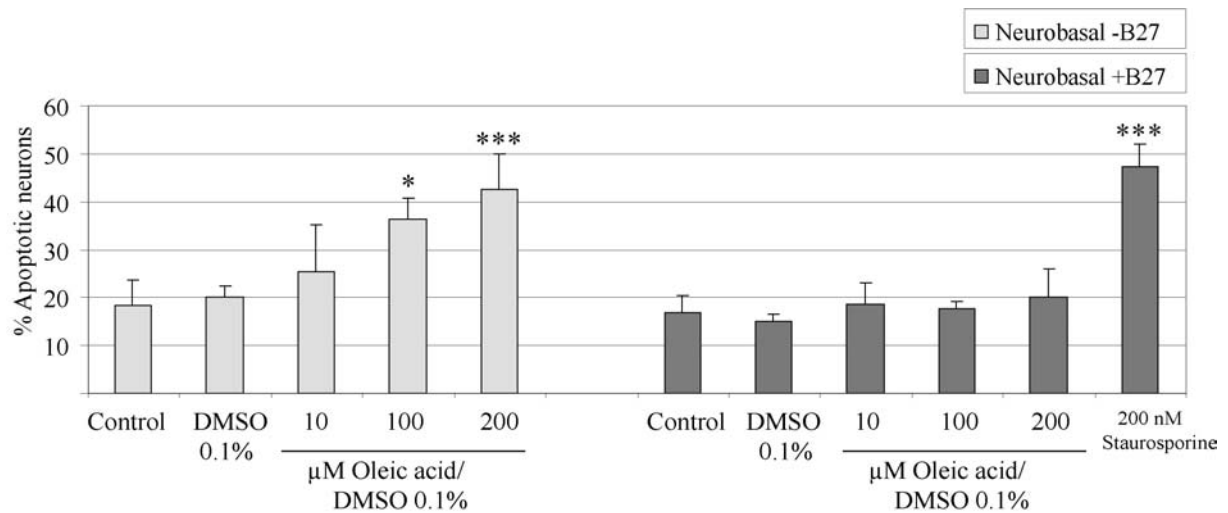


**Figure 24: The influence of B27 supplement on the induction of apoptosis by oleic acid in neonatal hippocampal neurons**

Treatment of primary hippocampal cultures with oleic acid/DMSO in NB-B27 led to a concentration-dependent increase in apoptotic neurons detected by nuclear staining. This damage was prevented when B27 was added to the culture medium. Staurosporine was used as a control apoptosis-inducing agent. (n=4)

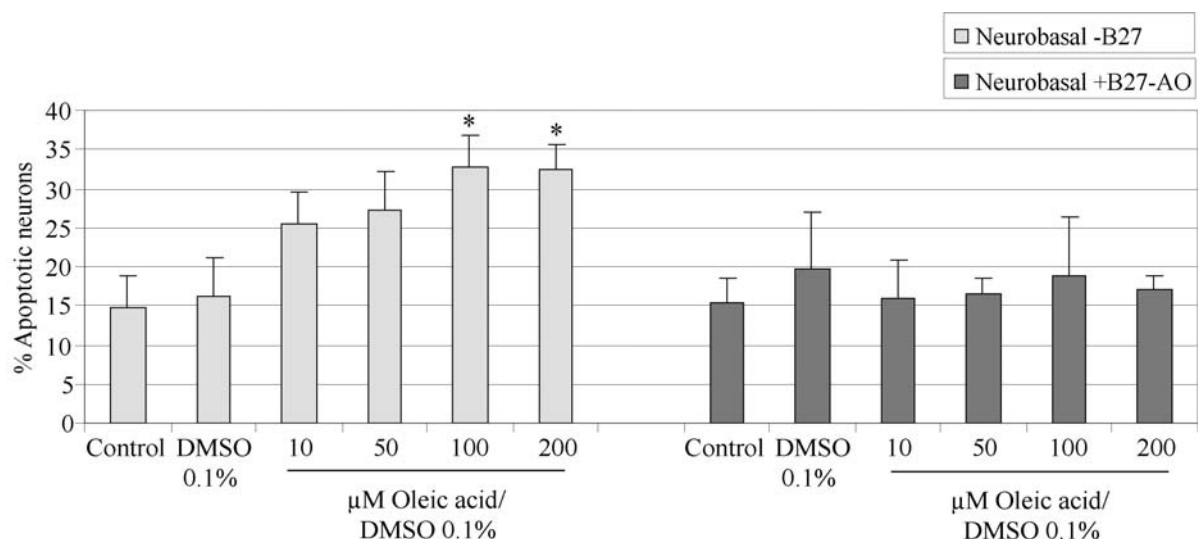


**Figure 25: Effect of B27-AO supplement on the induction of apoptosis by oleic acid in neonatal hippocampal neurons**

Treatment of primary hippocampal cultures with oleic acid/DMSO in NB-B27 led to a concentration-dependent increase of apoptotic neurons detected by Hoechst 33258-staining. When B27-AO was added to the culture medium, this damage was prevented even at high concentrations of oleic acid. (n=4)

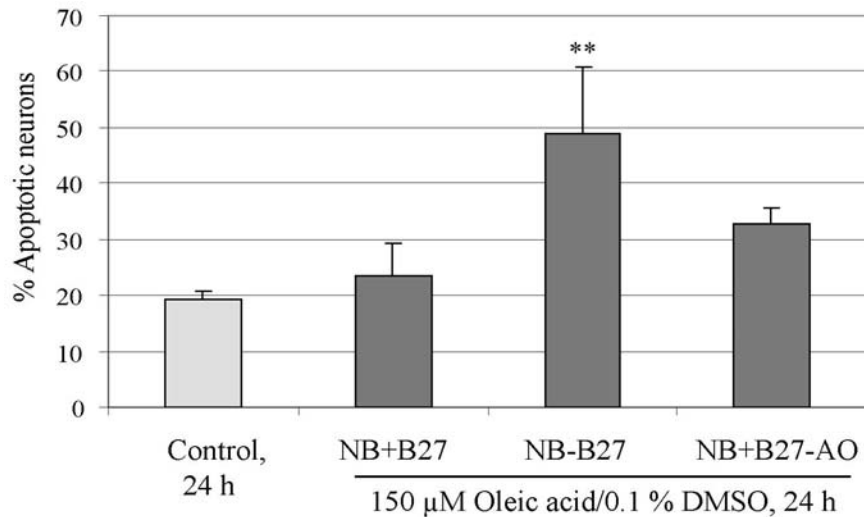


**Figure 26A: Effect of B27 and B27-AO supplement on the induction of apoptosis by oleic acid in embryonic cortical neurons**

A significant increase in apoptotic neurons, detected by Hoechst-33258-staining, was induced in primary cultures of embryonic cortical neurons at 24 h after treatment with oleic acid/DMSO in NB-B27. When B27-AO or B27 were added to the culture medium, this damage was inhibited. (n=2-4)

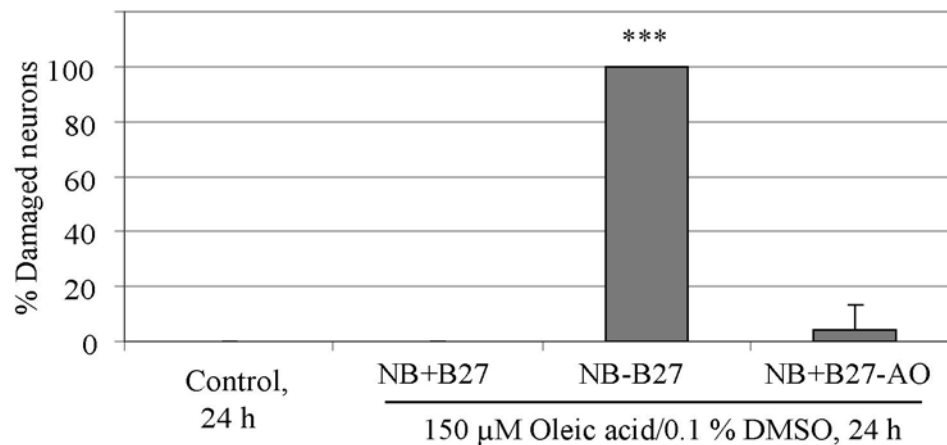


**Figure 26B: Effect of B27 and B27-AO supplement on morphological damage by oleic acid in embryonic cortical neurons**

At 24 h after treatment with oleic acid/DMSO in NB-B27, 100 % of embryonic cortical neurons showed features of damage. This damage was prevented by B27-AO or B27 supplements in the culture medium. Only neurons with both destroyed dendrites and droplets in the cytosol were counted damaged cells. (n=2-4)

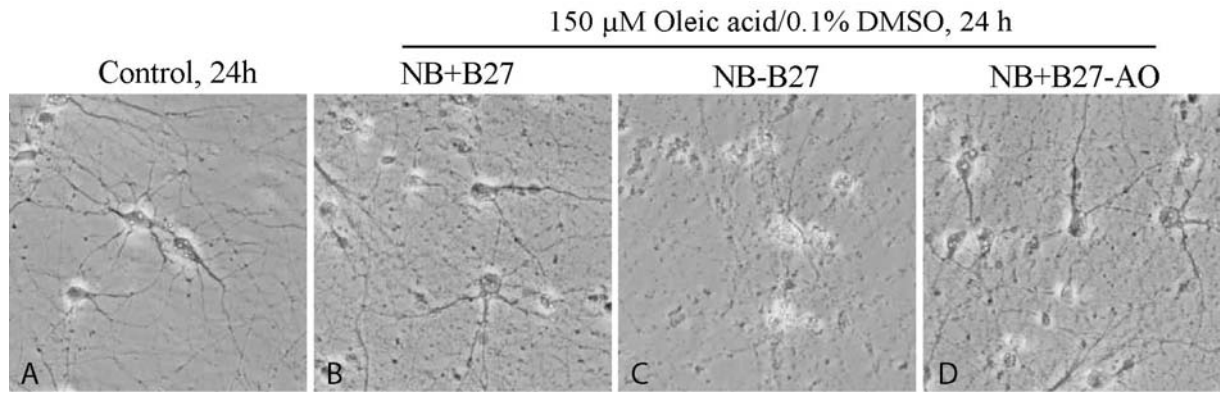


**Figure 26C: Morphology of embryonic cortical neurons after oleic acid treatment: Effect of B27 and B27-AO on damage by oleic acid**

At 24h after treatment with oleic acid/DMSO in NB-B27, embryonic cortical neurons showed features of damage like destroyed dendrites and droplets in the cytosol (C). This damage was prevented when B27-AO or B27 was added to the culture medium (B, D) and could not be found in the control group either (A).

### ***3.3.2.2 Influence of BSA or $\beta$ -cyclodextrin on solubility of oleic acid and its damaging effect***

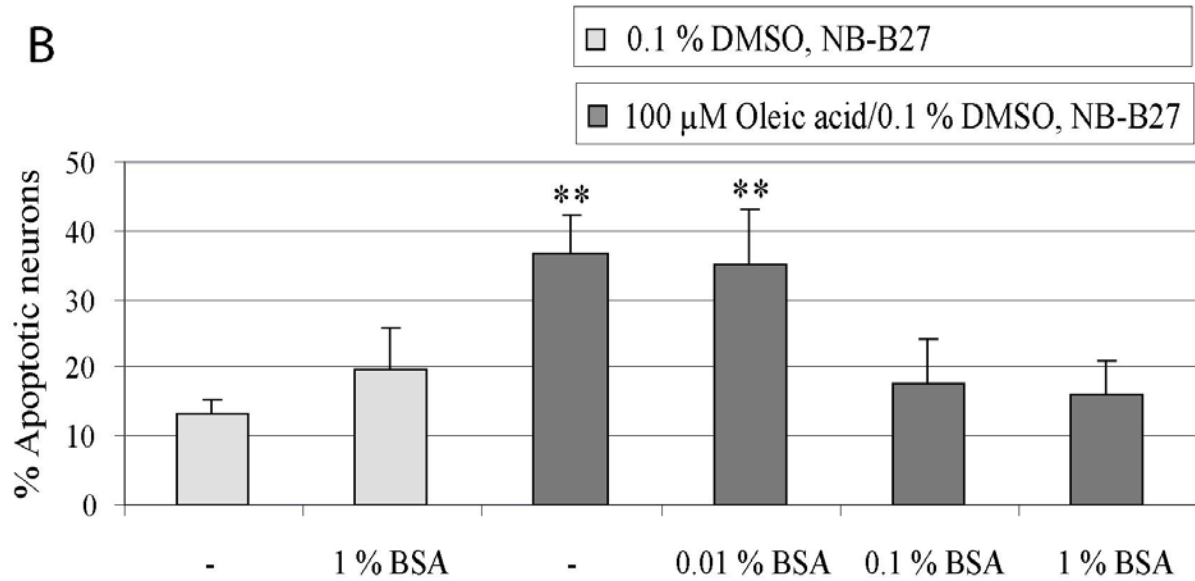
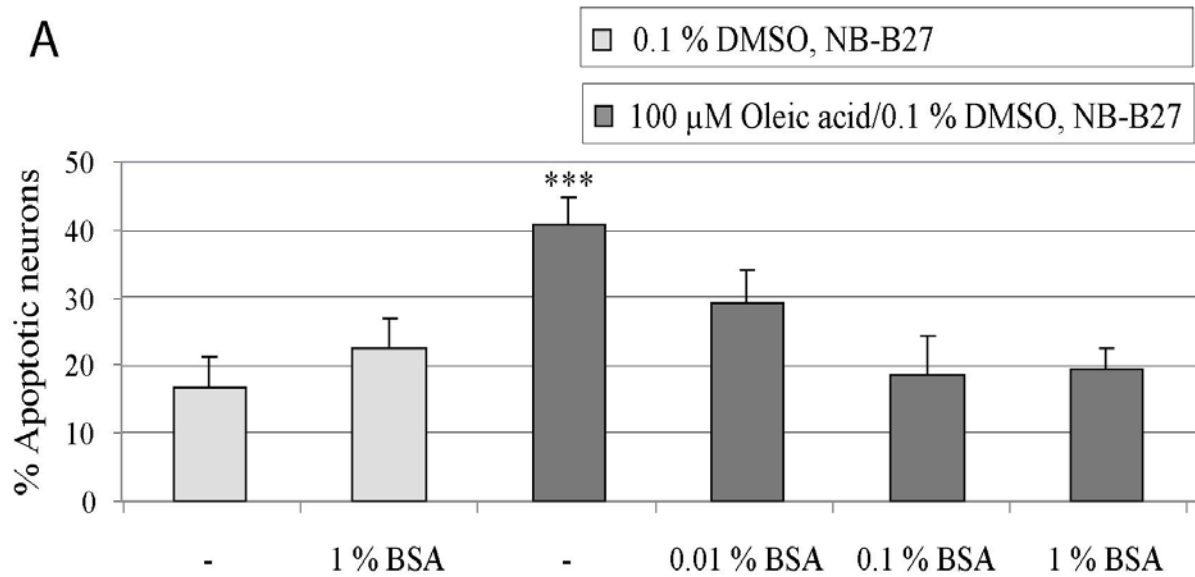
Oleic acid was soluble in Neurobasal without B27 in concentrations up to 50  $\mu$ M/0.1 % DMSO. Higher concentrations revealed visible particles of oleic acid in the culture medium. Although oleic acid significantly damaged neurons while it was not fully solved, approaches were made to increase the solubility of oleic acid in order to have a defined concentration of oleic acid in the culture medium. The options were to either increase the concentration of DMSO or to add some ingredient to improve the solubility of oleic acid. Since DMSO was known to have antioxidative properties which might affect the damage by oleic acid, the DMSO concentration of 0.1 % was not to be altered. Therefore, two different substances were tested improve the solubility of oleic acid:

- a) BSA, which is known to bind oleic acid and, thus, to increase its solubility and
- b)  $\beta$ -cyclodextrin, which is able to hold oleic acid in its hydrophobic cavity and, therefore, allows keeping very high concentrations of oleic acid in solution.

#### *a) Treatment with oleic acid + BSA*

BSA, bovine serum albumin, was dissolved in NB-B27 to concentrations of 0.01 %, 0.1 % and 1 %. These media were used to prepare solutions of 100  $\mu$ M oleic acid/ 0.1% DMSO. Although the damage by 100  $\mu$ M oleic acid was not as severe as after treatment with 150  $\mu$ M oleic acid which had been chosen as the optimal concentration, 100  $\mu$ M oleic acid was used for this experiment to potentially allow a full solution of oleic acid. The media were examined under a light microscope which revealed that oleic acid was only fully soluble in the medium containing 1 % BSA. At lower concentrations of BSA or in medium without BSA, particles of insoluble oleic acid were evident in the media.

Neonatal hippocampal and embryonic cortical neurons were treated with 100  $\mu$ M oleic acid/0.1 % DMSO in NB-B27 containing different concentrations of BSA. After 24 h, neurons were morphologically examined and stained with Hoechst-33258 to detect apoptotic nuclei. In medium containing BSA concentrations higher than 0.1 %, neither was neuronal damage by oleic acid observed morphologically (Fig. 28), nor did the number of apoptotic neurons increase significantly (Fig. 27A+B). It was not possible to find a concentration of BSA that would fully dissolve 100  $\mu$ M oleic acid/0.1 % DMSO and yet allow it to damage the neurons.



**Figures 27A+B: Effect of BSA on the induction of apoptosis by oleic acid in cultured neurons**

Increasing concentrations of BSA in culture medium blocked the apoptosis-inducing effect of oleic acid. The effect was lost at BSA-concentrations >0.1 %. An increase in solubility correlated with a loss of damage in neurons of primary neonatal hippocampal (A, n=4) or embryonic cortical cultures (B, n=5).

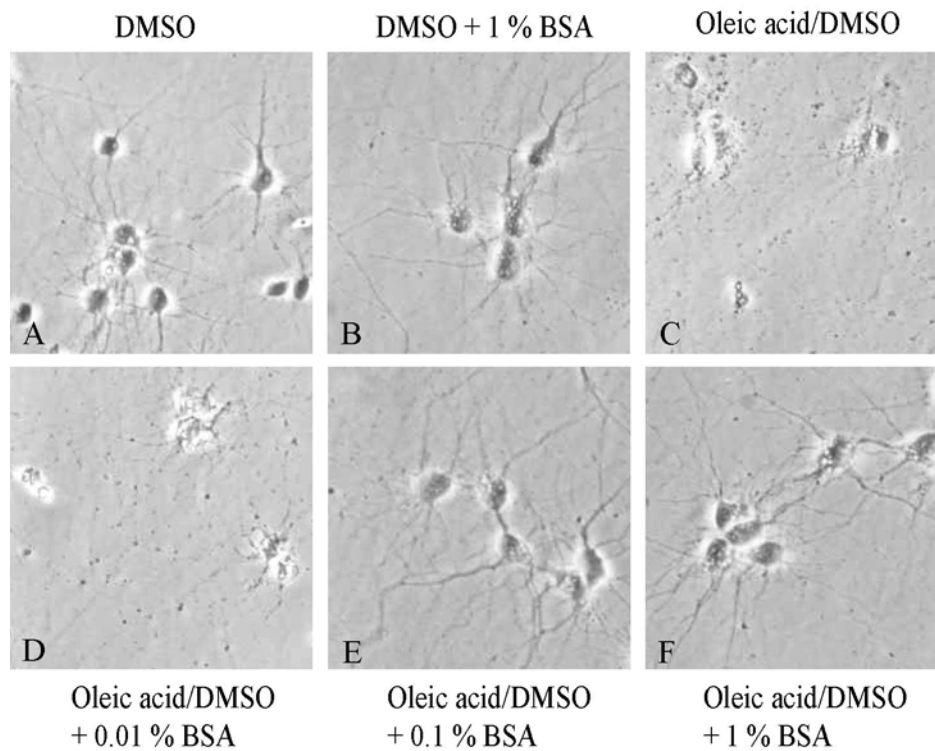


**Figure 28: Morphology of cultured embryonic cortical neurons showing the effect of BSA on neuronal damage by oleic acid**

BSA concentrations > 0.1 % blocked morphologically detectable damage induced by 100  $\mu$ M oleic acid/0.1 % DMSO in NB-B27 (E, F). An increase in solubility correlated with a loss of damage in embryonic cortical neurons. Neurons display features of damage like destruction of dendrites and "lipid droplets" in the cytosol after treatment with oleic acid/DMSO in medium without BSA or 0.01 % BSA (C, D). DMSO-treated controls in medium with or without BSA (A, B) and neurons treated with oleic acid/DMSO in medium containing either 0.1 % BSA or 1 % BSA appear undamaged.

*c) Treatment with oleic acid in  $\beta$ -cyclodextrin*

The application of oleic acid in cyclodextrin provided the advantage that oleic acid was soluble at higher concentrations than when the increase of solubility was mediated by DMSO. Embryonic cortical and primary hippocampal neurons growing in primary cultures were treated with oleic acid/ $\beta$ -cyclodextrin adding various amounts of a stock solution to NB+B27 (->2.5.11). By adding cyclodextrin the same concentration of cyclodextrin as in the group with the highest concentration of oleic acid /  $\beta$ -cyclodextrin was maintained in all groups. The

ratio of oleic acid to cyclodextrin in the stock remained unaltered at 10 mg oleic acid in 330 mg  $\beta$ -cyclodextrin as provided by the supplier.

Concentrations lower than 100  $\mu$ M oleic acid/0.0093 % cyclodextrin than did not damage embryonic cortical neurons as shown by Hoechst-33258 staining and even this concentration did only allow induction of apoptosis to a percentage of ~35 % (Fig. 29). Repetitions of this experiment showed that reproducible, significant induction of apoptosis in neurons was not possible with 100  $\mu$ M oleic acid. Since there were no solubility restrictions for oleic acid, a higher concentration of oleic acid (200  $\mu$ M) was used to increase the damage which resulted in a correlating cyclodextrin concentration of 0.0186 %. Unfortunately, increasing the concentration to 0.0186 % cyclodextrin induced apoptosis in cultured neurons. This damage proved to be independent of its combination with oleic acid (Fig. 30). Apoptosis was confirmed by correlating increase in activation of caspase-3.

The same effect was seen in neonatal hippocampal neurons: There was no significant difference between the percentage of apoptotic neurons after 200  $\mu$ M oleic acid /0.0186 % cyclodextrin treatment and the percentage after treatment with 0.0186 % cyclodextrin (Fig. 31A). Both induced apoptosis in a time-dependent manner as detected by Hoechst-33258 staining of cell nuclei and Western blotting of caspase-3 (Fig. 32). The number of apoptotic neurons did not significantly increase with increasing concentrations of oleic acid. However, the total number of neurons gradually decreased (Fig. 31B); damaged cells were floating in the medium and were therefore not countable. It could not be determined how many of these floating cells were apoptotic.

In both primary cultures the dramatic increase in apoptotic neurons occurred between 18 h and 24 h after treatment (Fig. 30, 33). Since high concentrations of cyclodextrin revealed a toxic effect of its own and because weak induction of apoptosis at lower concentrations of oleic acid/cyclodextrin revealed no advantages in comparison with oleic acid/DMSO treatment, cyclodextrin experiments were not further continued.  $\beta$ -Cyclodextrin, in concentrations associated with the amount of oleic acid necessary to induce apoptosis itself, induced apoptosis in embryonic cortical and neonatal hippocampal neurons.

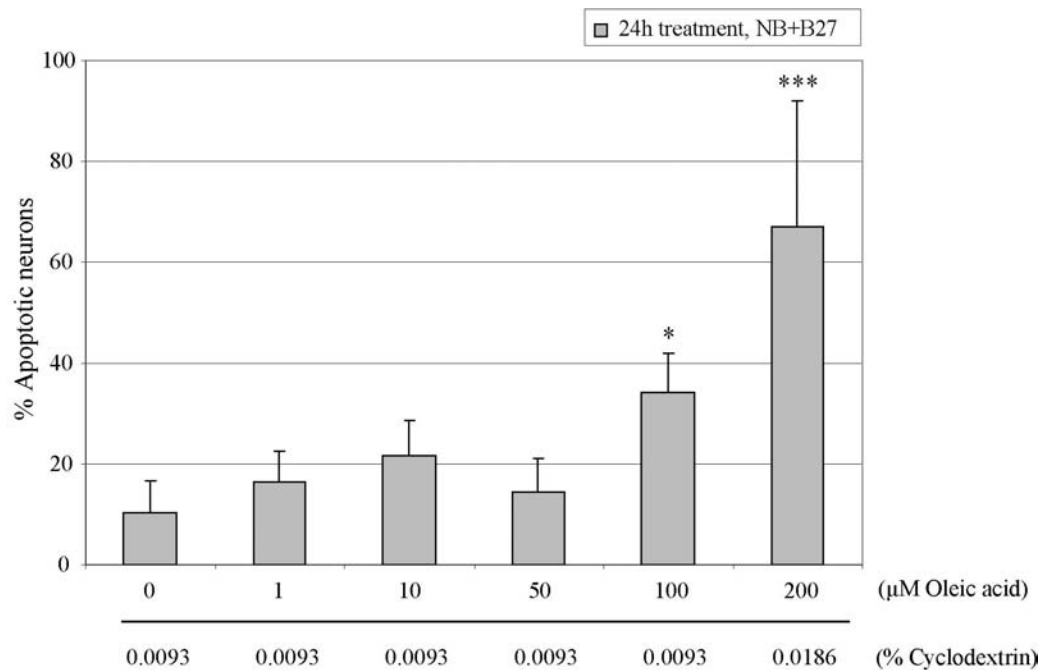


**Figure 29: Effect of oleic acid/cyclodextrin embryonic cortical neurons**

At 24 h, the number of apoptotic neurons was only significantly increased after treatment with 100 μM oleic acid/0.0093 % cyclodextrin or higher concentrations. When the concentration of oleic acid/cyclodextrin was doubled to 200 μM /0.0186 %, a dramatic increase in apoptotic cells could be observed. (n=8)

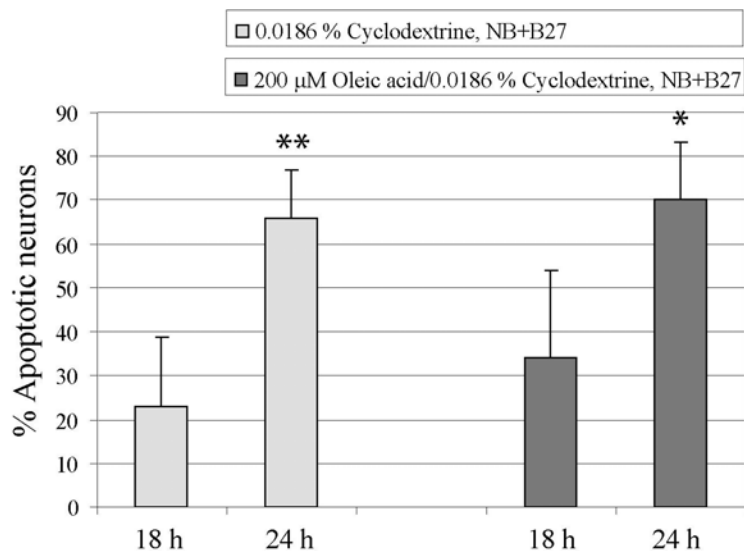


**Figure 30: Effect of cyclodextrin on embryonic cortical neurons**

At 24 h after treatment, cyclodextrin treatment alone induced the same dramatic increase in apoptotic neurons as treatment with oleic acid /cyclodextrin. There was no significant difference in the induction of apoptosis between these two groups. (n=5)



A

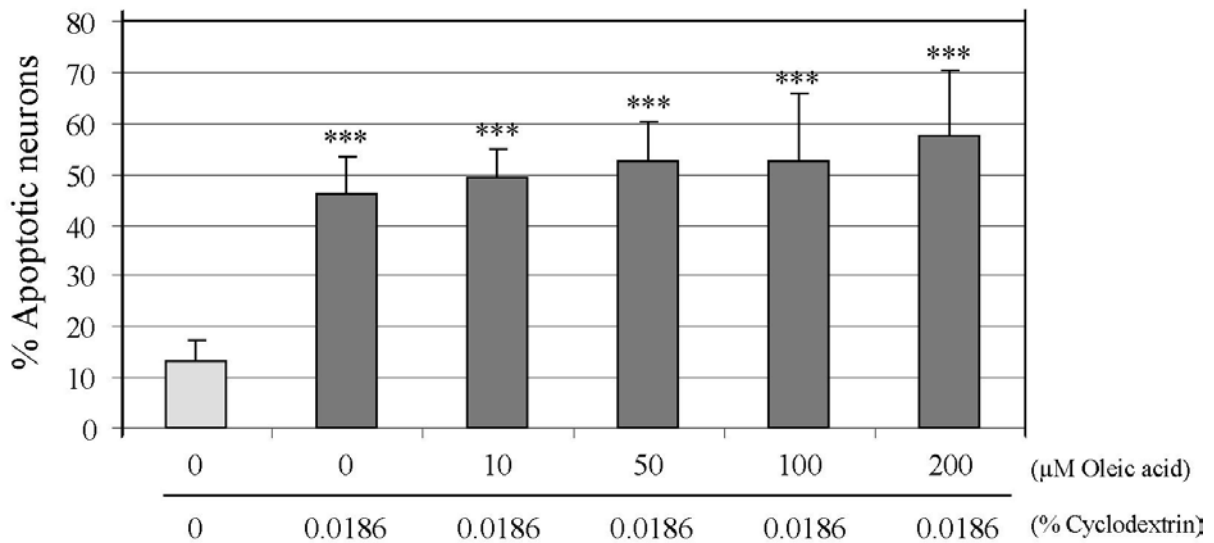


**Figure 31A: Effect of cyclodextrin on neonatal hippocampal neurons**

24 h treatment with 0.0186 % cyclodextrin increased the number of apoptotic neurons significantly.

The combination with oleic acid did not further exacerbate the damage. (n=4)

B

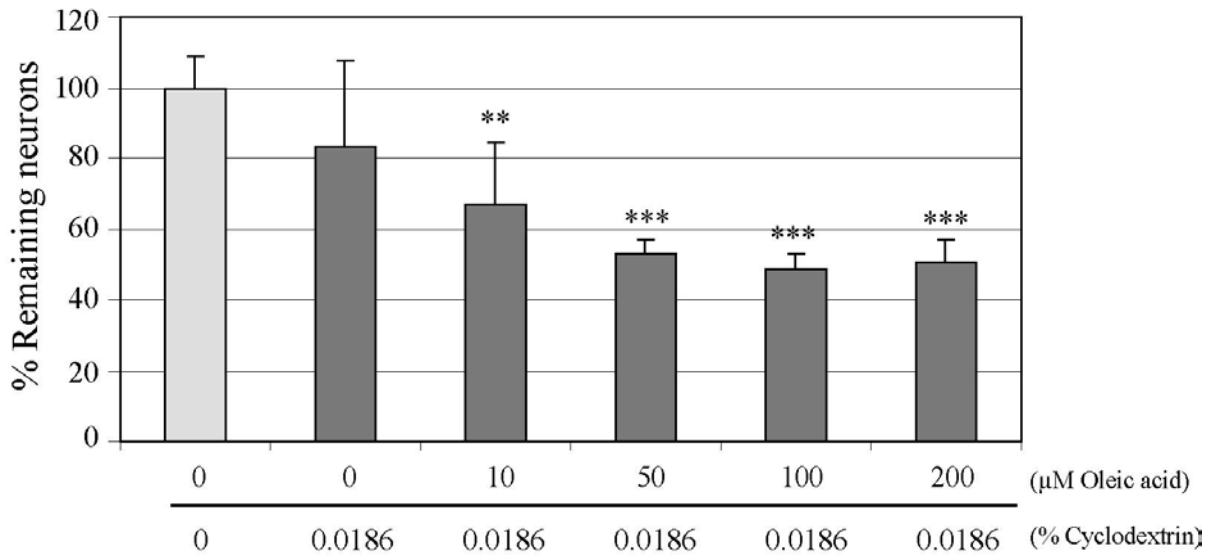


**Figure 31B: Effect of oleic acid/cyclodextrin on neonatal hippocampal neurons**

Increasing concentrations of oleic acid in combination with cyclodextrin reduced the number of remaining neurons growing in the Petri dishes. Cyclodextrin alone did not significantly reduce the number. (n=4)

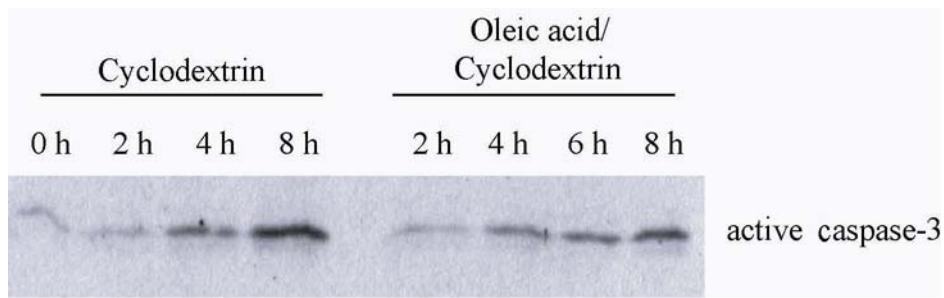


**Figure 32:** Western blot showing activation of caspase-3 in samples of primary hippocampal cultures after treatment with oleic acid/cyclodextrin and cyclodextrin alone. Treatment with 200  $\mu$ M oleic acid/ 0.0186 % cyclodextrin and 0.0186 % cyclodextrin alone both induced the cleavage of caspase-3 into its active form (at  $\sim$  20 kDa). The total amount of caspase-3 protein remained constant (not shown), while active caspase-3 increased in a time-dependent fashion in both oleic acid/cyclodextrin treated and cyclodextrin treated cells.

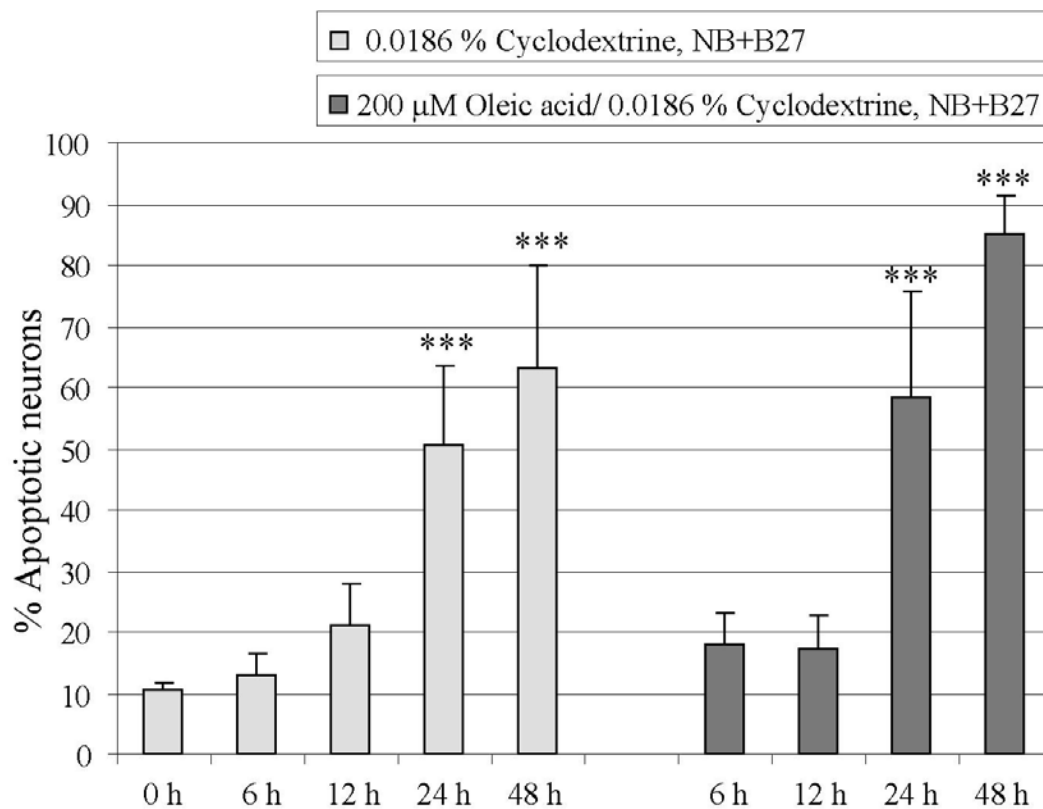


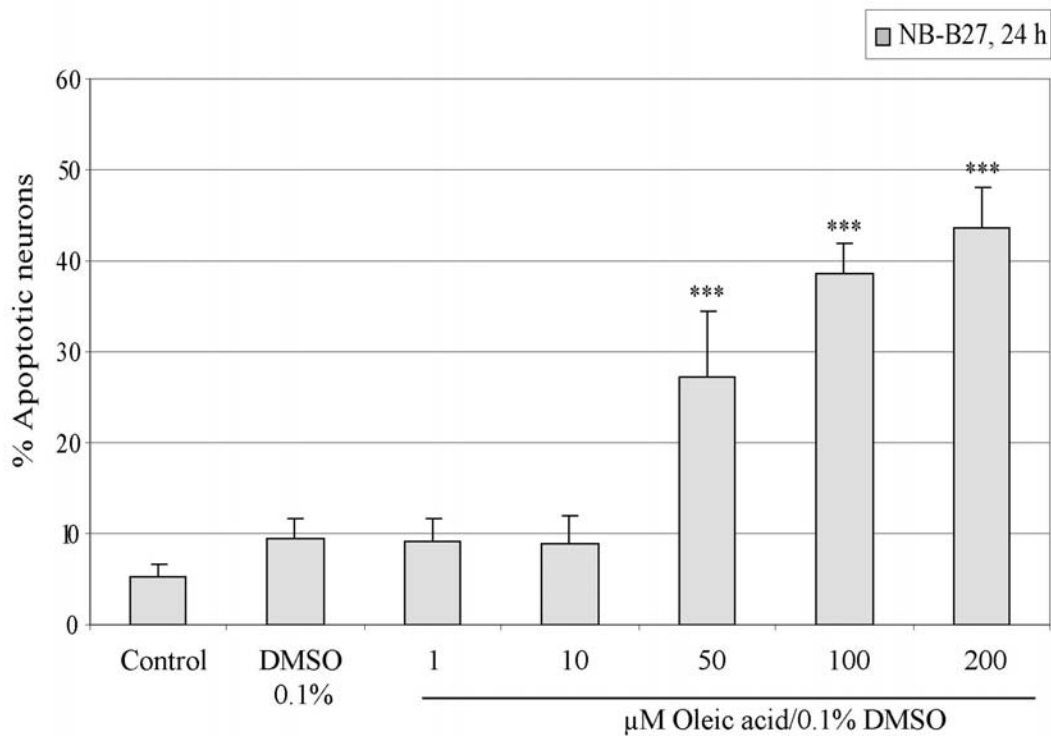
**Figure 33:** Time-dependent induction of apoptosis by oleic acid/cyclodextrin and cyclodextrin in neonatal hippocampal neurons

*Apoptotic nuclei count after Hoechst-33258 staining revealed the deleterious effect of both  $\beta$ -cyclodextrin and oleic acid/  $\beta$ -cyclodextrin. At 24 h and 48 h, there was a significant increase in apoptotic neurons compared to the 0 h control group. (n=5)*

### **3.3.2.3. Characterisation of neuronal damage after treatment of primary cultures with oleic acid/ DMSO in NB-B27**

After establishing oleic acid treatment in neurobasal medium without B27 which significantly induced apoptosis in neuronal culture (->2.3.2.2.), and after clarifying that neither BSA nor  $\beta$ -cyclodextrin were the appropriate tools to dissolve oleic acid in the cell culture medium, concentration- and time-dependent induction of apoptosis were examined in cultured neonatal hippocampal and embryonic cortical neurons. In both primary cultures it was observed that oleic acid treatment increased the number of apoptotic neurons in a concentration- (Fig. 34A, 36A) and time-dependant manner (Fig. 35A, 36B). Oleic acid 150  $\mu$ M/DMSO 0.1 % led to an increased of apoptotic neurons from control level of 10-20 % (DMSO-treated cultures) to 35-40 % after 24 h treatment and up to 80 % after 48 h treatment. In embryonic cortical neurons time- and concentration-dependant the morphological changes of neurons were examined, as well. While the formation of “lipid droplets” could be observed as early as 3 h after onset of treatment with 150  $\mu$ M oleic acid/0.1 % DMSO, destroyed dendrites and a significant increase in apoptotic nuclei could be observed as early as 12 h (Fig. 35B). At 24 h after treatment with different concentrations of oleic acid, cortical neurons showed the formation of vesicles in the cytosol at concentrations of 10  $\mu$ M; at 100  $\mu$ M oleic the dendrites were severely damaged (Fig. 34B).

A



B

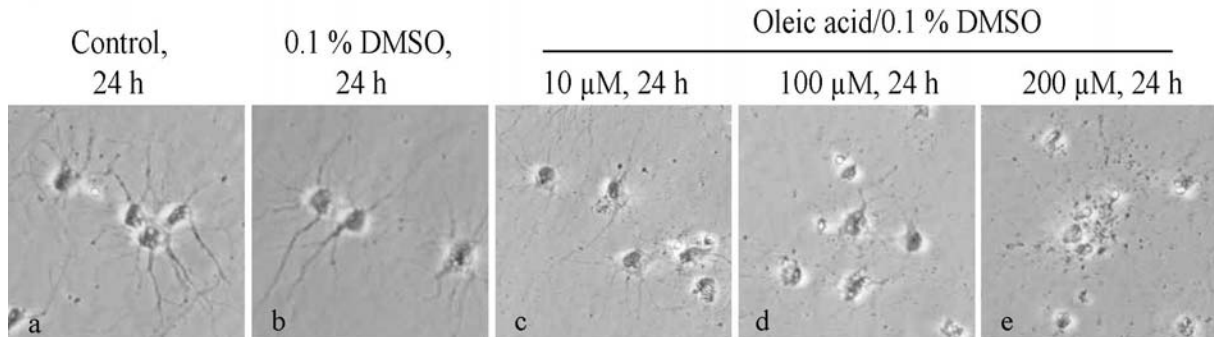


**Figure 34A+B: Concentration-dependency of damage to embryonic cortical neurons by oleic acid/0.1 % DMSO in Neurobasal medium without B27.**

At 24 h, oleic acid in concentrations higher than 50  $\mu\text{M}$  /0.1 % DMSO significantly induced apoptosis as shown by Hoechst-33258 staining (A). Morphological observation under light microscope (B) revealed lipid droplets in the cytosol at much lower concentrations (10  $\mu\text{M}$  oleic acid) (c); at concentrations of 100  $\mu\text{M}$  oleic acid and higher, all neurons additionally showed loss of dendrites. (d, e). Neurons treated with 0.1 % DMSO showed healthy, undamaged neurons (b) like non-treated neurons (a). (n=5)

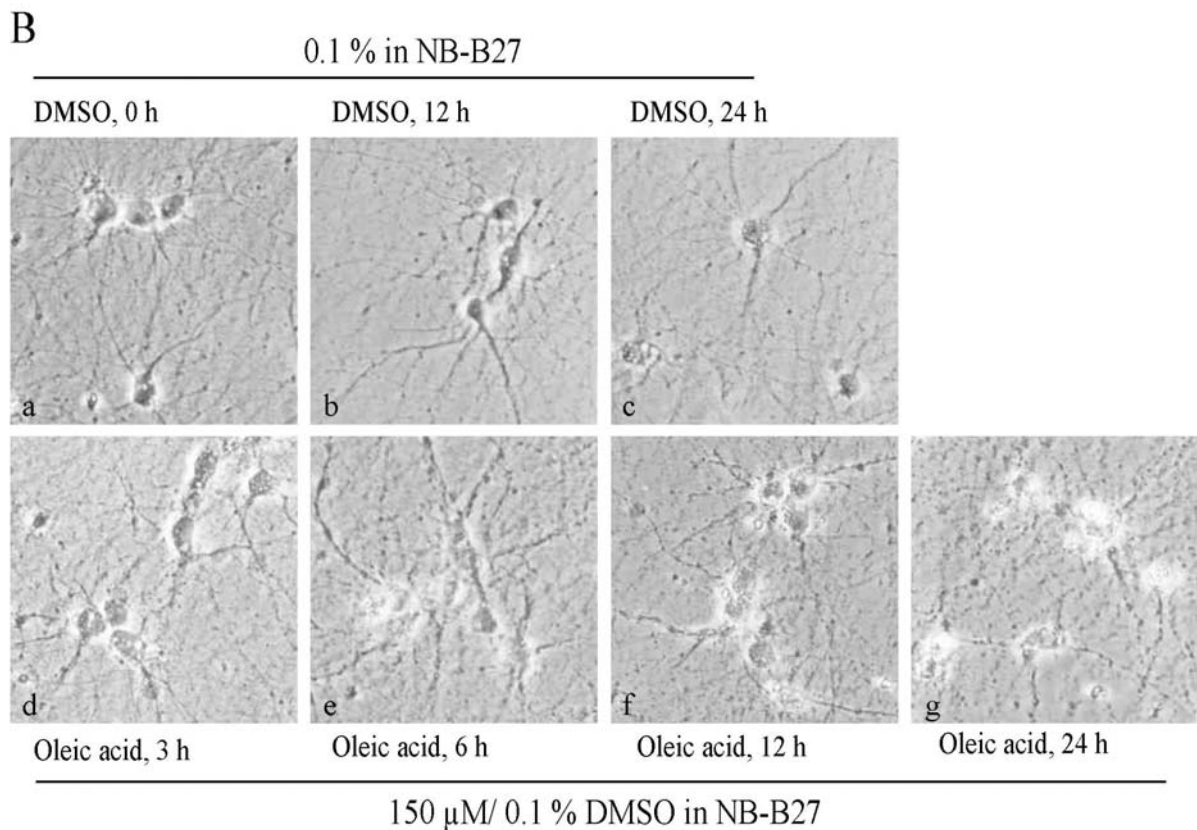
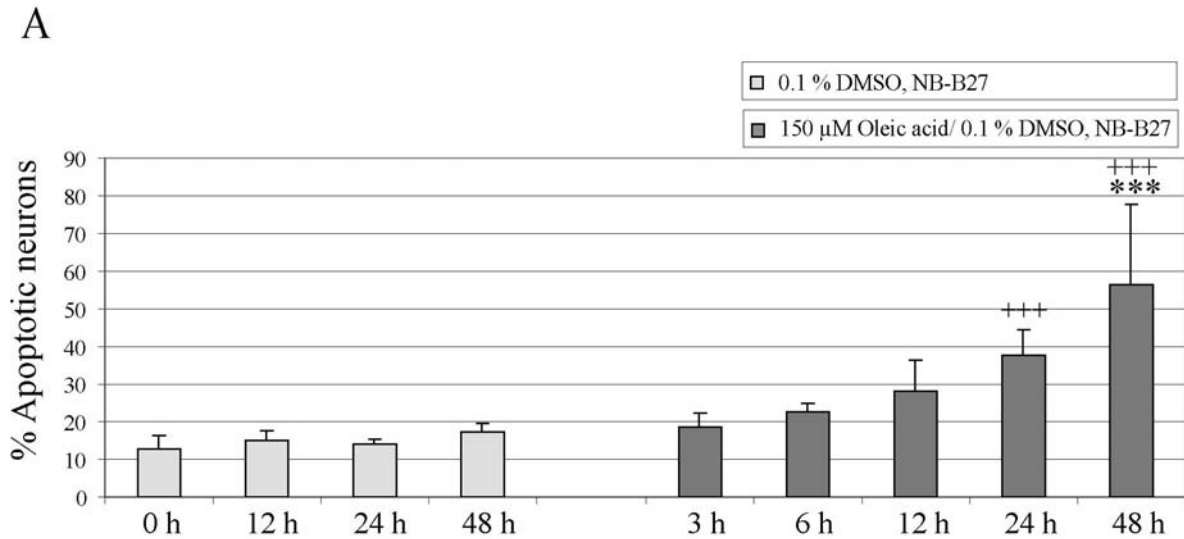
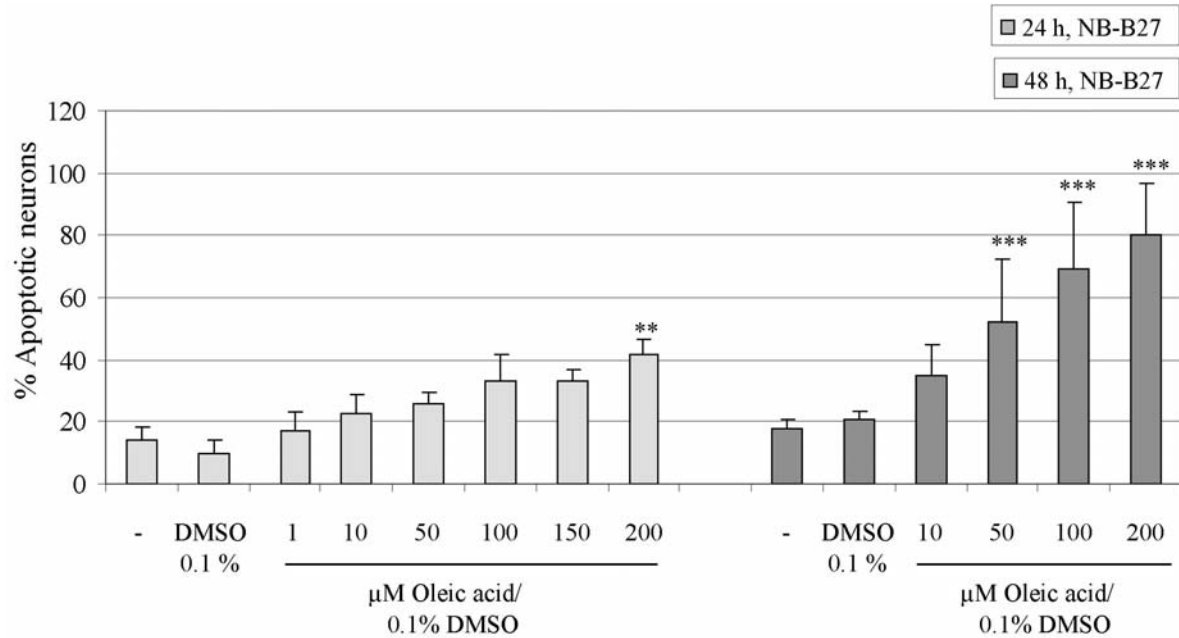


**Figure 35A+B: Time-dependency of damage by oleic acid/0.1 % DMSO in Neurobasal without B27 medium in embryonic cortical neurons**

*Treatment with 150  $\mu$ M oleic acid/ 0.1 % DMSO significantly induced apoptosis in cortical neurons, as detected nuclear staining, as early as 24 h (A, n=4). Morphological observations under a light microscope showed vesicles in the cytosol of cortical neurons as early as 3 h after treatment (B). At 12 h, some neurons showed loss of dendrites (f) which increased up to 24 h when most of the dendrites were fragmented or dissolved (g). Until 48 h after treatment,*

DMSO-treated controls neither showed a significant increase in apoptotic neurons nor did they look morphologically damaged (a-c).

**A**



**B**

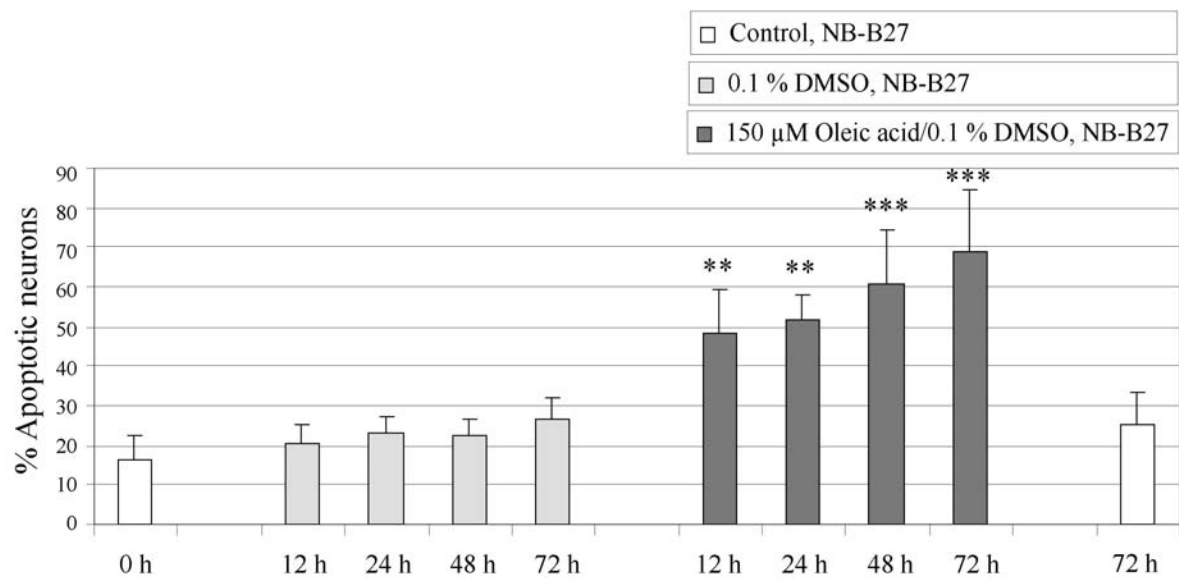


**Figure 36A:** Concentration-dependent induction of apoptosis in neonatal hippocampal neurons by oleic acid in NB-B27 (n=4-6)

**Figure 36B:** Time-dependent induction of apoptosis in neonatal hippocampal neurons by oleic acid in NB-B27 (n=6)

### 3.3.3. Nile blue staining of embryonic cortical neurons after oleic acid treatment

Nile blue staining revealed that the droplets which could be observed after treatment with 150  $\mu$ M oleic acid/ 0.1 % DMSO in NB-B27 contained free fatty acids. Under a fluorescent microscope the droplets showed strong, red fluorescence. Neither DMSO- nor staurosporine-treated neurons showed these fatty acids-filled vesicles/droplets (Fig. 37). Both oleic acid and staurosporine showed apoptotic features after Hoechst-33258 staining as fragmented, shrunken nuclei and intense Hoechst-labelling. Droplets appeared 3 h after onset of treatment, much earlier than apoptotic nuclei, and could be observed in oleic acid treated cells only.

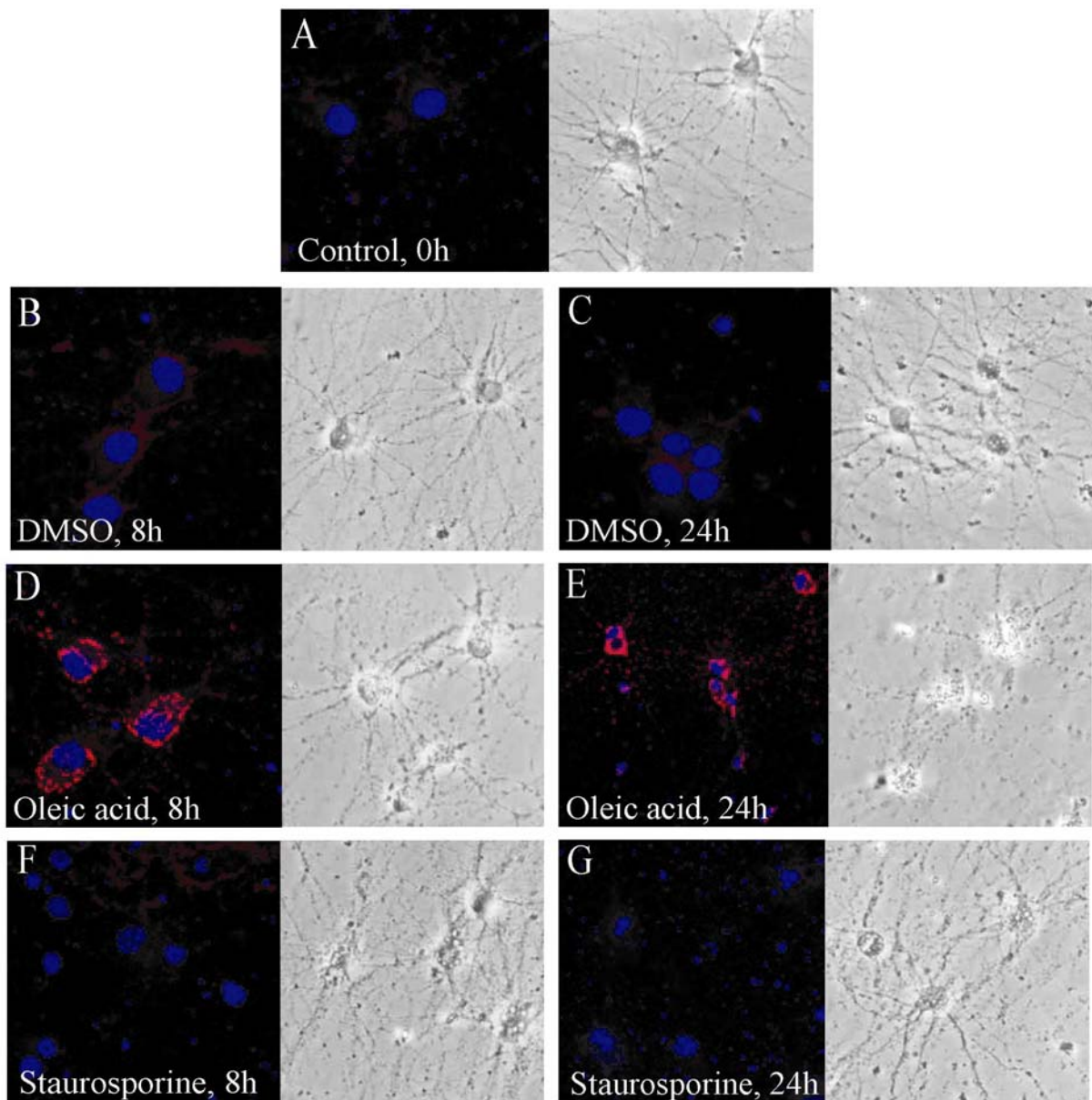


*Figure 37: Nile blue staining of embryonic cortical neurons after staurosporine and oleic acid treatment*

*Eight hours after treatment with 150  $\mu$ M oleic acid/0.1 % DMSO only few neurons showed apoptotic nuclei but all displayed lipid droplets in the cytoplasm (D). At 24 h, about 50 % of the oleic acid-treated neurons had apoptotic nuclei but 100 % revealed droplets and fully destroyed dendrites (E). Apoptosis, induced by 200 nM staurosporine/0.1 % DMSO, followed a different pattern: It was observed at 8 h (F) and 24 h (G) after treatment, while the neurons did not display lipid droplets at any time point. DMSO treatment did not induce apoptosis nor did it alter the morphology of neurons at 8 h (B) or 24 h (C) after treatment when compared with the 0 h control group (A).*

#### **3.3.4. Western blotting on Bad, Bad-155P and PP2C $\beta$ after oleic acid treatment in embryonic cortical and hippocampal cultures**

Cell extracts were prepared for Western blotting after treatment with 150  $\mu$ M oleic acid/ 0.1 % DMSO in NB-B27. Significant induction of neuronal apoptosis (~40 %) was controlled by nuclear staining of treated sister cultures. Protein samples were used for detection of Bad, Bad-155P and PP2C $\beta$ . In primary hippocampal cultures one blot each was prepared for the detection of proteins. Afterwards equal protein loading was controlled by  $\alpha$ -tubulin detection. In embryonic cortical neuronal cultures the same blot was used for all detections: Bad-155P was detected first, followed by Bad detection after stripping of the membrane. PP2C $\beta$  detection and  $\alpha$ -tubulin detection, as a control, followed using the same membrane without stripping since the remaining Bad band did not interfere with PP2C $\beta$  or  $\alpha$ -tubulin due to different molecular weights. In both primary cultures, Bad-155P protein was elevated as early as 1 h after onset of treatment, and decreased to below control level at later time points. Bad protein was slightly increased up to 3-4 h (Fig. 38, 39), however, this increase was not as pronounced as the one observed with Bad-155P. PP2C $\beta$  protein level was not altered throughout the treatment.



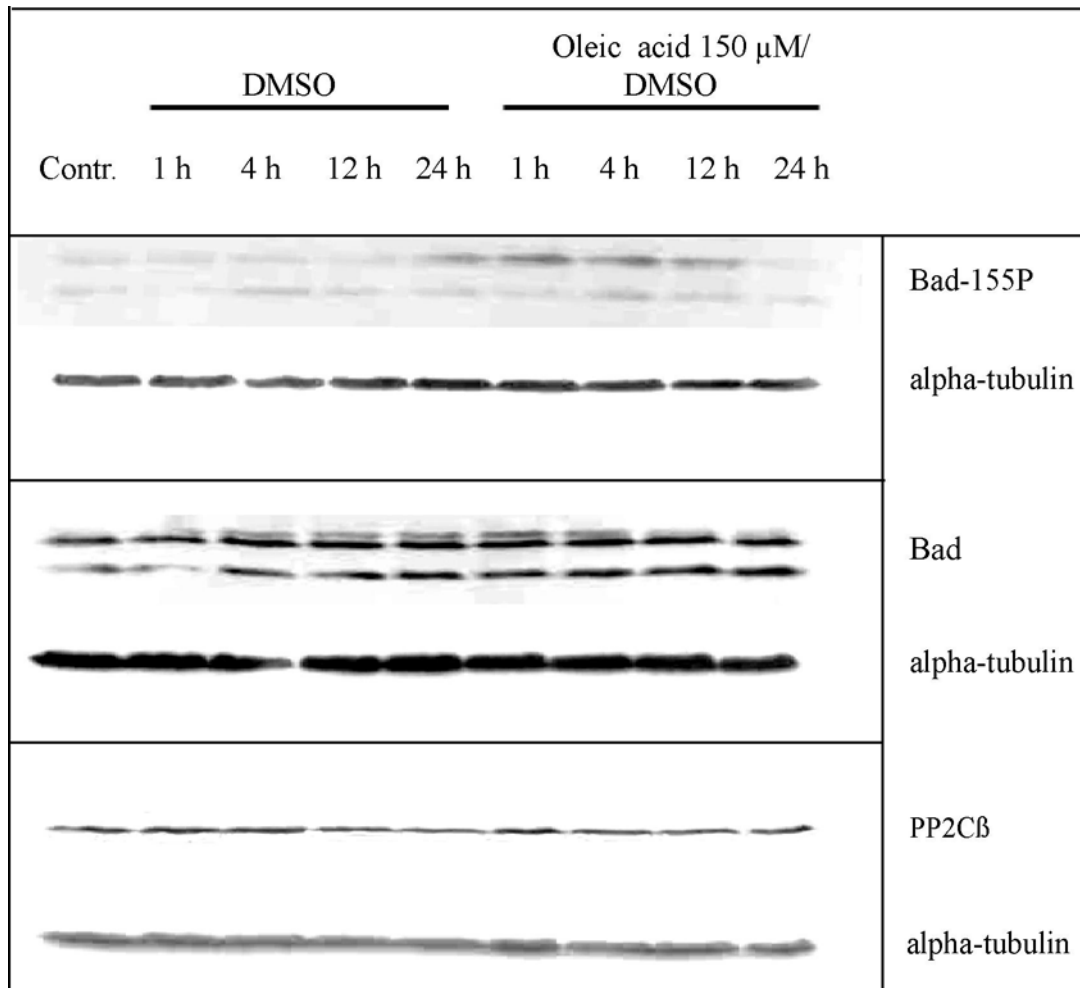


**Figure 38: Western blot detecting Bad-155P, Bad, PP2C $\beta$  and alpha-tubulin after treatment with 150  $\mu$ M oleic acid/0.1 % DMSO in samples of primary hippocampal mixed cultures**

At 1 h after treatment of primary hippocampal cultures with 150  $\mu$ M oleic acid/0.1 % DMSO in NB-B27, by Western blotting Bad-155P protein was observed to be strongly increased compared to 0 h control and decreased gradually, afterwards, until it fell under control level at 24 h. Bad was slightly increased at 1 h and 4 h, PP2C $\beta$  remained unaltered at all time points. Bad-155P, as well as Bad, slightly increased up to 24 h in cell extracts treated with 0.1 % DMSO in NB-B27 as controls. PP2C $\beta$  protein level remained constant in all treated and untreated cells at all time points.

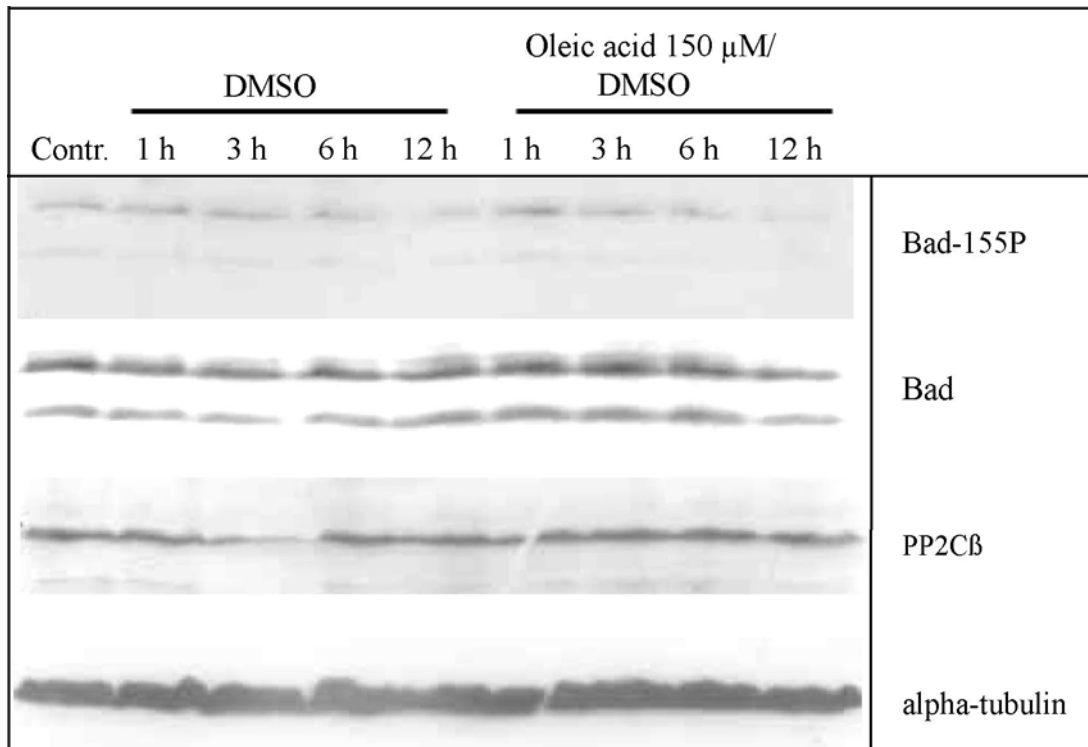


**Figure 39: Western blot detecting Bad-155P, Bad, PP2C $\beta$ , and alpha-tubulin in protein extracts of cultured embryonic cortical neurons after treatment with 150  $\mu$ M oleic acid/0.1 % DMSO**

*In embryonic cortical culture, Bad-155P protein was increased at 1 h compared to 0 h control after treatment with 150  $\mu$ M oleic acid/0.1 % DMSO in NB-B27 and gradually decreased under control level from 1 h to 12 h. Bad protein was slightly increased at 1 h and 3 h after treatment and returned to control level at 12 h. PP2C $\beta$  protein remained unaffected by the treatment at all time points. Bad-155P, as well as Bad and PP2C $\beta$  proteins levels remained constant in cell extracts treated with 0.1 % DMSO in NB-B27 as control at all time points.*

### 3.3.5. Apoptotic effect of ginkgolic acids in rat neuronal cultures

Ginkgolic acids, a composition of esters of ginkgolic acids, have been shown to increase PP2C activity *in vitro* and to induce apoptosis in cultured chick neurons at concentrations of 100  $\mu$ M after 24 h treatment (Ahlemeyer et al., 2001). Therefore, they fulfilled the same criteria as oleic acid to serve as a tool for the induction of apoptosis while activating PP2C which subsequently might influence Bad's phosphorylation state and therefore contribute to apoptosis. After establishing protocols to reproducibly induce apoptosis in rat embryonic

cortical and neonatal hippocampal neurons by treatment with ginkgolic acids, protein levels of Bad-155P, Bad and PP2C $\beta$  were examined by Western blotting in protein extracts of treated and untreated primary cultures to detect changes.

### ***3.3.5.1. Induction of apoptosis in rat neuronal cultures by ginkgolic acids***

Like oleic acid, ginkgolic acids proved to be almost insoluble in culture medium and had to be dissolved into a stock solution in DMSO. However, when mixing stock solution with Neurobasal culture medium with B27, concentrations of 250  $\mu$ M ginkgolic acids /0.1 % DMSO were not fully soluble.

Testing concentration-dependent induction of apoptosis by ginkgolic acids in either cultured embryonic cortical or neonatal hippocampal neurons, only concentrations  $\geq$  250  $\mu$ M ginkgolic acids/0.1 % DMSO were found to significantly increase the percentage of neurons with apoptotic nuclei at 24 h (Fig. 40, 42). Apoptotic damage could be detected as early as 24 h in both primary cultures while the DMSO-treated neurons remained at control level of  $\sim$ 15 % damage (Fig. 41, 43). While neurons appeared overall damaged under light microscope, the percentage of apoptotic cells after treatment with 250  $\mu$ M ginkgolic acids /0.1 % DMSO was unexpectedly low with 30 % in both lines of cultured neurons (Fig. 40, 42).

This raised the question whether another type of cell death like necrosis which can not be detected by nuclear staining might contribute to neuronal damage, as well. Therefore, Trypan blue staining (TB) was performed in embryonic cortical neurons, in addition to Hoechst-33258 staining, in order to examine whether apoptosis or necrosis was the predominant form of cell death after ginkgolic acids treatment. Sister cultures were used for these experiments since it was not possible to double-stain neurons with Trypan blue and Hoechst-33258. Neurons having picked up Trypan blue dye did not allow further nuclear Hoechst staining and Hoechst staining denaturalized the cells which did inhibit further TB staining. At 24 h after treatment with 250  $\mu$ M ginkgolic acids/0.1 % DMSO three times more Trypan blue-positive neurons were found in embryonic cortical cultures than neurons with apoptotic nuclei were detected by Hoechst staining (Fig. 41). While between 0 h and 24 h the percentage of apoptotic neurons remained unchanged (10 %) in the DMSO-treated control group, the value of damaged neurons doubled (18 %) as detected by Trypan blue staining. The ginkgolic treated group revealed an increase of apoptotic neurons to 32 % at 24 h while this increase could not be detected at earlier time points (6 h). The drastic increase of Trypan blue positive

neurons after ginkgolic acids treatment could already be observed at early time points and remained at this level (6 h: 84 %, 24 h: 86 %).

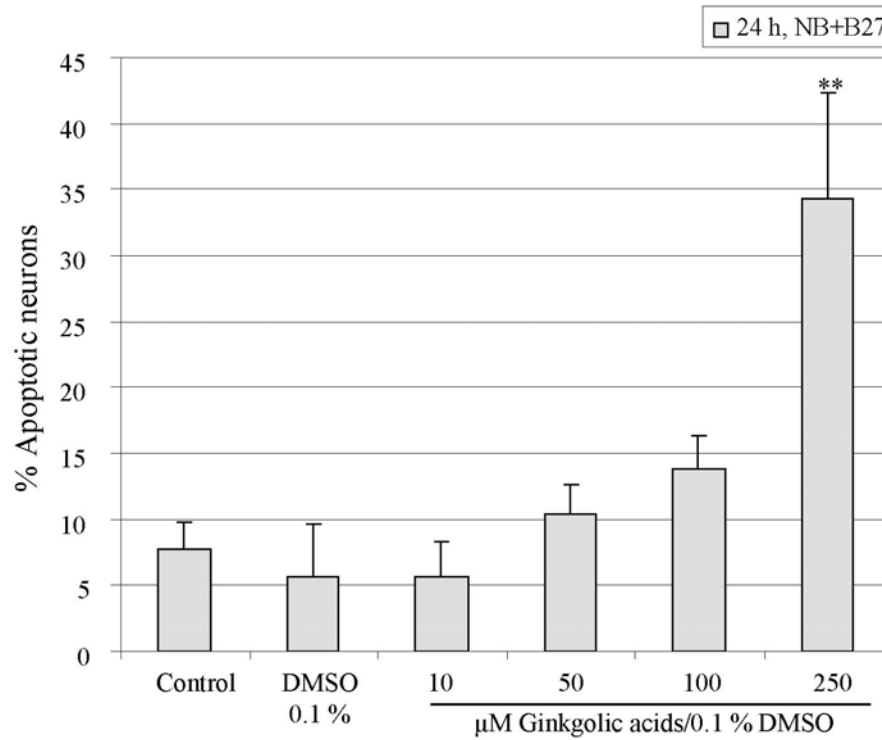


**Figure 40: Concentration-dependent induction of apoptosis in neonatal hippocampal neurons after ginkgolic acids treatment**

At 24 h hours after treatment of neonatal hippocampal neurons, significant induction of neuronal apoptosis was only observed at a concentration  $\geq 250 \mu\text{M}$  ginkgolic acids/0.1 % DMSO. Treatment with lower concentrations of ginkgolic acids did not significantly increase the percentage apoptotic neurons compared to the DMSO-treated control group. (n=4)

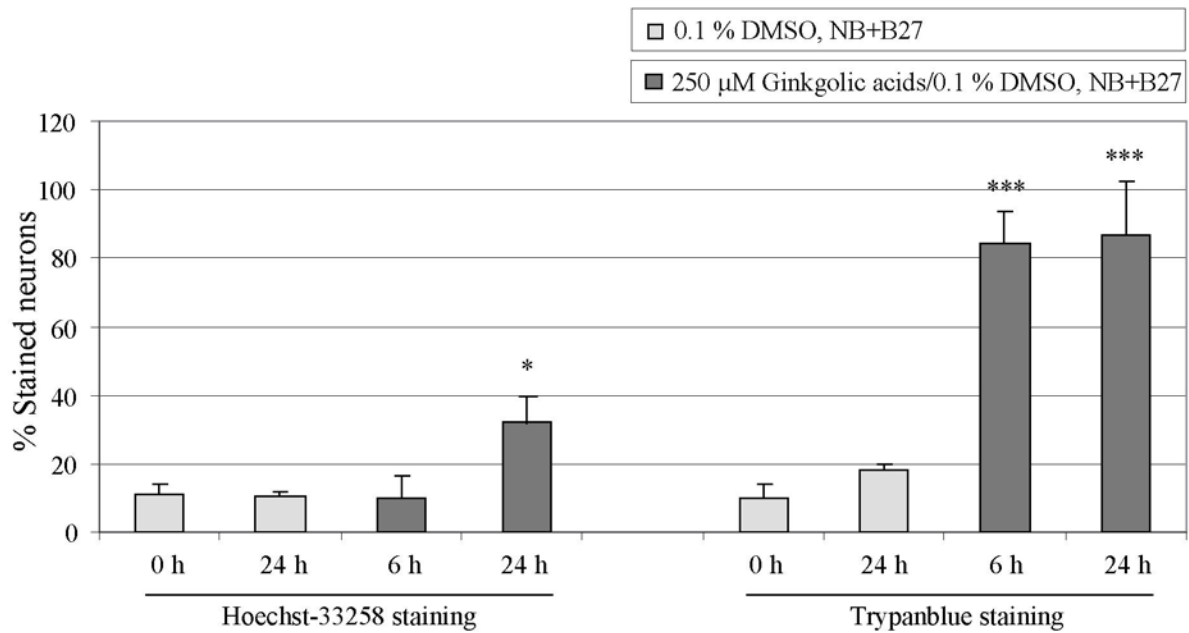


**Figure 41: Comparison of necrotic and apoptotic cell death in neonatal hippocampal neurons after ginkgolic acids treatment**

While only at 24 h after treatment with 250 μM ginkgolic acids the number of apoptotic nuclei was increased, Trypan blue (TB)-positive neurons were evident as early as 6 h in hippocampal neurons. The number of TB-stained neurons did not significantly increase from 6 h to 24 h indicating that the necrotic damage developed at early time points. (n=3-4)

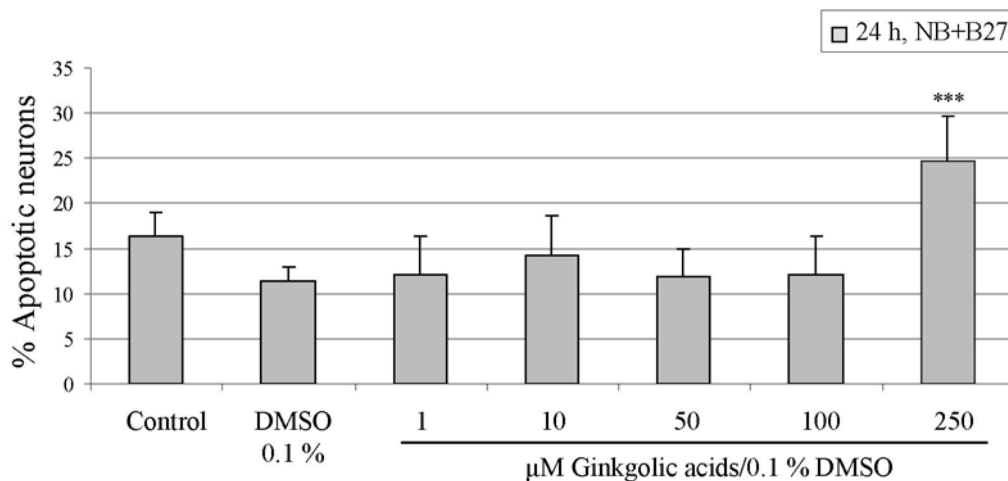


**Figure 42: Concentration-dependent induction of apoptosis after ginkgolic acids treatment in embryonic cortical neurons**

In embryonic cortical cultured neurons only treatment with 250 μM ginkgolic acids/0.1% DMSO significantly induced apoptosis at 24 h compared with DMSO-treated neurons. At lower ginkgolic acids concentrations the percentage of apoptotic neurons did not significantly differ from the percentage of DMSO-treated neurons. (n=5)

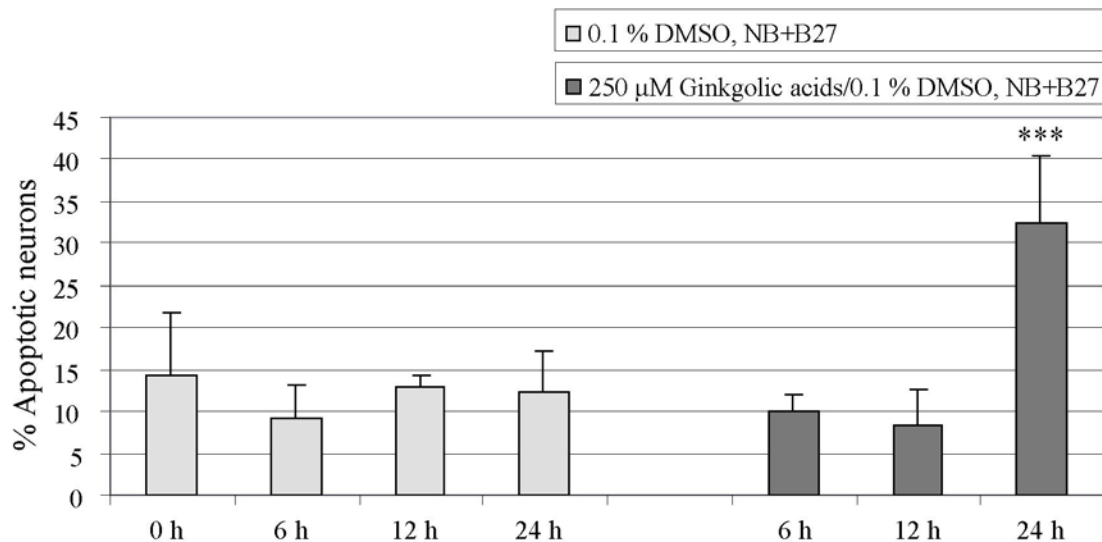


**Figure 43: Time-dependent induction of apoptosis after ginkgolic acids treatment in embryonic cortical neurons**

*In embryonic cortical neurons a significant increase of apoptosis was induced as early as 24 h after treatment with 250 μM ginkgolic acids/ 0.1 % DMSO. (n=4-5)*

### **3.3.5.2. Detection of Bad, Bad-155P and PP2Cβ protein levels by Western blotting after ginkgolic acids treatment of primary cultures**

To examine a possible regulation of the protein levels of Bad, Bad-155P or PP2Cβ after induction of apoptosis by ginkgolic acids treatment, primary embryonic cortical or hippocampal cultures were treated with 250 μM ginkgolic acid/0.1 % DMSO. Cell lysates prepared after various intervals of treatment were tested in Western blots for Bad, Bad-155P or PP2Cβ. The same blots were used for detection of Bad-155P and Bad. After Bad-155P detection, the membranes were stripped and reincubated with the Bad antibody. PP2Cβ was detected on a separate blot. None of these proteins appeared to be strongly regulated after ginkgolic acids treatment at any time point in either embryonic cortical (Fig. 44) or neonatal hippocampal culture. There was a slight increase in Bad-155P and Bad protein level at 3 h after treatment with 250 μM ginkgolic acids, which decreased at 6 h and fell under 0 h control level at 24 h.

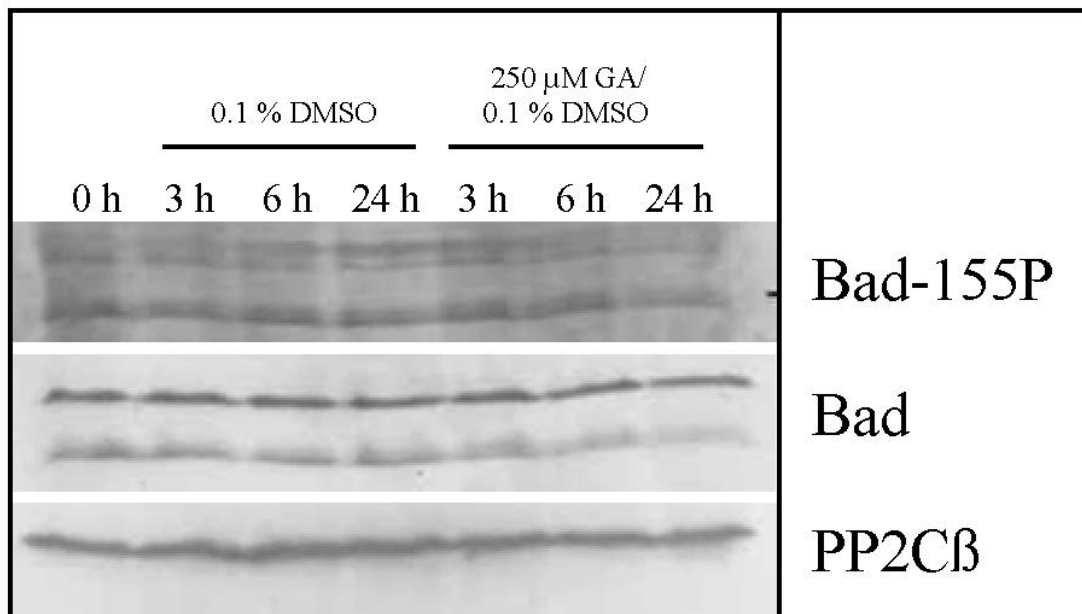


**Figure 44: Western blots detecting Bad-155P, Bad and PP2C $\beta$  in cultured embryonic cortical neurons after treatment with 250  $\mu$ M ginkgolic acids/0.1 % DMSO**

After treatment of embryonic cortical neurons with 250  $\mu$ M ginkgolic acids/0.1 % DMSO Bad-155P, Bad and PP2C $\beta$  protein levels were detected in protein extracts by Western blotting. Bad and PP2C $\beta$  proteins were not altered after ginkgolic acids/DMSO treatment, the Bad-155P protein level was slightly increased at 3 h, fell back on control level at 6 h and below the 0 h control at 24 h. The amounts of all detected proteins were not changed in the DMSO-treated neurons any time points up to 24 h.

### 3.3.6. Treatment of embryonic cortical culture with elaidic acid

Elaidic acid (“trans-oleic acid”) is known to neither activate PP2C *in vitro* nor induce apoptosis in cultured chick neurons in contrast to oleic acid (Klumpp et al., 2002). To verify that elaidic acid does not induce apoptosis in cultured rat neurons, either, we searched for apoptotic effects of elaidic acid in primary cultures of embryonic cortical neurons. Treatment with 150  $\mu$ M elaidic acid/0.1 % DMSO in NB-B27, applied up to 48 h, did neither significantly induce apoptosis (Fig. 45A) nor did it increase the number of morphologically damaged neurons (Fig. 45B). Up to 48 h, numbers of apoptotic cells remained on control niveau while the neurons showed a healthy morphology. No damaged dendrites or formation of lipid droplets in the cytosol were evident in contrast to neurons treated with 150  $\mu$ M oleic acid/0.1 % DMSO (Fig. 45B).

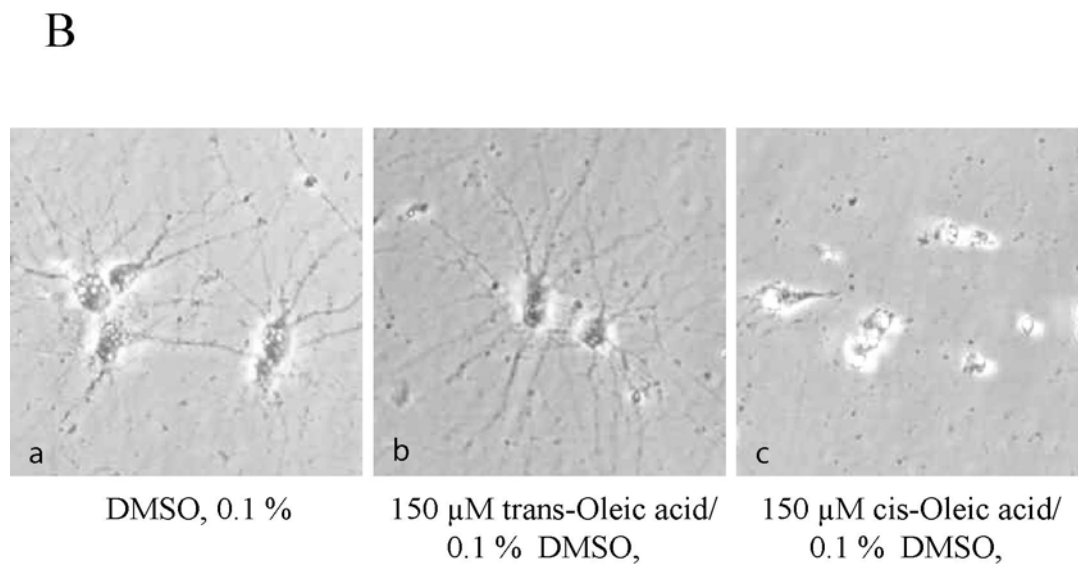
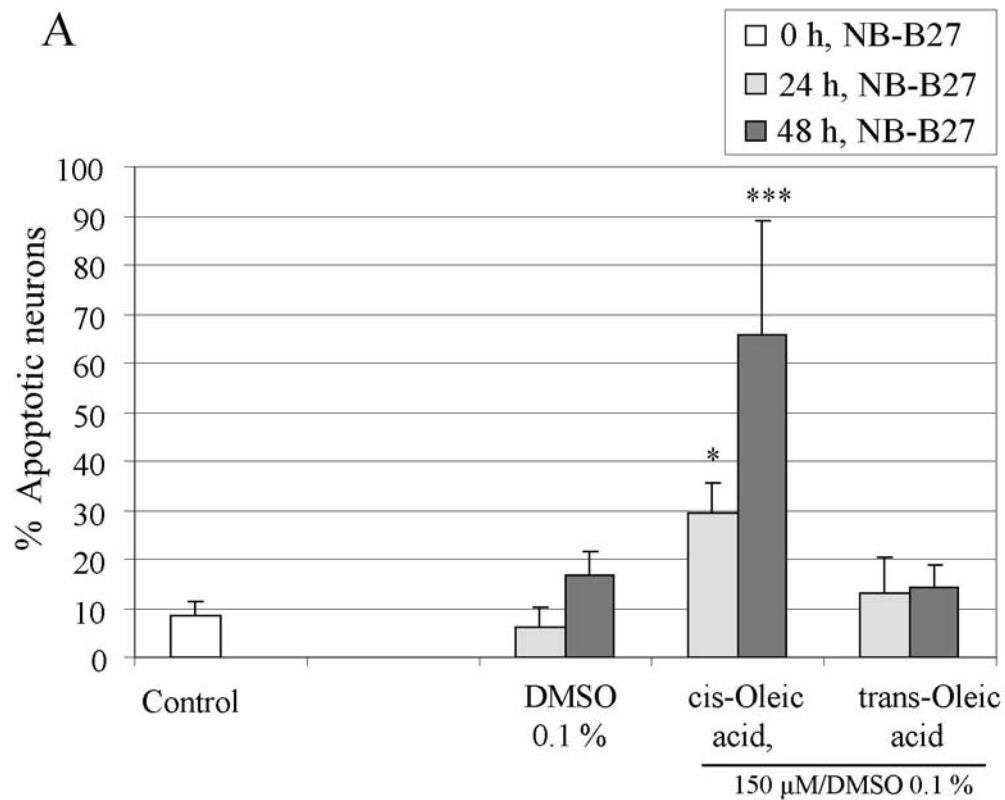


**Figure 45A+B: Comparison of damaging effects of oleic acid and elaidic acid (“trans-oleic acid”) on embryonic cortical neurons**

*In contrast to oleic acid, its trans-isomer elaidic acid did not induce apoptosis in embryonic cortical neurons. There was no significant increase in apoptotic nuclei (A, n=4) at 48 h after treatment with 150 μM elaidic acid/0.1 % DMSO. Morphologically (B), neurons looked*



*healthy at 48 h after treatment with elaidic acid, their dendrites were intact (b) while the same concentration of oleic acid made the neurons shrink, destroyed their dendrites and made them display vesicles in their cytoplasm (c). Control neurons treated with 0.1 % DMSO looked healthy at 48 h, their dendrites were intact.*

## **4. Discussion**

Cell death is involved a variety of biological events including embryogenesis, morphogenesis, differentiation, as well as cell and tissue homeostasis. In the mammalian nervous system, naturally occurring programmed cell death is required to form and refine the neuronal circuit (Raff et al., 1993). Following the emergence of functional neural networks, sustenance for neurons is required in order to maintain the nervous system because most mature neurons cannot proliferate. Inappropriate neuronal cell death results in dysfunction of the nervous system, as observed in neurodegenerative diseases, trauma, or stroke. Since the numbers of patients with neurodegenerative diseases and stroke are increasing in Western societies, the need for understanding the molecular machinery of cell death in order to find therapeutical targets to treat these diseases is great. In this thesis, the involvement of specific factors, the enzymes superoxide dismutases (SODs) and PP2C, in neuronal cell death was investigated by their modulation in different models of neurodegeneration. The roles of superoxide dismutases which function as endogenous free radical scavengers were tested *in vivo* in a model of cold injury-induced brain trauma (CIBT) and after intrastriatal injection of the toxin 3-nitropropionic acid in mice. The function of protein phosphatase type 2C (PP2C) in neuronal apoptosis was examined by measuring changes in Bad phosphorylation after treatment of rat neuronal cultures with oleic acid or ginkgolic acids, activators of PP2C.

### **4.1. Neuroprotective effect of SOD1 in a model of intrastriatal 3-nitropropionic acid injection**

One aim of this thesis was to examine the role of SOD1 in a model of intrastriatal 3-nitropropionic acid (3-NP) injection. Mycotoxin 3-NP has been shown to irreversibly inhibit the enzyme succinate dehydrogenase which is part the electron transport chain in the mitochondria and to lead to cellular depletion of adenosine triphosphate (ATP) (Ludolph et al., 1992). Both chronic or subacute systemic intoxication with 3-NP induces specific striatal brain damage (Alston et al., 1977) (Palfi et al., 1996). Chronic systemic treatment with low doses of 3-NP has been demonstrated to produce selective striatal lesions sparing aspiny NADPH-diaphorase-positive neurons and thus replicating some features of Huntington's disease (HD), a progressive neurodegenerative disorder associated with severe degeneration of basal ganglia neurons, especially of intrinsic neurons of the striatum (Martin and Gusella, 1986) (Brouillet et al., 1999) (Beal et al., 1993b) (Palfi et al., 1996) (Borlongan et al., 1997).

After subacute systemic and intrastriatal injection, however, both intrinsic striatal neurons and the nigrostriatal dopaminergic system degenerate, suggesting that this lesion may provide an animal model of multiple system atrophy rather than Huntington's disease (Nakao and Brundin, 1997). Though the origin for striatal lesion is different for HD and 3-NP intoxication, in both cases energy depletion leads to neuronal cell death. Investigations of cell death mechanisms in Huntington's disease have evolved around energy depletion and increased sensitivity for excitatory amino acids (EAA, i.e. glutamate) as a primary cause of neuronal cell death (Zorumski and Olney, 1993). Likewise, excitotoxicity seems to be a major factor in the pathogenesis of 3-NP lesions after both systemic and intrastriatal treatment and is required for the occurrence of striatal damage. Elimination of excitatory signals by removal of the cortex attenuates the lesion after acute systemic and intrastriatal treatment alike (Kim et al., 2000) (Beal et al., 1993a). The activation of NMDA and non-NMDA receptors has been implicated after energy depletion in 3-NP toxicity, but it remained unclear which type of receptor plays a pivotal role in which treatment regimen: Beal and co-workers proposed that chronic systemic administration of 3-NP with mild energy impairment leads to selective NMDA receptor activation by postsynaptic mechanisms which can be blocked by NMDA-antagonists like MK801. Damage by intrastriatal 3-NP injection was only blocked by a combination of both NMDA- and non-NMDA-antagonists indicating that a non-NMDA mechanism might be involved (Beal et al., 1993b). Opposite results have been described by Ikonomidou and colleagues: Slow progression of neuronal death induced by systemic treatment with 3-NP was enhanced by NMDA-antagonists but ameliorated by AMPA-(non-NMDA)-antagonists while rapidly progressing neuronal death induced by intrastriatal treatment with 3-NP was prevented by NMDA antagonists (Ikonomidou et al., 2000). These authors concluded that glutamate could determine the fate of neurons by saving them through activation of NMDA receptors or inducing neuronal cell death by activating AMPA/kainate receptors. Even though there is no full agreement about the precise mechanisms of receptor activation and modulation, all previous publications strongly suggest profound differences in morphological, biochemical and behavioural outcome between chronic systemic treatment of low doses 3-NP, acute/subacute systemic treatment and intrastriatal injection of 3-NP.

In this thesis, the role of cytosolic SOD1, an endogenous free radical scavenger, in the development of lesion after intrastriatal 3-NP injection was elucidated by testing whether changes in SOD1 levels affect the outcome of the lesion. Excitotoxicity induced by 3-NP, a prerequisite for striatal lesion (Schulz et al., 1996) (Kim et al., 2000), has been linked to free radical production (Coyle and Puttfarcken, 1993) causing lipid peroxidation, protein oxidation

and DNA damage. Mechanisms of free radical production due to 3-NP intoxication and subsequent excitotoxicity have been elucidated: By inhibition of the succinate dehydrogenase, ROS are produced in the dysfunctional mitochondria due to incomplete utilisation of oxygen. Additionally, inhibition of the succinate dehydrogenase stops the mitochondrial ATP production. Energy depletion leads to loss of membrane potential, activation of glutamate receptors and generation of toxic superoxide radicals in vitro (Lafon-Cazal et al., 1993). Opening glutamate receptor-associated  $\text{Ca}^{2+}$ -channels triggers  $\text{Ca}^{2+}$  influx into the cell and disrupts the intracellular  $\text{Ca}^{2+}$  homeostasis. This further enhances mitochondrial dysfunction and ROS production in the mitochondria. Free oxygen radicals themselves can target and damage mitochondria and further reduce their function (Wullner et al., 1994). In vivo, it has been shown by increased protein oxidation following administration of 3-NP to rats that oxidative stress precedes the formation of striatal lesions (Fontaine et al., 2000). Endogenous and exogenous antioxidants affect the outcome of the 3-NP lesion as well as endogenous free radical scavengers like members of the superoxide dismutase family (Nakao et al., 1996) (Fontaine et al., 2000) (Beal et al., 1995). Both cytosolic SOD1 (copper-zinc-superoxide dismutase, Cu-Zn-SOD) and mitochondrial SOD2 (manganese-superoxide dismutase, Mn-SOD) have been shown to contribute to cellular defense mechanisms counteracting the deleterious effects of ROS generated after systemic 3-NP intoxication. SOD1 had neuroprotective effects after subacute systemic injection of 3-NP into SOD1-TG mice (Beal et al., 1995). Knock-out mice with a partial deficiency of SOD2 showed an increased neuronal vulnerability to 3-NP intoxication after subacute systemic injection (Andreassen et al., 2001). All these findings indicated that ROS production plays an important role in 3-NP intoxication, but so far it has not been examined whether cytosolic SOD1 could be protective in a model of intrastriatal injection of 3-NP. In this study, SOD1-TG transgenic animals with a three-fold increase of cytosolic SOD1 and homozygous SOD1-KO mice that totally lacked SOD1 were used as tools to modulate SOD1 levels. The established protocol of intrastriatal 3-NP injection in wild type mice allowed creating a reproducible, medium-sized lesion within the striatum that did not extend into damage of hippocampus or cortex. The lesion size of ~ 30 % of the striatum did not significantly change between 4 h and 72 h after injection but decreased significantly from 72 h to 7 days. Edema measured as hemisphere enlargement was evident at all time points, peaked at 24 h, and decreased afterwards. Since both necrosis and apoptosis have been reported to occur after acute 3-NP intoxication (Ankarcrona et al., 1995) (Sato et al., 1997a; Sato et al., 1998), it was necessary to define the type of cell death by in-situ-labelling of fragmented DNA (TUNEL-staining). Strongly labelled cells with features like

blebbing, shrinking or fragmentation of the nucleus would indicate apoptosis. However, the 3-NP dose chosen in this study did not induce apoptosis. The majority of damaged cells were neither shrunk, nor did they have condensed, strongly labelled nuclei. On the contrary, the nuclei of damaged cells were increased in size compared to healthy ones in the contralateral hemisphere. Some apoptotic cells could be observed in the needle track area, but they were presumably the result of mechanical damage induced by the needle. Since the majority of dying cells did not show apoptotic morphology, biochemical markers of apoptosis such as active caspase-3 or caspase-9 were investigated by immunohistochemistry. These experiments revealed that, indeed, immunoreactivity occurred only in the needle track area but not in the 3-NP-damaged cells of the striatum, supporting the notion that necrosis and not apoptosis was the predominating cell death mechanism in this model.

After establishing parameters of this model such as development of lesion, edema formation and type of cell death in WT animals, the influence of SOD1-dosage on the outcome of intrastriatal 3-NP injection was examined. Since edema peaked at 24 h after injection in wild type animals, this time point was chosen to measure differences between SOD1-TG mice, their wild type littermates and SOD1-KO animals. At 24 h after 3-NP injection, SOD1-TG mice showed a significant decrease in both lesion size and edema formation compared to their WT littermates. SOD1 proved to be neuroprotective after this acute 3-NP treatment which supports the hypothesis that free radical production is a major factor in the pathogenesis of this intoxication. At 72 h, lesion size was still significantly smaller in SOD1-TG mice compared to the WT animals whereas the difference in edema had vanished at this time point. SOD1-KO mice failed to reveal a significant increase of lesion size at 24 h after injection when compared with WT animals while showing a significant increase in edema formation. That SOD1 overexpression, a 3-fold increase in SOD1, affected both lesion size and edema development while complete loss of SOD1 did only affect the edema formation can be explained as follows: Edema formation, on the one hand, is associated with BBB breakdown after damage of endothelial cells of the vessels, while lesion size, on the other hand, reflects the overall damage of brain tissue including astrocytes and neurons. SOD1 reduction could have increased the level of free oxygen radicals after 3-NP intoxication but the damage on neurons and astrocytes might have been already too high in WT animals to be exacerbated in SOD1-KO mice. In the more robust endothelial cells, however, the maximum damage by ROS and subsequent BBB breakdown was not reached in WT animals and therefore could be enhanced by reduction of SOD1. A reduction of ROS levels by SOD1 overexpression, on the

other hand, improved the conditions for both brain tissue and endothelial cells and therefore affected both lesion size and edema formation.

In conclusion, intrastriatal 3-NP treatment of mice proved to be a model of necrotic cell death in which ROS production contributed to the development of the lesion. Overexpression of cytosolic free radical scavenger SOD1 could reduce lesion and edema after BBB breakdown by decreasing the level of free radicals after 3-NP injection. SOD1 reduction did not significantly exacerbate of the size of the lesion, however, it enhanced edema formation and blood brain barrier breakdown. Thus, this study confirms that oxidative stress plays an important role in 3-NP toxicity.

#### **4.2. Effect of SOD2 reduction on cold injury-induced brain trauma**

Using animals deficient in SOD2 (SOD2-KO mice), the role of the inducible mitochondrial antioxidative enzyme SOD2 in the development of secondary brain damage following severe traumatic injury was examined. Traumatic brain injury involves immediate neuronal cell death in the primary lesion site, disruption of blood-brain barrier integrity and cerebral edema. This process is accompanied by secondary damage being believed to be mediated by free radicals and leads to progressive extinction of brain parenchyma. Experimental evidence from various brain trauma models had shown that focal tissue necrosis following a traumatic insult is caused, to a large extent, by oxygen radical-mediated oxidation of lipids, proteins, and nucleic acids, which can critically alter cellular function (Lewen et al., 2000). Since cerebral edema is one of the most important prognostic factors in traumatic brain injury, a non-invasive model of cold injury-induced brain trauma was used that results in vasogenic edema and allows reproducible cortical damage without the pathophysiological complexity of mechanical injury (Chan et al., 1991). The parameters compared between SOD2-KO animals and their wild type littermates (WT) were lesion size, edema development, number and distribution of apoptotic cells, as well as MPO-positive neutrophils and hemorrhagic transformations at time points from 24 h up to 7 days. Additionally, superoxide anion radical production in the injured cortex was measured in the first two hours after CIBT. The results of this study revealed that in the CIBT model a 50 % reduction in SOD2 activity did not alter the injury response according to the parameters measured. This lack of an effect of SOD2-deficiency in this study is puzzling, particularly since SOD2-KO animals showed exacerbation of the lesion following global ischemia, permanent and transient focal ischemia,

traumatic brain injury (TBI) and subarachnoid hemorrhage (Matz et al., 2001) (Maier, Tannous, 2002) (Fujimura et al., 1999b) (Murakami et al., 1998b) (Noshita et al., 2001).

In the present study, total superoxide anion production during the first 2 hours after CIBT was increased in the injured hemisphere as compared to the contralateral side. However, this increase in ROS formation in the injured brain hemisphere was not different between SOD2-KO mice and WT animals. ROS increase in the injured hemisphere demonstrates that free oxygen radicals were, indeed, produced in the lesion after CIBT and supports the hypothesis of ROS production as a key event in the damage of CIBT. Chan et al. had uncovered the role of ROS in CIBT, showing that overexpression of SOD1 and exogenous administration of liposome entrapped SOD were neuroprotective and reduced brain edema after CIBT (Chan et al., 1991) (Chan et al., 1987). Previous work by Vagnozzi and colleagues in a closed head injury rodent model had shown that the lipid peroxidation level in the injured brain which was already present 1 minute after trauma, reached maximal values by 2 hours, and decreased progressively thereafter (Vagnozzi et al., 1999). These authors indicated that significant ROS production takes place in a very early phase of traumatic injury processes.

In this study, a decrease of SOD2 levels did not increase the total amount of free oxygen radicals after CIBT nor did it influence any other parameter for measuring the effect of trauma. Two explanations might be invoked: either the production of free radicals did not co-localize with SOD2 in the mitochondria in which case SOD2 could not have an influence on the ROS level, or the levels of ROS were already too deleterious in wild type animals to allow a further increase after reduction of SOD2.

If the mitochondria were not the main source of ROS production in this model but the cytosol via mechanisms like the arachidonic acid cascade (Hillered and Chan, 1988b), mitochondrial SOD2 could influence the burst of ROS production less than cytosolic SOD1 whose overexpression has been shown to be neuroprotective after CIBT (Chan et al., 1991). Evidence for site-specific protection of SODs has been demonstrated previously: Overexpression of SOD1 did not prevent neonatal lethality in SOD2 knockout mice (Copin et al., 2000) implicating that not only the total amount of SODs but rather their localisation in the cell is important for their protective function. In previous studies SOD2-KO mice showed an exacerbation of the infarct in a model of permanent focal cerebral ischemia (Murakami et al., 1998b) while in the same model overexpression of SOD1 was not neuroprotective (Fujimura et al., 2001). This indicated that SOD2 modulation mainly affects models in which mitochondrial ROS production follows reperfusion of ischemic brain tissue. Such reperfusion may not occur after CIBT due to edema-induced ischemia which lasts for at least 72 h. Due to

edema and blood flow reduction, O<sub>2</sub> supply might be permanently lowered leading to a drop of oxygen utilisation in the mitochondria which would, in turn, result in a reduced production of mitochondrial ROS.

A different reason why reduced SOD2 levels did not influence the outcome of the lesion might be a devastating amount of superoxide anions formed in the injured cells following CIBT. The endogenous antioxidant systems might be completely overrun already in WT animals, making differences in ROS levels between WT and SOD2-KO mice undetectable. This explanation is attractive considering the severity of damage revealed by in-situ labelling of DNA-strand breaks (TUNEL-staining). After CIBT, cells inside the lesion area showed predominantly morphological features of necrosis. Though quite a few cells were strongly labelled, very few had condensed nuclei or were fragmented. Only a small number of TUNEL-positive cells met the morphologic criteria of apoptosis, suggesting that this type of cell death was not involved in the expansion of the lesion. This finding is in line with a previous report defining necrosis as the predominant form of cell death after CIBT (Stoffel et al., 2001). Other groups had stressed a role for apoptosis as a cause for cell death after CIBT as indicated by TUNEL-staining, detection of “DNA-laddering”, cytochrome C release from the mitochondria, and activation of caspases (Murakami et al., 1998a) (Murakami et al., 1999) (Morita-Fujimura et al., 1999b) (Morita-Fujimura et al., 1999a). Yet none of these methods allowed quantitative comparison of apoptosis versus necrotic cell death. In contrast to these studies, in this thesis TUNEL-staining was performed on paraffin sections being much thinner and allowing detailed analysis of individual cells.

Lesion size did not significantly increase from 24 h to 3 days post injury, rather, due to tissue loss in the affected area the lesion appeared to be decreased by 1 week. This finding is corroborated by the observation of Murakami and colleagues that the lesion did not significantly increase between 30 min and 3 days after CIBT. The distribution of apoptotic cells found in our study was similar to previous findings (Murakami et al., 1998a) (Murakami et al., 1999): Apoptotic cells could be observed in the outer layer (penumbra) rather than in the core of the lesion. If significant apoptosis would have occurred there at any timepoint, a progressive enlargement of the damaged area would have been observed. In other, probably milder models of traumatic injury, a significant number of apoptotic cells have been described to contribute to the development of secondary brain damage (Lewen et al., 2000). In the approach followed in this thesis, however, the core of the lesion was probably too severely damaged by permanent ischemia and mechanical damage to allow a programmed cell death.



This study was also designed to study edema formation in WT-animals at later time points after CIBT, as well as hemorrhagic transformations after BBB breakdown, inflammatory response, and the role of SOD2 in these processes. CIBT has been described to be a model for vasogenic edema (Chan et al., 1983), therefore, edema formation was followed up to 7 days after CIBT by measuring enlargement of the affected hemisphere. Significantly higher swelling was found in the injured hemisphere of all animals up to 7 days compared with the contralateral side, indicating occurrence of BBB breakdown and vasogenic edema, and confirming the results of previous studies regarding the effects of experimental CIBT on brain edema (Unterberg et al., 1994) (Ikeda et al., 1994) (Erdinçler et al., 2002). Murakami and colleagues described vasogenic edema, visualized by Evans blue extravasation, peaking as early as 30 min after CIBT and returning to control levels at 24 h while the measured water content of the injured hemisphere remained increased up to 72 h (Murakami et al., 1998a).

In this study, edema formation measured as hemisphere enlargement decreased between 1 and 7 days in all animals, while the appearance of hemorrhagic transformations increased significantly at 3 days post insult, particularly in the periphery of the lesion. By 7 days no new hemorrhagic transformations could be observed. Staining for neutrophils and microglial cell activation showed that a significant amount of inflammatory cells was already present in the injured hemisphere at 24 h post CIBT. Neutrophil infiltration and microglial activation peaked at 3 days post insult and was at this time point found at the same site as the hemorrhagic transformations. Obviously, the inflammatory response correlated with hemorrhagic transformations but none of both correlated with the edema formation. This observation raises the question whether inflammatory cells are actively involved in delayed BBB breakdown. A biphasic BBB breakdown after CIBT is considered to be a likely mechanism, the first phase describing the acute breakdown within 24 h after the insult by primary freezing damage followed by BBB opening due to secondary damage, the second phase, at 3 days, featuring hemorrhagic transformations caused by inflammatory response but not generalized vasogenic edema. Biphasic opening of the BBB has also been observed after controlled cortical impact, where the second opening of the BBB at 3 days post insult did not contribute to further increases in edema formation either (Baskaya et al., 1997). In the present study, neutrophils might have contributed to secondary BBB breakdown after CIBT by different mechanisms. By secreting lysosomal enzymes or cytokines they may damage the BBB. In addition, phagocytes such as neutrophils and macrophages have been described to produce reactive oxygen species (ROS) during phagocytosis (Forman and Torres, 2002). Finding leukocyte recruitment only in regions of BBB disruption, Soares and colleagues

implicated inflammatory cells in BBB breakdown in a model of traumatic brain injury (Soares et al., 1995). Inducible nitric oxide synthase (iNOS) expression and nitric oxide production by polymorph nuclear leukocytes and macrophages has also been observed after CIBT (Nag et al., 2001) and may also contribute to the BBB breakdown. In that study, BBB breakdown was immediate in lesional vessels but was delayed in perilesional vessels that showed maximal BBB breakdown between 2-4 days, with complete restoration by 6 days post-lesion.

We did not observe any differences in HT rates between WT and SOD2-KO animals at any time point up to 7 days. Again, if lysosomal enzymes as cytokines, extracellular ROS produced by phagocytes or nitric oxide production lead to this BBB breakdown, decreased SOD2 levels in the mitochondria would hardly affect this process.

Our observations suggest, that two different phases of damage occur after CIBT, a) an acute one which is defined by physical destruction of the tissue (freezing) resulting in necrosis and b) a delayed one, secondary damage, which at earlier time points is characterized by vasogenic edema, free radical production, and predominant induction of necrosis rather than apoptosis and at later time points by hemorrhagic transformations and inflammatory processes. In the acute phase, the cold injury-inducing probe freezes the cortical tissue underneath the skull leading to necrosis, destroying cortical brain tissue, neurons, astrocytes and vessels alike, in the core of the lesion. A temperature gradient can be assumed throughout the lesion, therefore, cells with more distance to the core are less affected by cold injury. In the core of the lesion the blood brain barrier is disrupted by mechanical destruction of frozen vessels. Additionally, successive BBB breakdown of perilesional vessels can be observed, possibly due to mechanisms that include a) release of mediators such as arachidonic acid-analogues and other polyunsaturated fatty acids (PUFA) that are produced by phospholipid degradation of the membranes, free radicals, bradykinin, vascular endothelial growth factor and b) activation of enzymes of the matrix metalloproteinase family (MMPs) (Chan et al., 1983) (Hillered and Chan, 1988a) (Nag et al., 1997) (Morita-Fujimura et al., 2000). The BBB becomes permeable for electrolytes and serum proteins which results in vasogenic edema observable almost immediately after the insult (Murakami et al., 1998a). Secondary damage is initiated when the tissue of the lesion becomes ischemic due to edema formation and when free radicals are formed around the edema which result in lipid peroxidation of the cellular membranes and increases in intracellular calcium, thus aggravating vasogenic edema (Erdinler et al., 2002). Among their many deleterious effects ROS increase the extracellular concentration of excitatory amino acids (e.g. glutamate) by inhibiting their re-uptake (Trotti et al., 1998). Glutamate mediated increase of the intracellular  $\text{Ca}^{2+}$  concentration results in both

dysfunction of the mitochondria being unable to further produce ATP, and the increase of intracellular ROS production via activation of the xanthin oxidase pathway, nitric oxide synthase, and phospholipase A cyclooxygenase. ROS, again, peroxidize lipids of cellular membranes, proteins, DNA (Lewen et al., 2000). The damaged cells run out of energy and undergo necrosis, burst and release their intracellular components. Although free radicals contribute to this pathological event of necrosis, mitochondrial ROS production does not play an important role: Due to immediately occurring edema and destruction of vessel in the lesion site the supply with oxygen is strongly reduced and the metabolic rate and utilisation of oxygen is decreased due to hypothermia in the tissue. Oxygen is absolutely necessary for the production of ROS in the mitochondria, however, vasogenic edema is evident for at least 3 days and during that time perfusion of the damaged tissue can only be found in the outer layers of the lesion. In this “penumbra” supply with oxygen is restored which leads to a burst of ROS in the damaged mitochondria of the cells. If these cells have enough energy left they undergo apoptosis, if not they die via necrosis. This process should be comparable to cell death occurring during reperfusion after transient focal ischemia, however, the percentage of necrotic cells in this area was too high in wild type animals to allow a further increase due to the reduction of SOD2 in KO-animals.

At 24 h the expansion of the lesion reaches its maximum. As a sign of inflammatory processes, neutrophils invade the lesion, astrocytes get activated, and microglial cells transform into monocytes and easily intrude into edematous tissue. These cells clean the tissue from debris and microglia cells and astrocytes resorb edema fluid. Moreover, after closure of the injured small vasculature a healing process takes place around the cold lesion characterized by proliferation of microvasculature (Orita et al., 1988).

In summary, these data show that CIBT provides a good model to follow the biphasic progress of BBB breakdown and development of the vasogenic edema. However, this model is not well suited to study the effect of SOD2 reduction in brain injury. Either the damage in this model is already too severe in wild type animals to allow the detection of an exacerbated injury as a consequence of a decreased amount of SOD2 in KO animals or the preferred site of free radical production after CIBT is not in the mitochondria and, therefore, cannot be influenced by the amount of SOD2.

### 4.3. Role of PP2C in neuronal apoptosis

Reversible phosphorylation of proteins by protein kinases and phosphatases is an important mechanism to regulate cellular functions including signal transduction, cell division or control of cell death pathways. While the protein kinases involved in these processes have been widely examined for many years, the importance of protein phosphatases has been recognized only very recently. One of the less examined phosphatases is protein phosphatase 2C (PP2C). It is a member of the magnesium-dependent protein phosphatase family (PPM) and requires  $Mg^{2+}$  (or  $Mn^{2+}$ ) -ions for its activation. A possible role of PP2C in cell physiology was previously underestimated because unphysiologically high concentrations of  $Mg^{2+}$  were known to be required for full PP2C activation *in vitro*. Recently, Klumpp and colleagues exposed that unsaturated fatty acids, such as oleic acid, linoleic acid and arachidonic acid, can activate PP2C, probably by affecting its response to divalent cations (Klumpp et al., 1998), which implicates that in the presence of these fatty acids PP2C could be active under physiological  $Mg^{2+}$  concentrations. All chemical compounds, mostly fatty acids, which were found to activate PP2C had in common that they were lipophilic, unsaturated molecules with a negatively charged group while *trans*-isomers and esterified derivatives of fatty acids like oleic acid were found to be inactive.

An astonishing correlation between PP2C activation by these compounds and their ability to induce apoptosis has been observed in chick neuronal culture (Klumpp et al., 2002) hinting at PP2C as an important player in neuronal apoptosis. How the apoptotic pathway is influenced by PP2C, however, is unresolved so far. Various endogenous substrates of PP2C have been identified in protozoan and mammalian cells such as Bad, translation elongation factor 1 $\beta$  (Mamoun and Goldberg, 2001), cyclin-dependent kinases (Cheng et al., 1999) and a number of stress-activated MAP kinases (Hanada et al., 1998) (Hanada et al., 2001) (Nguyen and Shiozaki, 1999). There is strong indication that dephosphorylation of Bad by PP2C might be one major underlying pro-apoptotic mechanism (Klumpp and Krieglstein, 2002): Bad, a member of the Bcl-2 family consisting of anti- and proapoptotic members which control a critical intracellular checkpoint within an evolutionary preserved cell death pathway (Wang and Reed, 1998), is dephosphorylated by PP2C at Ser<sup>112</sup>, Ser<sup>136</sup>, and preferably at Ser<sup>155</sup> “*in vitro*” (Krieglstein, Klumpp, unpublished data). Dephosphorylation has been shown to unleash Bad's proapoptotic properties by triggering heterodimerization of Bad with Bcl-x<sub>L</sub> whose protective function in the mitochondrial membrane is, thereby, ameliorated. Phosphorylation of Bad at Ser<sup>155</sup> inhibits Bad/Bcl-x<sub>L</sub> dimerisation and prevents Bad-induced apoptosis, moreover, phosphorylation at Ser<sup>112</sup> and Ser<sup>136</sup> allows Bad to bind to 14-3-3

proteins in the cytosol. So far it has not been demonstrated whether PP2C dephosphorylates Bad *in vivo* and, thereby, induces apoptosis. One aim of this thesis was to elucidate the proapoptotic role of PP2C in rat neuronal cultures after treatment with PP2C-activating compounds and to define apoptotic pathways regulated by PP2C *in vivo*.

As a first step to show Bad dephosphorylation after PP2C activation, it was investigated whether Bad and PP2C proteins, possibly involved in a PP2C-related pathway of neuronal apoptosis, were expressed in rat neuronal cultures and co-localized in the same cellular compartment which is a precondition for their interaction. In this study, Bad, phospho-Bad-155 and PP2C $\beta$  proteins were detectable in both rat embryonic cortical (CC) and neonatal hippocampal (HC) neuronal cultures by Western blotting analysis. Cellular PP2C $\beta$  protein distribution was examined by immunocytochemistry (ICC) in CC and PP2C $\beta$  was found being localized in the cytosol but not in the nucleus. Since Bad has been described to be localized in the cytosol and at the outer mitochondrial matrix (Zha et al., 1997) an interaction between PP2C $\beta$  and Bad “*in vivo*” could be hypothesized.

Afterwards, oleic acid treatment was optimized in both rat neuronal cultures to induce apoptosis which had been observed in cultured chick neurons at oleic acid concentrations  $\geq 100$   $\mu\text{M}$  (Klumpp et al., 2002). In this study, significant damage could be achieved by treating the cell cultures for 24 h with 150  $\mu\text{M}$  oleic acid while excluding serum proteins from the cell culture medium. In the presence of serum proteins, such as bovine serum albumin (BSA), the apoptotic effect was diminished in a dose dependant manner. While increasing the solubility of oleic acid in cell culture medium, BSA presumably bound oleic acid, thus, lowered the concentration of free oleic acid in the cell culture medium and prevented cellular damage. No ratio of oleic acid and BSA could be found which allowed full solubility of oleic acid and simultaneously induced apoptosis in rat neuronal cell culture. Therefore, not only BSA was inappropriate as a tool to dissolve oleic acid, but also B27 supplement, a component of the Neurobasal medium, had to be excluded since it contained BSA.

Since oleic acid was not fully soluble in the culture medium at 150  $\mu\text{M}$ /0.1 % DMSO, and lower doses did not reproducibly induce apoptosis in rat neuronal culture,  $\beta$ -cyclodextrin was tested as a solvent mediator to achieve higher concentrations of oleic acid. Although,  $\beta$ -cyclodextrin allowed dissolving oleic acid to considerably high concentrations in cell culture medium, it proved to be ill-suited for treatment of rat embryonic cortical and neonatal hippocampal neuronal culture due to toxic effects of its own. In high concentrations, cyclodextrin induced apoptosis in cultured neurons being demonstrated by nuclear staining and confirmed by detection of active caspase-3, a biochemical marker for apoptosis, by

Western blot analysis. Since, for technical reasons, it was impossible to reduce the concentration of  $\beta$ -cyclodextrin without reducing oleic acid's concentration,  $\beta$ -cyclodextrin, too, was not useful to study the influence of oleic acid on PP2C.

Because neither  $\beta$ -cyclodextrin nor BSA could be used to increase oleic acid solubility, high concentrations of oleic acid were prepared in NB-B27 even if oleic acid was not fully dissolved. Interestingly, the concentration of dissolved oleic acid seemed to be less important for induction of apoptotic damage than the total amount of oleic acid in culture medium including non-dissolved parts. This can be explained by the finding that fatty acids, assumingly oleic acid, were found in the cytosol in "lipid droplets". Under light microscopy, neuronal morphology revealed the formation of droplets inside the cytosol of neurons as early as 2 h and fragmented dendrites at 12 h after onset of treatment with 150  $\mu$ M oleic acid. These vesicles contained free fatty acids or lipids as visualized by Nile blue staining, indicating that oleic acid had entered the cells and could potentially activate PP2C. Although Nile blue staining could not discriminate whether these "lipid droplets" contained acid oleic or some other acidic lipid, it is quite likely that oleic acid was a major compound. Formation of such lipid droplets has also been described in oleic acid-treated macrophages (Chen et al., 2002). In this study, the neurons presumably lowered the concentration of oleic acid in the culture medium by storing in droplets inside their cytosol, thus allowing undissolved oleic acid to subsequently dissolve.

To confirm the postulated specificity of oleic acid in inducing apoptosis in these cell culture systems, elaidic acid ("trans oleic acid") was tested in rat embryonic cortical neurons. Previously, elaidic acid had been described to neither induce apoptosis in chick neuronal culture nor activate PP2C in vitro (Klumpp et al., 2002). In this study, 150  $\mu$ M elaidic acid/0.1 % DMSO in culture medium without B27 did not induce apoptosis nor morphological damage the cells up to 48 h, implicating that, indeed, only oleic acids with *cis*-conformation had negative effects on cell survival.

To demonstrate changes in Bad phosphorylation after PP2C activation by oleic acid, protein levels of Bad, Bad-155P and PP2C $\beta$  were examined in oleic acid-treated rat neuronal cultures by Western blot analysis. For technical reasons, only phospho-Bad-155 and total Bad including all phosphorylated and non-phosphorylated forms could be detected by Western blotting but not unphosphorylated Bad which should ideally have been measured. The only way to approach regulation of unphosphorylated Bad was to detect changes in ratios of Bad to Bad-155P and by that to draw conclusions about unphosphorylated Bad levels.

The Western blot analysis revealed a pronounced increase of Bad-155P protein as early as 1 h after onset of treatment in both neuronal cultures instead of an expected decrease due to PP2C activation. Total Bad was only very mildly upregulated at this time point while PP2C $\beta$  levels remained unchanged. These results indicate that Bad-155P protein levels increased to a much higher percentage than Bad protein levels. However, since by Western blot analysis the ratio of Bad/Bad-155P under physiological, non-damaging conditions could not be determined, the changes of Bad-155P and Bad did not allow drawing conclusions about changes in unphosphorylated Bad. Therefore, the results of these experiments do not prove that after induction of apoptosis by oleic acid Bad-155P is dephosphorylated via activation of PP2C nor do they necessarily contradict this hypothesis.

If increase of Bad-155P, however, was a real effect, this discrepancy could be explained by oleic acid as the substance of choice for induction of apoptosis in neuronal cell culture. Oleic acid is by no means a very specific activator of PP2C. It has been described to directly activate the protein kinases 2C which has been observed to phosphorylate Bad (Lu et al., 1996) (Bertolotto et al., 2000). Oleic acid induces the release of neurotransmitters from synaptosomes and inhibits their re-uptake (Rhoads et al., 1983) (Troeger et al., 1984). It even triggers the production of ROS which could possibly damage cells as well (Lu et al., 1998). Bad dephosphorylation by PP2C might not be detectable due to strong phosphorylation of Bad by an activated kinase.

Treatment of rat neurons with ginkgolic acids which have been shown to activate PP2C and induce apoptosis (Ahlemeyer et al., 2001) did not reveal any advantages over treatment with oleic acid. Not only did the same solubility problems occur, but both Bad-155P and total Bad proteins levels slightly increased at early time points and decreased at later time points and, therefore, did not allow to draw conclusions about regulation of unphosphorylated Bad. Ginkgolic acids also had the general disadvantage that they are composed of many compounds and, therefore, a possible effect could hardly be connected to one compound.

For further studies to assess a role of PP2C in neuronal apoptosis, it is necessary to regulate the amount or the activity of PP2C either via specific inhibitors or activators. Potential strategies to down-regulate PP2C expression could be the use of anti-sense nucleotides or the RNA-interference (RNAi) method blocking the translation of PP2C. Specific activators of PP2C might be found by testing compounds fulfilling the same structural criteria of PP2C activators known so far.

Comparing each of the three experimental model systems employed in this thesis for the study of neuronal cell death and the answers obtained with other approaches from the literature which used apparently similar procedures allows to draw the conclusion, that already minor experimental variations affecting the fine tuned concert of interacting molecules can lead to contradictory results. Specific conclusions on the events after brain trauma at the cellular and molecular level apply preferentially or exclusively to the set of conditions chosen. General conclusions on factors and pathways involved in neuronal cell death emerge only gradually. On this background the results obtained in this thesis form small, although interesting, pieces in a puzzle the general picture of which is beginning to be visible, hopefully, guiding the development to a better therapeutic management of brain injuries.



## 5. Summary

The purpose of this study was to elucidate the role of enzymes, the endogenous free radical scavengers superoxide dismutase 1 and 2 (SOD1/2) as well as protein phosphatase type 2C (PP2C), in different models of neuronal cell death. This should improve the understanding of cellular mechanisms after neuronal damage like stroke, trauma, or neurodegenerative diseases like Huntington's disease in order to reveal new therapeutic targets. Two different *in vivo*-models of neuronal damage, cold injury-induced brain trauma (CIBT) and intrastriatal injection of the toxin 3-nitropropionic (3-NP) acid in mice, were employed to study the influence of quantitative modulation of SODs on brain damage. The possible role of PP2C, an enzyme participating in the reversible phosphorylation of proteins, in the induction of apoptosis was elucidated in cultured rat neurons.

In the first part of this study it was demonstrated that the cytosolic Cu/Zn-superoxide dismutase (SOD1) influences the development of the lesion after intrastriatal injection of 3-NP. Overexpression of SOD1 in transgenic mice was neuroprotective in this predominantly necrotic model of 3-NP injection, reducing lesion size and edema development, while diminished expression of this enzyme in knock-out mutants only significantly enhanced edema formation.

The results of this study support the notion that also in this model of intrastriatal injection free oxygen radical production is a crucial factor of 3-NP intoxication as had been previously demonstrated in milder, systemic models of 3-NP intoxication. Cellular energy deficits, the underlying mechanism for 3-NP toxicity, play an important role in neurodegenerative disease like Huntington's disease. Therefore, understanding neuronal cell death due to lack of energy allows insight into neurodegenerative diseases and guides the search for therapeutic targets to treat these diseases.

As a next step, the role of mitochondrial Mn-superoxide dismutase (SOD2) in mice was examined using a model of cold injury-induced brain trauma (CIBT). The results of these experiments elucidate, on the one hand, the role of mitochondrial free oxygen radical production and, on the other hand, the development of the lesion after cold injury brain trauma (CIBT) at later time points, especially BBB breakdown and inflammatory response.

Reduced expression of SOD2 in knock-out mutants did not influence the development of damage after CIBT. However, increased free oxygen radical production inside the lesion of CIBT was detected by hydroethidine assay. This result supports findings of previous publications postulating reactive oxygen species (ROS) production to play a crucial role in the

damage after CIBT. Since SOD2 is localized in the mitochondria, this result allows to draw the conclusion that either the production of free radicals did not co-localize with SOD2 in the mitochondria, in which case SOD2 could not have an influence on the ROS level, or the amounts of ROS were already too devastating in wild type animals to allow an exacerbation of the lesion after reduction of SOD2.

By observing the development of vasogenic edema and finding hemorrhagic transformations and inflammation at later time points, this study proved CIBT to be a reproducible model of a biphasic breakdown of the BBB. Stroke as well as trauma research might benefit from this model, since biphasic BBB breakdown and inflammation are factors contributing to the deterioration of these brain damages. Augmented knowledge gained from this study can contribute to the development of new therapies for improved prognosis of patients.

The involvement of PP2C's role in neuronal apoptosis was the third focus of research of this thesis. Protein kinases and phosphatases, including PP2C, regulate numerous cellular mechanisms by reversible phosphorylation of proteins. The results of this study support the hypothesis of PP2C being involved in programmed neuronal cell death (apoptosis).

Activators of PP2C, such as oleic acid or ginkgolic acids, were shown to induce apoptosis in a time- and concentration-dependent manner in cultured rat neurons while using the enantiomer "trans-oleic acid" (elaidic acid), known not to activate PP2C *in vitro*, instead of *cis*-oleic acid, did not induce apoptosis. A possible apoptotic mechanism, the induction of programmed cell death by dephosphorylation of the proapoptotic protein Bad by activated PP2C, was analyzed by Western blotting experiments. Bad phosphorylated at Ser<sup>155</sup> and total Bad (phosphorylated + unphosphorylated) were detected in cultivated rat neurons which had been treated with oleic acid or ginkgolic acids. By the Western blotting method, changes in the amount of unphosphorylated Bad were not detectable since no antibody against unphosphorylated Bad was available. Without knowledge of the ratio of phosphorylated Bad to total Bad in non-treated cultured neurons, the proportion of phospho-Bad/total Bad in oleic acid-treated cells did not allow to draw conclusions about quantitative changes of unphosphorylated Bad.

Oleic acid as well as ginkgolic acids are relatively unspecific activators. By their impact on other pathways of the cellular metabolism possible effects of PP2C activation might be masked. Therefore, in addition to searching for more specific activators, one important goal in the future must be to find specific substrates of PP2C whose dephosphorylation is measurable. Specific activators or inhibitors of PP2C could contribute to unequivocally prove the role of this enzyme in neuronal apoptosis.

## 6. Zusammenfassung

Das Ziel dieser Arbeit war es, die Rolle von Enzymen, den endogenen Sauerstoffradikalfängern Superoxiddismutase 1 und 2 (SOD1/2) sowie der Proteinphosphatase Typ 2C (PP2C), in verschiedenen Modellen von neuronalem Zelltod zu beleuchten. Damit sollte ein Beitrag geleistet werden, das Verständnis der zellulären Vorgänge nach neuronaler Schädigung, wie Schlaganfall, Trauma oder neurodegenerativen Erkrankungen, wie Morbus Huntington, zu verbessern, mit dem Ziel, neue therapeutische Ansätze aufzuzeigen. Zwei verschiedene *in vivo*-Modelle, das Kälte-induzierte Hirntrauma (Cold injury-induced brain trauma, CIBT) und die intrastriale Injektion des Toxins 3-Nitropropionsäure (3-NP), fanden Anwendung in Mäusen, um den Einfluss der Menge an SOD auf das Ausmaß von Hirnschädigung zu untersuchen. Die mögliche Rolle der PP2C bei der Induktion der Apoptose, eines Enzyms, welches an der reversiblen Phosphorylierung von Proteinen beteiligt ist, wurde an kultivierten Rattenneuronen beleuchtet.

Im ersten Teil dieser Arbeit wurde demonstriert, dass das zytosolische Enzym Cu/Zn-Superoxiddismutase (SOD1) den Verlauf der Schädigung nach intrastrialer Injektion von 3-NP beeinflusst. Vermehrte Expression von SOD1 in transgenen Mäusen wirkte in diesem überwiegend nekrotischen Schädigungsmodell neuroprotektiv, verkleinerte die Läsion und verminderte Ödembildung, während eine Verminderung dieses Enzyms in „knock-out“-Mutanten allein die Ödembildung signifikant verstärkte.

Die Ergebnisse dieser Studie untermauern die Hypothese, welche zuvor anhand von mildereren, systemischen 3-NP-Intoxikationsmodellen formuliert wurde, dass auch im Modell der intrastrialen Injektion die Bildung von freien Sauerstoffradikalen ein wichtiger Faktor der Intoxikation durch 3-NP ist. Zelluläre Energiedefizite, welche die Ursache für die Schädigung durch 3-NP sind, spielen auch bei neurodegenerativen Erkrankungen, wie der Chorea Huntington, eine wichtige Rolle. Daher erlauben Erkenntnisse über den Zelluntergang durch Energiemangel Einblicke in neurodegenerative Erkrankungen und erleichtern so die Suche nach therapeutischen Zielen zur Behandlung dieser Erkrankungen.

Weiterhin wurde in dieser Arbeit die Rolle der mitochondrialen Mn-Superoxiddismutase (SOD2) anhand eines Modells von Gehirntrauma durch Kälteschädigung (CIBT) untersucht. Die Ergebnisse dieser Experimente beleuchteten auf der einen Seite die Rolle der mitochondrialen Produktion von freien Sauerstoffradikalen, auf der anderen Seite die Entwicklung der Läsion nach CIBT, im Besonderen den Zusammenbruch der Blut-Hirnschranke und Entzündungsreaktionen zu späteren Zeitpunkten.

Es zeigte sich, dass die verminderte Expression von SOD2 in “knock-out” Mutanten den Schädigungsverlauf nach CIBT nicht beeinflusst. Allerdings wurde ein Anstieg der Produktion von freien Sauerstoffradikalen in der Läsion durch den Hydroethidin-Test detektiert. Dieses Resultat unterstützt Funde in früheren Publikationen, welche postulieren, dass die Bildung reaktiver Sauerstoffspezies (ROS) eine wichtige Rolle in der Schädigung nach CIBT spielt. Da SOD2 in den Mitochondrien lokalisiert ist, erlaubt dieses Ergebnis den Rückschluss, dass entweder die Produktion von freien Radikalen nicht mit der SOD2 in den Mitochondrien kolokalisiert war, wobei SOD2 keinen Einfluss auf den Spiegel freier Sauerstoffradikale haben konnte, oder dass die Menge an freigesetzten Sauerstoffradikalen in Wildtypen schon zu schädigend war, um eine Verschlimmerung der Läsion nach Verringerung von SOD2 zuzulassen. Außerdem zeigte diese Studie durch Verfolgen der Ödementwicklung und den Befund von haemorrhagischen Veränderungen und Entzündungsreaktionen, dass CIBT ein reproduzierbares Modell für einen biphasischen Zusammenbruch der Blut-Hirnschranke ist. Dieses Modell kann sowohl in der Schlaganfall- als auch der Trauma- Forschung genutzt werden, da dort ein biphasischer Zusammenbruch der Blut-Hirnschranke und Entzündungsreaktionen Faktoren sind, welche zur Verschlechterung des Krankheitsbildes dieser Hirnschädigungen führen. Das an diesen Modellen erarbeitete Wissen kann dazu beitragen, neue Therapien zu entwickeln, um die Prognose der Patienten zu verbessern.

Die Untersuchung der Rolle der PP2C in der neuronalen Apoptose war der dritte Forschungsschwerpunkt dieser Arbeit. Proteinkinasen und Phosphatasen, darunter PP2C, üben durch reversible Proteinphosphorylierung eine entscheidende regulierende Funktion in vielen zellulären Mechanismen aus. Die Ergebnisse dieser Arbeit unterstreichen die Hypothese, daß PP2C am programmierten neuronalen Zelltod (Apoptose) beteiligt sein könnte. Es wurde gezeigt, daß Aktivatoren der PP2C, wie Ölsäure oder Ginkgolsäuren, in kultivierten Rattenneuronen zeit- und konzentrationsabhängig Apoptose hervorrufen. Dagegen zeigt sich bei Verwendung des Enantiomers *trans*-Ölsäure (Elaidinsäure), welche PP2C *in-vitro* nicht aktiviert, anstelle von *cis*-Ölsäure keine Induktion von Apoptose. Ein möglicher apoptotischer Mechanismus, die Induktion von Apoptose durch Dephosphorylierung des proapoptotischen Proteins Bad durch aktivierte PP2C, wurde durch Bestimmung der Menge an Ser<sup>155</sup>-phosphoryliertem Bad sowie von Gesamt-Bad (phosphoryliert + unphosphoryliert) in kultivierten Rattenneuronen, welche mit Ölsäure oder Ginkgolsäuren behandelt wurden, beleuchtet. Veränderungen von unphosphoryliertem Bad konnten durch die hier eingesetzte Westernblot-Methode nicht bestimmt werden, denn für den

Nachweis von unphosphoryliertem Bad standen keine Antikörper zu Verfügung. Andererseits ließen die gemessenen Phospho-Bad/Gesamt-Bad-Veränderungen in behandelten Zellen ohne die Kenntnis über das Verhältnis von Gesamt-Bad zu phosphoryliertem Bad in unbehandelten Zellen ebenfalls keinen indirekten Rückschluss auf unphosphoryliertes Bad zu.

Sowohl Ölsäure als auch Ginkgolsäuren sind relativ unspezifische Aktivatoren. Durch deren Einfluss auf andere Stoffwechselwege können mögliche Effekte der PP2C-Aktivierung verdeckt werden. Außer der Suche nach spezifischen Aktivatoren muß es ein wichtiges Ziel in der näheren Zukunft sein, spezifische Substrate für PP2C zu finden, deren Dephosphorylierung messbar ist. Spezifische Aktivatoren oder Hemmstoffe der PP2C können wesentlich zur Aufklärung einer möglichen Rolle dieses Enzyms in der neuronalen Apoptose beitragen.

## **7. Publications**

### **7.1 Journals**

Grzeschik SM, Maier CM, Chan PH (2003) Effects of cold injury-induced trauma in SOD2-deficient mice. *J Neurotrauma* (in press)

Kim GW, Gasche Y, Grzeschik SM, Maier CM, Chan PH. Neurodegeneration in striatum induced by the mitochondrial toxin 3-Nitropropionic acid; role of matrix metalloproteinase-9 in early blood brain barrier disruption? (submitted to *J Neuroscience*)

### **7.2 Meetings**

Grzeschik SM, Maier CM, Chan PH (2001) Temporal pattern of brain edema and apoptosis following cold injury in SOD2<sup>+/-</sup> mice (Brain'01, Taipei)

## 8. References

- Ahlemeyer B, Selke D, Schaper C, Klumpp S, Krieglstein J (2001) Ginkgolic acids induce neuronal death and activate protein phosphatase type-2C. *Eur J Pharmacol* 430:1-7.
- Albin RL, Greenamyre JT (1992) Alternative excitotoxic hypotheses. *Neurology* 42:733-738.
- Alston TA, Mela L, Bright HJ (1977) 3-Nitropropionate, the toxic substance of *Indigofera*, is a suicide inactivator of succinate dehydrogenase. *Proc Natl Acad Sci U S A* 74:3767-3771.
- Andreassen OA, Ferrante RJ, Dedeoglu A, Albers DW, Klivenyi P, Carlson EJ, Epstein CJ, Beal MF (2001) Mice with a partial deficiency of manganese superoxide dismutase show increased vulnerability to the mitochondrial toxins malonate, 3-nitropropionic acid, and MPTP. *Exp Neurol* 167:189-195.
- Ankarcrona M, Dybukt JM, Bonfoco E, Zhivotovsky B, Orrenius S, Lipton SA, Nicotera P (1995) Glutamate-induced neuronal death: a succession of necrosis or apoptosis depending on mitochondrial function. *Neuron* 15:961-973.
- Ayllon V, Martinez AC, Garcia A, Cayla X, Rebollo A (2000) Protein phosphatase 1alpha is a Ras-activated Bad phosphatase that regulates interleukin-2 deprivation-induced apoptosis. *Embo J* 19:2237-2246.
- Bae J, Hsu SY, Leo CP, Zell K, Hsueh AJ (2001) Underphosphorylated BAD interacts with diverse antiapoptotic Bcl-2 family proteins to regulate apoptosis. *Apoptosis* 6:319-330.
- Baskaya MK, Rao AM, Dogan A, Donaldson D, Dempsey RJ (1997) The biphasic opening of the blood-brain barrier in the cortex and hippocampus after traumatic brain injury in rats. *Neurosci Lett* 226:33-36.
- Bast A, Goris RJ (1989) Oxidative stress. *Biochemistry and human disease. Pharm Weekbl Sci* 11:199-206.

- Beal MF, Brouillet E, Jenkins B, Henshaw R, Rosen B, Hyman BT (1993a) Age-dependent striatal excitotoxic lesions produced by the endogenous mitochondrial inhibitor malonate. *J Neurochem* 61:1147-1150.
- Beal MF, Ferrante RJ, Henshaw R, Matthews RT, Chan PH, Kowall NW, Epstein CJ, Schulz JB (1995) 3-Nitropropionic acid neurotoxicity is attenuated in copper/zinc superoxide dismutase transgenic mice. *J Neurochem* 65:919-922.
- Beal MF, Brouillet E, Jenkins BG, Ferrante RJ, Kowall NW, Miller JM, Storey E, Srivastava R, Rosen BR, Hyman BT (1993b) Neurochemical and histologic characterization of striatal excitotoxic lesions produced by the mitochondrial toxin 3-nitropropionic acid. *J Neurosci* 13:4181-4192.
- Beckman JS, Beckman TW, Chen J, Marshall PA, Freeman BA (1990) Apparent hydroxyl radical production by peroxynitrite: implications for endothelial injury from nitric oxide and superoxide. *Proc Natl Acad Sci U S A* 87:1620-1624.
- Bertolotto C, Maulon L, Filippa N, Baier G, Auberger P (2000) Protein kinase C theta and epsilon promote T-cell survival by a rsk-dependent phosphorylation and inactivation of BAD. *J Biol Chem* 275:37246-37250.
- Blume-Jensen P, Janknecht R, Hunter T (1998) The kit receptor promotes cell survival via activation of PI 3-kinase and subsequent Akt-mediated phosphorylation of Bad on Ser136. *Curr Biol* 8:779-782.
- Bonni A, Brunet A, West AE, Datta SR, Takasu MA, Greenberg ME (1999) Cell survival promoted by the Ras-MAPK signaling pathway by transcription-dependent and -independent mechanisms. *Science* 286:1358-1362.
- Borlongan CV, Koutouzis TK, Sanberg PR (1997) 3-Nitropropionic acid animal model and Huntington's disease. *Neurosci Biobehav Rev* 21:289-293.
- Brennan WA, Jr., Bird ED, Aprille JR (1985) Regional mitochondrial respiratory activity in Huntington's disease brain. *J Neurochem* 44:1948-1950.
- Bronner LL, Kanter DS, Manson JE (1995) Primary prevention of stroke. *N Engl J Med* 333:1392-1400.



- Brouillet E, Conde F, Beal MF, Hantraye P (1999) Replicating Huntington's disease phenotype in experimental animals. *Prog Neurobiol* 59:427-468.
- Brouillet E, Hantraye P, Ferrante RJ, Dolan R, Leroy-Willig A, Kowall NW, Beal MF (1995) Chronic mitochondrial energy impairment produces selective striatal degeneration and abnormal choreiform movements in primates. *Proc Natl Acad Sci U S A* 92:7105-7109.
- Butterworth NJ, Williams L, Bullock JY, Love DR, Faull RL, Dragunow M (1998) Trinucleotide (CAG) repeat length is positively correlated with the degree of DNA fragmentation in Huntington's disease striatum. *Neuroscience* 87:49-53.
- Cadet JL, Sheng P, Ali S, Rothman R, Carlson E, Epstein C (1994) Attenuation of methamphetamine-induced neurotoxicity in copper/zinc superoxide dismutase transgenic mice. *J Neurochem* 62:380-383.
- Carriedo SG, Yin HZ, Sensi SL, Weiss JH (1998) Rapid Ca<sup>2+</sup> entry through Ca<sup>2+</sup>-permeable AMPA/Kainate channels triggers marked intracellular Ca<sup>2+</sup> rises and consequent oxygen radical production. *J Neurosci* 18:7727-7738.
- Chan PH, Longar S, Fishman RA (1983) Phospholipid degradation and edema development in cold-injured rat brain. In: *Brain Res*, pp 329-337.
- Chan PH, Longar S, Fishman RA (1987) Protective effects of liposome-entrapped superoxide dismutase on posttraumatic brain edema. *Ann Neurol* 21:540-547.
- Chan PH, Chen SF, Yu AC (1988) Induction of intracellular superoxide radical formation by arachidonic acid and by polyunsaturated fatty acids in primary astrocytic cultures. *J Neurochem* 50:1185-1193.
- Chan PH, Fishman RA, Wesley MA, Longar S (1990a) Pathogenesis of vasogenic edema in focal cerebral ischemia. Role of superoxide radicals. *Adv Neurol* 52:177-183.
- Chan PH, Chu L, Chen SF, Carlson EJ, Epstein CJ (1990b) Reduced neurotoxicity in transgenic mice overexpressing human copper-zinc-superoxide dismutase. *Stroke* 21:III80-82.

- Chan PH, Yang GY, Chen SF, Carlson E, Epstein CJ (1991) Cold-induced brain edema and infarction are reduced in transgenic mice overexpressing CuZn-superoxide dismutase. *Ann Neurol* 29:482-486.
- Chan PH, Kamii H, Yang G, Gafni J, Epstein CJ, Carlson E, Reola L (1993) Brain infarction is not reduced in SOD-1 transgenic mice after a permanent focal cerebral ischemia. *Neuroreport* 5:293-296.
- Chen JS, Greenberg AS, Wang SM (2002) Oleic acid-induced PKC isozyme translocation in RAW 264.7 macrophages. *J Cell Biochem* 86:784-791.
- Cheng A, Ross KE, Kaldis P, Solomon MJ (1999) Dephosphorylation of cyclin-dependent kinases by type 2C protein phosphatases. *Genes Dev* 13:2946-2957.
- Chiang CW, Harris G, Ellig C, Masters SC, Subramanian R, Shenolikar S, Wadzinski BE, Yang E (2001) Protein phosphatase 2A activates the proapoptotic function of BAD in interleukin-3-dependent lymphoid cells by a mechanism requiring 14-3-3 dissociation. *Blood* 97:1289-1297.
- Clark RS, Chen J, Watkins SC, Kochanek PM, Chen M, Stetler RA, Loeffert JE, Graham SH (1997) Apoptosis-suppressor gene bcl-2 expression after traumatic brain injury in rats. *J Neurosci* 17:9172-9182.
- Cohen P (2001) The role of protein phosphorylation in human health and disease. The Sir Hans Krebs Medal Lecture. *Eur J Biochem* 268:5001-5010.
- Cohen P, Holmes CF, Tsukitani Y (1990) Okadaic acid: a new probe for the study of cellular regulation. *Trends Biochem Sci* 15:98-102.
- Copin JC, Gasche Y, Chan PH (2000) Overexpression of copper/zinc superoxide dismutase does not prevent neonatal lethality in mutant mice that lack manganese superoxide dismutase. *Free Radic Biol Med* 28:1571-1576.
- Coyle JT, Puttfarcken P (1993) Oxidative stress, glutamate, and neurodegenerative disorders. *Science* 262:689-695.
- Datta SR, Brunet A, Greenberg ME (1999) Cellular survival: a play in three Akts. *Genes Dev* 13:2905-2927.

- Datta SR, Dudek H, Tao X, Masters S, Fu H, Gotoh Y, Greenberg ME (1997) Akt phosphorylation of BAD couples survival signals to the cell-intrinsic death machinery. *Cell* 91:231-241.
- Datta SR, Katsov A, Hu L, Petros A, Fesik SW, Yaffe MB, Greenberg ME (2000) 14-3-3 proteins and survival kinases cooperate to inactivate BAD by BH3 domain phosphorylation. *Mol Cell* 6:41-51.
- Datta SR, Ranger AM, Lin MZ, Sturgill JF, Ma YC, Cowan CW, Dikkes P, Korsmeyer SJ, Greenberg ME (2002) Survival factor-mediated BAD phosphorylation raises the mitochondrial threshold for apoptosis. *Dev Cell* 3:631-643.
- de Freitas GR, Carruzzo A, Tsiskaridze A, Lobrinus JA, Bogousslavsky J (2001) Massive haemorrhagic transformation in cardioembolic stroke: the role of arterial wall trauma and dissection. *J Neurol Neurosurg Psychiatry* 70:672-674.
- del Peso L, Gonzalez-Garcia M, Page C, Herrera R, Nunez G (1997) Interleukin-3-induced phosphorylation of BAD through the protein kinase Akt. *Science* 278:687-689.
- Eguchi Y, Shimizu S, Tsujimoto Y (1997) Intracellular ATP levels determine cell death fate by apoptosis or necrosis. *Cancer Res* 57:1835-1840.
- Epstein CJ, Avraham KB, Lovett M, Smith S, Elroy-Stein O, Rotman G, Bry C, Groner Y (1987) Transgenic mice with increased Cu/Zn-superoxide dismutase activity: animal model of dosage effects in Down syndrome. *Proc Natl Acad Sci U S A* 84:8044-8048.
- Erdinçler P, Tuzgen S, Erdinçler UD, Oguz E, Korpınar A, Ciplak N, Kuday C (2002) Influence of aging on blood-brain barrier permeability and free radical formation following experimental brain cold injury. *Acta Neurochir (Wien)* 144:195-199; discussion 199-200.
- Fontaine MA, Geddes JW, Banks A, Butterfield DA (2000) Effect of exogenous and endogenous antioxidants on 3-nitrotyrosine acid-induced in vivo oxidative stress and striatal lesions: insights into Huntington's disease. *J Neurochem* 75:1709-1715.
- Forman HJ, Torres M (2002) Reactive oxygen species and cell signaling: respiratory burst in macrophage signaling. *Am J Respir Crit Care Med* 166:S4-8.

- Forsman M, Fleischer JE, Milde JH, Steen PA, Michenfelder JD (1988) Superoxide dismutase and catalase failed to improve neurologic outcome after complete cerebral ischemia in the dog. *Acta Anaesthesiol Scand* 32:152-155.
- Fridovich I (1995) Superoxide radical and superoxide dismutases. *Annu Rev Biochem* 64:97-112.
- Fujimura M, Morita-Fujimura Y, Copin J, Yoshimoto T, Chan PH (2001) Reduction of copper, zinc-superoxide dismutase in knockout mice does not affect edema or infarction volumes and the early release of mitochondrial cytochrome c after permanent focal cerebral ischemia. *Brain Res* 889:208-213.
- Fujimura M, Morita-Fujimura Y, Narasimhan P, Copin JC, Kawase M, Chan PH (1999a) Copper-zinc superoxide dismutase prevents the early decrease of apurinic/apyrimidinic endonuclease and subsequent DNA fragmentation after transient focal cerebral ischemia in mice. *Stroke* 30:2408-2415.
- Fujimura M, Morita-Fujimura Y, Noshita N, Sugawara T, Kawase M, Chan PH (2000) The cytosolic antioxidant copper/zinc-superoxide dismutase prevents the early release of mitochondrial cytochrome c in ischemic brain after transient focal cerebral ischemia in mice. *J Neurosci* 20:2817-2824.
- Fujimura M, Morita-Fujimura Y, Kawase M, Copin JC, Calagui B, Epstein CJ, Chan PH (1999b) Manganese superoxide dismutase mediates the early release of mitochondrial cytochrome C and subsequent DNA fragmentation after permanent focal cerebral ischemia in mice. *J Neurosci* 19:3414-3422.
- Geddes JW, Pang Z, Wiley DH (1996) Hippocampal damage and cytoskeletal disruption resulting from impaired energy metabolism. Implications for Alzheimer disease. *Mol Chem Neuropathol* 28:65-74.
- Hamilton BF, Gould DH (1987) Nature and distribution of brain lesions in rats intoxicated with 3-nitropropionic acid: a type of hypoxic (energy deficient) brain damage. *Acta Neuropathol (Berl)* 72:286-297.

- Hamner S, Arumae U, Li-Ying Y, Sun YF, Saarma M, Lindholm D (2001) Functional characterization of two splice variants of rat bad and their interaction with Bcl-w in sympathetic neurons. *Mol Cell Neurosci* 17:97-106.
- Hanada M, Ninomiya-Tsuji J, Komaki K, Ohnishi M, Katsura K, Kanamaru R, Matsumoto K, Tamura S (2001) Regulation of the TAK1 signaling pathway by protein phosphatase 2C. *J Biol Chem* 276:5753-5759.
- Hanada M, Kobayashi T, Ohnishi M, Ikeda S, Wang H, Katsura K, Yanagawa Y, Hiraga A, Kanamaru R, Tamura S (1998) Selective suppression of stress-activated protein kinase pathway by protein phosphatase 2C in mammalian cells. *FEBS Lett* 437:172-176.
- Harada H, Becknell B, Wilm M, Mann M, Huang LJ, Taylor SS, Scott JD, Korsmeyer SJ (1999) Phosphorylation and inactivation of BAD by mitochondria-anchored protein kinase A. *Mol Cell* 3:413-422.
- Haun SE, Kirsch JR, Helfaer MA, Kubos KL, Traystman RJ (1991) Polyethylene glycol-conjugated superoxide dismutase fails to augment brain superoxide dismutase activity in piglets. *Stroke* 22:655-659.
- Hengartner MO (2000) The biochemistry of apoptosis. *Nature* 407:770-776.
- Henneberry RC, Novelli A, Vigano MA, Reilly JA, Cox JA, Lysko PG (1989) Energy-related neurotoxicity at the NMDA receptor: a possible role in Alzheimer's disease and related disorders. *Prog Clin Biol Res* 317:143-156.
- Hillered L, Chan PH (1988a) Effects of arachidonic acid on respiratory activities in isolated brain mitochondria. *J Neurosci Res* 19:94-100.
- Hillered L, Chan PH (1988b) Role of arachidonic acid and other free fatty acids in mitochondrial dysfunction in brain ischemia. *J Neurosci Res* 20:451-456.
- Hirai I, Wang HG (2001) Survival-factor-induced phosphorylation of Bad results in its dissociation from Bcl-x(L) but not Bcl-2. *Biochem J* 359:345-352.
- Huang DC, Strasser A (2000) BH3-Only proteins-essential initiators of apoptotic cell death. *Cell* 103:839-842.

- Ikeda Y, Anderson JH, Long DM (1989) Oxygen free radicals in the genesis of traumatic and peritumoral brain edema. *Neurosurgery* 24:679-685.
- Ikeda Y, Toda S, Wang M, Nakazawa S (1994) Early changes of blood-brain barrier and superoxide scavenging activity in rat cryogenic brain injury. *Acta Neurochir Suppl (Wien)* 60:136-138.
- Ikonomidou C, Stefovskaja V, Turski L (2000) Neuronal death enhanced by N-methyl-D-aspartate antagonists. *Proc Natl Acad Sci U S A* 97:12885-12890.
- Imaizumi S, Woolworth V, Kinouchi H, Chen SF, Fishman RA, Chan PH (1990) Liposome-entrapped superoxide dismutase ameliorates infarct volume in focal cerebral ischaemia. *Acta Neurochir Suppl (Wien)* 51:236-238.
- Ingebritsen TS, Cohen P (1983) Protein phosphatases: properties and role in cellular regulation. *Science* 221:331-338.
- Kamii H, Kato I, Kinouchi H, Chan PH, Epstein CJ, Akabane A, Okamoto H, Yoshimoto T (1999) Amelioration of vasospasm after subarachnoid hemorrhage in transgenic mice overexpressing CuZn-superoxide dismutase. *Stroke* 30:867-871; discussion 872.
- Kawase M, Murakami K, Fujimura M, Morita-Fujimura Y, Gasche Y, Kondo T, Scott RW, Chan PH (1999) Exacerbation of delayed cell injury after transient global ischemia in mutant mice with CuZn superoxide dismutase deficiency. *Stroke* 30:1962-1968.
- Kim GW, Chan PH (2002) Involvement of superoxide in excitotoxicity and DNA fragmentation in striatal vulnerability in mice after treatment with the mitochondrial toxin, 3-nitropropionic acid. *J Cereb Blood Flow Metab* 22:798-809.
- Kim GW, Kondo T, Noshita N, Chan PH (2002) Manganese superoxide dismutase deficiency exacerbates cerebral infarction after focal cerebral ischemia/reperfusion in mice: implications for the production and role of superoxide radicals. *Stroke* 33:809-815.
- Kim GW, Lewen A, Copin J, Watson BD, Chan PH (2001) The cytosolic antioxidant, copper/zinc superoxide dismutase, attenuates blood-brain barrier disruption and oxidative cellular injury after photothrombotic cortical ischemia in mice. *Neuroscience* 105:1007-1018.

- Kim GW, Copin JC, Kawase M, Chen SF, Sato S, Gobbel GT, Chan PH (2000) Excitotoxicity is required for induction of oxidative stress and apoptosis in mouse striatum by the mitochondrial toxin, 3- nitropropionic acid. *J Cereb Blood Flow Metab* 20:119-129.
- Kinouchi H, Epstein CJ, Mizui T, Carlson E, Chen SF, Chan PH (1991) Attenuation of focal cerebral ischemic injury in transgenic mice overexpressing CuZn superoxide dismutase. *Proc Natl Acad Sci U S A* 88:11158-11162.
- Kinouchi H, Kamii H, Mikawa S, Epstein CJ, Yoshimoto T, Chan PH (1998) Role of superoxide dismutase in ischemic brain injury: a study using SOD-1 transgenic mice. *Cell Mol Neurobiol* 18:609-620.
- Klumpp S, Krieglstein J (2002) Serine/threonine protein phosphatases in apoptosis. *Curr Opin Pharmacol* 2:458-462.
- Klumpp S, Selke D, Hermesmeier J (1998) Protein phosphatase type 2C active at physiological Mg<sup>2+</sup>: stimulation by unsaturated fatty acids. *FEBS Lett* 437:229-232.
- Klumpp S, Selke D, Ahlemeyer B, Schaper C, Krieglstein J (2002) Relationship between protein phosphatase type-2C activity and induction of apoptosis in cultured neuronal cells. *Neurochem Int* 41:251-259.
- Koeppen AH (1995) The history of iron in the brain. *J Neurol Sci* 134 Suppl:1-9.
- Kogure K, Busto R, Scheinberg P (1981) The role of hydrostatic pressure in ischemic brain edema. *Ann Neurol* 9:273-282.
- Kondo T, Sharp FR, Honkaniemi J, Mikawa S, Epstein CJ, Chan PH (1997a) DNA fragmentation and Prolonged expression of c-fos, c-jun, and hsp70 in kainic acid-induced neuronal cell death in transgenic mice overexpressing human CuZn-superoxide dismutase. *J Cereb Blood Flow Metab* 17:241-256.
- Kondo T, Reaume AG, Huang TT, Carlson E, Murakami K, Chen SF, Hoffman EK, Scott RW, Epstein CJ, Chan PH (1997b) Reduction of CuZn-superoxide dismutase activity exacerbates neuronal cell injury and edema formation after transient focal cerebral ischemia. *J Neurosci* 17:4180-4189.

- Konishi Y, Lehtinen M, Donovan N, Bonni A (2002) Cdc2 phosphorylation of BAD links the cell cycle to the cell death machinery. *Mol Cell* 9:1005-1016.
- Kontos HA (1985) George E. Brown memorial lecture. Oxygen radicals in cerebral vascular injury. *Circ Res* 57:508-516.
- Kontos HA, Wei EP (1986) Superoxide production in experimental brain injury. *J Neurosurg* 64:803-807.
- Koutouzis TK, Borlongan CV, Freeman TB, Cahill DW, Sanberg PR (1994) Intrastratial 3-nitropropionic acid: a behavioral assessment. *Neuroreport* 5:2241-2245.
- Lafon-Cazal M, Pietri S, Culcasi M, Bockaert J (1993) NMDA-dependent superoxide production and neurotoxicity. *Nature* 364:535-537.
- Levasseur JE, Patterson JL, Jr., Ghatak NR, Kontos HA, Choi SC (1989) Combined effect of respirator-induced ventilation and superoxide dismutase in experimental brain injury. *J Neurosurg* 71:573-577.
- Lewen A, Matz P, Chan PH (2000) Free radical pathways in CNS injury. *J Neurotrauma* 17:871-890.
- Lewen A, Fujimura M, Sugawara T, Matz P, Copin JC, Chan PH (2001) Oxidative stress-dependent release of mitochondrial cytochrome c after traumatic brain injury. *J Cereb Blood Flow Metab* 21:914-920.
- Li Y, Chopp M, Jiang N, Yao F, Zaloga C (1995a) Temporal profile of in situ DNA fragmentation after transient middle cerebral artery occlusion in the rat. *J Cereb Blood Flow Metab* 15:389-397.
- Li Y, Copin JC, Reola LF, Calagui B, Gobbel GT, Chen SF, Sato S, Epstein CJ, Chan PH (1998) Reduced mitochondrial manganese-superoxide dismutase activity exacerbates glutamate toxicity in cultured mouse cortical neurons. *Brain Res* 814:164-170.
- Li Y, Huang TT, Carlson EJ, Melov S, Ursell PC, Olson JL, Noble LJ, Yoshimura MP, Berger C, Chan PH, et al. (1995b) Dilated cardiomyopathy and neonatal lethality in mutant mice lacking manganese superoxide dismutase. *Nat Genet* 11:376-381.



- Lieberthal W, Menza SA, Levine JS (1998) Graded ATP depletion can cause necrosis or apoptosis of cultured mouse proximal tubular cells. *Am J Physiol* 274:F315-327.
- Liu G, Hinch B, Davatol-Hag H, Lu Y, Powers M, Beavis AD (1996a) Temperature dependence of the mitochondrial inner membrane anion channel. The relationship between temperature and inhibition by protons. *J Biol Chem* 271:19717-19723.
- Liu TH, Beckman JS, Freeman BA, Hogan EL, Hsu CY (1989) Polyethylene glycol-conjugated superoxide dismutase and catalase reduce ischemic brain injury. *Am J Physiol* 256:H589-593.
- Liu X, Kim CN, Yang J, Jemmerson R, Wang X (1996b) Induction of apoptotic program in cell-free extracts: requirement for dATP and cytochrome c. *Cell* 86:147-157.
- Lizcano JM, Morrice N, Cohen P (2000) Regulation of BAD by cAMP-dependent protein kinase is mediated via phosphorylation of a novel site, Ser155. *Biochem J* 349:547-557.
- Lu G, Greene EL, Nagai T, Egan BM (1998) Reactive oxygen species are critical in the oleic acid-mediated mitogenic signaling pathway in vascular smooth muscle cells. *Hypertension* 32:1003-1010.
- Lu G, Morinelli TA, Meier KE, Rosenzweig SA, Egan BM (1996) Oleic acid-induced mitogenic signaling in vascular smooth muscle cells. A role for protein kinase C. *Circ Res* 79:611-618.
- Ludolph AC, Seelig M, Ludolph AG, Sabri MI, Spencer PS (1992) ATP deficits and neuronal degeneration induced by 3-nitropropionic acid. *Ann N Y Acad Sci* 648:300-302.
- MacManus JP, Buchan AM, Hill IE, Rasquinha I, Preston E (1993) Global ischemia can cause DNA fragmentation indicative of apoptosis in rat brain. *Neurosci Lett* 164:89-92.
- Maeda M, Akai F, Yanagihara T (1997) Neuronal integrity and astrocytic reaction in cold injury: an immunohistochemical investigation. *Acta Neuropathol (Berl)* 94:116-123.
- Maher P, Schubert D (2000) Signaling by reactive oxygen species in the nervous system. *Cell Mol Life Sci* 57:1287-1305.

- Mamoun CB, Goldberg DE (2001) Plasmodium protein phosphatase 2C dephosphorylates translation elongation factor 1beta and inhibits its PKC-mediated nucleotide exchange activity in vitro. *Mol Microbiol* 39:973-981.
- Martin JB, Gusella JF (1986) Huntington's disease. Pathogenesis and management. *N Engl J Med* 315:1267-1276.
- Masters SC, Yang H, Datta SR, Greenberg ME, Fu H (2001) 14-3-3 inhibits Bad-induced cell death through interaction with serine-136. *Mol Pharmacol* 60:1325-1331.
- Mattson MP, Culmsee C, Yu ZF (2000) Apoptotic and antiapoptotic mechanisms in stroke. *Cell Tissue Res* 301:173-187.
- Matz PG, Fujimura M, Lewen A, Morita-Fujimura Y, Chan PH (2001) Increased cytochrome c-mediated DNA fragmentation and cell death in manganese-superoxide dismutase-deficient mice after exposure to subarachnoid hemolysate. *Stroke* 32:506-515.
- Ment LR, Stewart WB, Duncan CC (1985) Beagle puppy model of intraventricular hemorrhage. Effect of superoxide dismutase on cerebral blood flow and prostaglandins. *J Neurosurg* 62:563-569.
- Michelson AM, Jadot G, Puget K (1988) Treatment of brain trauma with liposomal superoxide dismutase. *Free Radic Res Commun* 4:209-224.
- Mikawa S, Kinouchi H, Kamii H, Gobbel GT, Chen SF, Carlson E, Epstein CJ, Chan PH (1996) Attenuation of acute and chronic damage following traumatic brain injury in copper, zinc-superoxide dismutase transgenic mice. *J Neurosurg* 85:885-891.
- Morita-Fujimura Y, Fujimura M, Kawase M, Chan PH (1999a) Early decrease in apurinic/aprimidinic endonuclease is followed by DNA fragmentation after cold injury-induced brain trauma in mice. *Neuroscience* 93:1465-1473.
- Morita-Fujimura Y, Fujimura M, Kawase M, Chen SF, Chan PH (1999b) Release of mitochondrial cytochrome c and DNA fragmentation after cold injury-induced brain trauma in mice: possible role in neuronal apoptosis. *Neurosci Lett* 267:201-205.
- Morita-Fujimura Y, Fujimura M, Gasche Y, Copin JC, Chan PH (2000) Overexpression of copper and zinc superoxide dismutase in transgenic mice prevents the induction and

- activation of matrix metalloproteinases after cold injury-induced brain trauma. *J Cereb Blood Flow Metab* 20:130-138.
- Murakami K, Kondo T, Epstein CJ, Chan PH (1997) Overexpression of CuZn-superoxide dismutase reduces hippocampal injury after global ischemia in transgenic mice. *Stroke* 28:1797-1804.
- Murakami K, Kawase M, Kondo T, Chan PH (1998a) Cellular accumulation of extravasated serum protein and DNA fragmentation following vasogenic edema. *J Neurotrauma* 15:825-835.
- Murakami K, Kondo T, Yang G, Chen SF, Morita-Fujimura Y, Chan PH (1999) Cold injury in mice: a model to study mechanisms of brain edema and neuronal apoptosis. *Prog Neurobiol* 57:289-299.
- Murakami K, Kondo T, Kawase M, Li Y, Sato S, Chen SF, Chan PH (1998b) Mitochondrial susceptibility to oxidative stress exacerbates cerebral infarction that follows permanent focal cerebral ischemia in mutant mice with manganese superoxide dismutase deficiency. *J Neurosci* 18:205-213.
- Nag S, Takahashi JL, Kilty DW (1997) Role of vascular endothelial growth factor in blood-brain barrier breakdown and angiogenesis in brain trauma. *J Neuropathol Exp Neurol* 56:912-921.
- Nag S, Picard P, Stewart DJ (2001) Expression of nitric oxide synthases and nitrotyrosine during blood-brain barrier breakdown and repair after cold injury. *Lab Invest* 81:41-49.
- Nakao N, Brundin P (1997) Effects of alpha-phenyl-tert-butyl nitrone on neuronal survival and motor function following intrastriatal injections of quinolinate or 3-nitropropionic acid. *Neuroscience* 76:749-761.
- Nakao N, Grasbon-Frodl EM, Widner H, Brundin P (1996) Antioxidant treatment protects striatal neurons against excitotoxic insults. *Neuroscience* 73:185-200.

- Neshat MS, Raitano AB, Wang HG, Reed JC, Sawyers CL (2000) The survival function of the Bcr-Abl oncogene is mediated by Bad-dependent and -independent pathways: roles for phosphatidylinositol 3-kinase and Raf. *Mol Cell Biol* 20:1179-1186.
- Nguyen AN, Shiozaki K (1999) Heat-shock-induced activation of stress MAP kinase is regulated by threonine- and tyrosine-specific phosphatases. *Genes Dev* 13:1653-1663.
- Nicotera P, Leist M, Ferrando-May E (1998) Intracellular ATP, a switch in the decision between apoptosis and necrosis. *Toxicol Lett* 102-103:139-142.
- Nishino H, Shimano Y, Kumazaki M, Sakurai T (1995) Chronically administered 3-nitropropionic acid induces striatal lesions attributed to dysfunction of the blood-brain barrier. *Neurosci Lett* 186:161-164.
- Nishino H, Fujimoto I, Shimano Y, Hida H, Kumazaki M, Fukuda A (1996) 3-Nitropropionic acid produces striatum selective lesions accompanied by iNOS expression. *J Chem Neuroanat* 10:209-212.
- Noshita N, Sugawara T, Fujimura M, Morita-Fujimura Y, Chan PH (2001) Manganese Superoxide Dismutase Affects Cytochrome c Release and Caspase-9 Activation After Transient Focal Cerebral Ischemia in Mice. *J Cereb Blood Flow Metab* 21:557-567.
- Oltvai ZN, Milliman CL, Korsmeyer SJ (1993) Bcl-2 heterodimerizes in vivo with a conserved homolog, Bax, that accelerates programmed cell death. *Cell* 74:609-619.
- Orita T, Nishizaki T, Kamiryo T, Harada K, Aoki H (1988) Cerebral microvascular architecture following experimental cold injury. *J Neurosurg* 68:608-612.
- Palfi S, Ferrante RJ, Brouillet E, Beal MF, Dolan R, Guyot MC, Peschanski M, Hantraye P (1996) Chronic 3-nitropropionic acid treatment in baboons replicates the cognitive and motor deficits of Huntington's disease. *J Neurosci* 16:3019-3025.
- Patel M, Day BJ, Crapo JD, Fridovich I, McNamara JO (1996) Requirement for superoxide in excitotoxic cell death. *Neuron* 16:345-355.
- Peter ME, Krammer PH (1998) Mechanisms of CD95 (APO-1/Fas)-mediated apoptosis. *Curr Opin Immunol* 10:545-551.

- Phelan AM, Lange DG (1991) Ischemia/reperfusion-induced changes in membrane fluidity characteristics of brain capillary endothelial cells and its prevention by liposomal-incorporated superoxide dismutase. *Biochim Biophys Acta* 1067:97-102.
- Phillis JW (1994) A "radical" view of cerebral ischemic injury. *Prog Neurobiol* 42:441-448.
- Pigott JP, Donovan DL, Fink JA, Sharp WV (1988) Experimental pharmacologic cerebroprotection. *J Vasc Surg* 7:625-630.
- Raff M (1998) Cell suicide for beginners. *Nature* 396:119-122.
- Raff MC, Barres BA, Burne JF, Coles HS, Ishizaki Y, Jacobson MD (1993) Programmed cell death and the control of cell survival: lessons from the nervous system. *Science* 262:695-700.
- Reaume AG, Elliott JL, Hoffman EK, Kowall NW, Ferrante RJ, Siwek DF, Wilcox HM, Flood DG, Beal MF, Brown RH, Jr., Scott RW, Snider WD (1996) Motor neurons in Cu/Zn superoxide dismutase-deficient mice develop normally but exhibit enhanced cell death after axonal injury. *Nat Genet* 13:43-47.
- Reulen HJ, Graham R, Spatz M, Klatzo I (1977) Role of pressure gradients and bulk flow in dynamics of vasogenic brain edema. *J Neurosurg* 46:24-35.
- Rhoads DE, Osburn LD, Peterson NA, Raghupathy E (1983) Release of neurotransmitter amino acids from synaptosomes: enhancement of calcium-independent efflux by oleic and arachidonic acids. *J Neurochem* 41:531-537.
- Riepe M, Hori N, Ludolph AC, Carpenter DO, Spencer PS, Allen CN (1992) Inhibition of energy metabolism by 3-nitropropionic acid activates ATP-sensitive potassium channels. *Brain Res* 586:61-66.
- Rink A, Fung KM, Trojanowski JQ, Lee VM, Neugebauer E, McIntosh TK (1995) Evidence of apoptotic cell death after experimental traumatic brain injury in the rat. *Am J Pathol* 147:1575-1583.
- Salomoni P, Wasik MA, Riedel RF, Reiss K, Choi JK, Skorski T, Calabretta B (1998) Expression of constitutively active Raf-1 in the mitochondria restores antiapoptotic

- and leukemogenic potential of a transformation-deficient BCR/ABL mutant. *J Exp Med* 187:1995-2007.
- Sato S, Gobbel GT, Honkaniemi J, Li Y, Kondo T, Murakami K, Sato M, Copin JC, Chan PH (1997a) Apoptosis in the striatum of rats following intraperitoneal injection of 3-nitropropionic acid. *Brain Res* 745:343-347.
- Sato S, Gobbel GT, Honkaniemi J, Li Y, Kondo T, Murakami K, Sato M, Copin JC, Sharp FR, Chan PH (1998) Decreased expression of bcl-2 and bcl-x mRNA coincides with apoptosis following intracerebral administration of 3-nitropropionic acid. *Brain Res* 808:56-64.
- Sato S, Gobbel GT, Li Y, Kondo T, Murakami K, Sato M, Hasegawa K, Copin JC, Honkaniemi J, Sharp FR, Chan PH (1997b) Blood-brain barrier disruption, HSP70 expression and apoptosis due to 3-nitropropionic acid, a mitochondrial toxin. *Acta Neurochir Suppl* 70:237-239.
- Scaffidi C, Fulda S, Srinivasan A, Friesen C, Li F, Tomaselli KJ, Debatin KM, Kramer PH, Peter ME (1998) Two CD95 (APO-1/Fas) signaling pathways. *Embo J* 17:1675-1687.
- Scheid MP, Duronio V (1998) Dissociation of cytokine-induced phosphorylation of Bad and activation of PKB/akt: involvement of MEK upstream of Bad phosphorylation. *Proc Natl Acad Sci U S A* 95:7439-7444.
- Schulz JB, Henshaw DR, MacGarvey U, Beal MF (1996) Involvement of oxidative stress in 3-nitropropionic acid neurotoxicity. *Neurochem Int* 29:167-171.
- Schurer L, Groggaard B, Gerdin B, Arfors KE (1990) Superoxide dismutase does not prevent delayed hypoperfusion after incomplete cerebral ischaemia in the rat. *Acta Neurochir (Wien)* 103:163-170.
- Schurmann A, Mooney AF, Sanders LC, Sells MA, Wang HG, Reed JC, Bokoch GM (2000) p21-activated kinase 1 phosphorylates the death agonist bad and protects cells from apoptosis. *Mol Cell Biol* 20:453-461.

- Sengpiel B, Preis E, Krieglstein J, Prehn JH (1998) NMDA-induced superoxide production and neurotoxicity in cultured rat hippocampal neurons: role of mitochondria. *Eur J Neurosci* 10:1903-1910.
- Simpson JR, Isacson O (1993) Mitochondrial impairment reduces the threshold for in vivo NMDA-mediated neuronal death in the striatum. *Exp Neurol* 121:57-64.
- Skoglosa Y, Lewen A, Takei N, Hillered L, Lindholm D (1999) Regulation of pituitary adenylate cyclase activating polypeptide and its receptor type 1 after traumatic brain injury: comparison with brain-derived neurotrophic factor and the induction of neuronal cell death. *Neuroscience* 90:235-247.
- Soares HD, Hicks RR, Smith D, McIntosh TK (1995) Inflammatory leukocytic recruitment and diffuse neuronal degeneration are separate pathological processes resulting from traumatic brain injury. *J Neurosci* 15:8223-8233.
- Stoffel M, Rinecker M, Plesnila N, Eriskat J, Baethmann A (2001) Role of nitric oxide in the secondary expansion of a cortical brain lesion from cold injury. *J Neurotrauma* 18:425-434.
- Sugawara T, Lewen A, Gasche Y, Yu F, Chan PH (2002) Overexpression of SOD1 protects vulnerable motor neurons after spinal cord injury by attenuating mitochondrial cytochrome c release. *Faseb J* 16:1997-1999.
- Tan Y, Ruan H, Demeter MR, Comb MJ (1999) p90(RSK) blocks bad-mediated cell death via a protein kinase C-dependent pathway. *J Biol Chem* 274:34859-34867.
- Tanno H, Nockels RP, Pitts LH, Noble LJ (1992) Breakdown of the blood-brain barrier after fluid percussive brain injury in the rat. Part 1: Distribution and time course of protein extravasation. *J Neurotrauma* 9:21-32.
- Troeger MB, Rafalowska U, Erecinska M (1984) Effect of oleate on neurotransmitter transport and other plasma membrane functions in rat brain synaptosomes. *J Neurochem* 42:1735-1742.

- Trotti D, Danbolt NC, Volterra A (1998) Glutamate transporters are oxidant-vulnerable: a molecular link between oxidative and excitotoxic neurodegeneration? *Trends Pharmacol Sci* 19:328-334.
- Tsuiki S, Hiraga A, Kikuchi K, Tamura S (1988) Purification of an Mg<sup>2+</sup>-dependent protein phosphatase. *Methods Enzymol* 159:437-446.
- Unterberg A, Schneider GH, Gottschalk J, Lanksch WR (1994) Development of traumatic brain edema in old versus young rats. *Acta Neurochir Suppl (Wien)* 60:431-433.
- Vagnozzi R, Marmarou A, Tavazzi B, Signoretti S, Di Pierro D, del Bolgia F, Amorini AM, Fazzina G, Sherkat S, Lazzarino G (1999) Changes of cerebral energy metabolism and lipid peroxidation in rats leading to mitochondrial dysfunction after diffuse brain injury. *J Neurotrauma* 16:903-913.
- Vaux DL, Korsmeyer SJ (1999) Cell death in development. *Cell* 96:245-254.
- Virdee K, Parone PA, Tolkovsky AM (2000) Phosphorylation of the pro-apoptotic protein BAD on serine 155, a novel site, contributes to cell survival. *Curr Biol* 10:1151-1154.
- Wang HG, Reed JC (1998) Mechanisms of Bcl-2 protein function. *Histol Histopathol* 13:521-530.
- Wang HG, Rapp UR, Reed JC (1996) Bcl-2 targets the protein kinase Raf-1 to mitochondria. *Cell* 87:629-638.
- Wang HG, Pathan N, Ethell IM, Krajewski S, Yamaguchi Y, Shibasaki F, McKeon F, Bobo T, Franke TF, Reed JC (1999) Ca<sup>2+</sup>-induced apoptosis through calcineurin dephosphorylation of BAD. *Science* 284:339-343.
- Wang X (2001) The expanding role of mitochondria in apoptosis. *Genes Dev* 15:2922-2933.
- Wei EP, Kontos HA, Dietrich WD, Povlishock JT, Ellis EF (1981) Inhibition by free radical scavengers and by cyclooxygenase inhibitors of pial arteriolar abnormalities from concussive brain injury in cats. *Circ Res* 48:95-103.
- Wullner U, Young AB, Penney JB, Beal MF (1994) 3-Nitropropionic acid toxicity in the striatum. *J Neurochem* 63:1772-1781.



- Yaffe MB, Elia AE (2001) Phosphoserine/threonine-binding domains. *Curr Opin Cell Biol* 13:131-138.
- Yang E, Zha J, Jockel J, Boise LH, Thompson CB, Korsmeyer SJ (1995) Bad, a heterodimeric partner for Bcl-XL and Bcl-2, displaces Bax and promotes cell death. *Cell* 80:285-291.
- Yang G, Chan PH, Chen J, Carlson E, Chen SF, Weinstein P, Epstein CJ, Kamii H (1994) Human copper-zinc superoxide dismutase transgenic mice are highly resistant to reperfusion injury after focal cerebral ischemia. *Stroke* 25:165-170.
- Yang JC, Cortopassi GA (1998) Induction of the mitochondrial permeability transition causes release of the apoptogenic factor cytochrome c. *Free Radic Biol Med* 24:624-631.
- Zha J, Harada H, Yang E, Jockel J, Korsmeyer SJ (1996) Serine phosphorylation of death agonist BAD in response to survival factor results in binding to 14-3-3 not BCL-X(L). *Cell* 87:619-628.
- Zha J, Harada H, Osipov K, Jockel J, Waksman G, Korsmeyer SJ (1997) BH3 domain of BAD is required for heterodimerization with BCL-XL and pro-apoptotic activity. *J Biol Chem* 272:24101-24104.
- Zhang XM, Ellis EF (1991) Superoxide dismutase decreases mortality, blood pressure, and cerebral blood flow responses induced by acute hypertension in rats. *Stroke* 22:489-494.
- Zhou H, Li XM, Meinkoth J, Pittman RN (2000) Akt regulates cell survival and apoptosis at a postmitochondrial level. *J Cell Biol* 151:483-494.
- Zorumski CF, Olney JW (1993) Excitotoxic neuronal damage and neuropsychiatric disorders. *Pharmacol Ther* 59:145-162.

## 9. Abbreviations

3-NP	3-Nitropropionic acid
dUTP	Deoxyuridine triphosphate
AB	Antibody
APS	Ammonium persulfate
ATP	Adenosine triphosphate
Bad	Bcl-2/Bcl-x <sub>L</sub> -antagonist, causing cell death
Bad-GST	Bad, Glutathione-S-transferase-tagged
Bad-155P	Bad, phosphorylated at Ser <sup>155</sup>
BBB	Blood brain barrier
BH3	Bcl-2 homology 3
BSA	Bovine serum albumine
cAMP	Cyclic adenosine monophosphate
cA-PK	Catalytic subunit of protein kinase type A
CIBT	Cold injury-induced brain trauma
CNS	Central nervous system
DAB	N-N'-Diaminobenzidine
DMF	Dimethylformamide
DMSO	Dimethylsulfoxide
DNA	Desoxyribonucleic acid
dNTP	Deoxynucleosid triphosphate
EAA	Excitatory amino acids
EDTA	Ethylendiamin tetraacetic acid
EGTA	Ethylenglycol tetraacetic acid
HD	Huntington's disease
H&E	Hematoxylin and eosin
HEPES	N-(2-Hydroxyethyl)piperazine-N'-(2-ethanesulfonic acid)
HEt	Hydroethidine
HRP	Horseradish peroxidase
ICC	Immunocytochemistry
IgG	Immunoglobuline Type G
kDa	Kilo Dalton
MAP-kinase	Mitogen-activated protein kinase
MEM	Minimal essential medium

MOPS	3-(N-Morpholino) propanesulfonic acid
MPO	Myeloperoxidase
M <sub>r</sub>	Relative molecular weight
mRNA	Messenger-RNA
NADPH	Nicotinamide adenine dinucleotide phosphate
NB	Neurobasal medium
NB-B27	Neurobasal medium without supplement B27
NB+B27-AO	Neurobasal medium with supplement B27 without antioxidants
NBT	Nitro-blue tetrazolium
NMDA	N-methyl-D-aspartate
N <sub>2</sub> O	Nitrogen dioxide
NO·	Nitric oxide
O <sub>2</sub>	Oxygen
O <sub>2</sub> <sup>-·</sup>	Superoxide anion radical
PBS	Phosphate buffered saline
PCR	Polymerase chain reaction
PEG	Polyethylene glycole
PEI	Polyethylenimine
PK	Protein kinase
PKA/PKB	Protein kinase type-A/B
PP	Protein phosphatase
PP2C	Protein phosphatase type-2C
PPP	Phosphoprotein phosphatases
PPM	Protein phosphatase Mg <sup>2+</sup> -dependent
p-Ser	Phospho-serine
PTP	Protein tyrosine phosphatase
RNA	Ribonucleic acid
ROS	Reactive oxygen species
RT	Room temperature
SDS	Sodiumdodecylsulfate
Ser	Serine
SOD	Superoxide dismutase
SOD1	Cu/Zn-Superoxide dismutase, Cu/Zn-SOD
SOD1-TG	SOD1 transgenic mice

SOD1-KO	SOD1 knock-out mice
SOD2	Mn-Superoxide dismutase, Mn-SOD
SOD2-KO	SOD2 knock-out mice
TB	Trypan blue
TBI	Traumatic brain injury
TEMED	N,N,N',N'-tetramethyl-ethylene-diamine
TdT	Terminal deoxynucleotidyl transferase
Thr	Threonine
TNF- $\alpha$	Tumor necrosis factor alpha
Tris	Tris-hydroxymethyl aminomethan
TUNEL	Transferase-dUTP-Nick-End-Labeling
U	Unit
UV	Ultra violet
WT	Wild-type mice

## 10. Curriculum vitae

Susanna Grzeschik

Hubgraben 4

35041 Marburg

Date of birth	22. 06. 1974
Place of birth	Münster (Westf.), Germany
Family status	unmarried
Nationality	German

### School education

1980-1984	Elementary school
1984-1988	Gymnasium Paulinum, Münster
1988-1993	Gymnasium Philippinum, Marburg

### University training

10/1993-05/1998	Student of Pharmacy at the Philipps-University, Marburg
09/1995	First state examination
05/1998	Second state examination
05/1999	Final state examination, qualification as registered pharmacist
06/1999	Start of Ph.D. work at the faculty of Pharmacy, Institute of Pharmacology and Toxicology, Philipps-University, Marburg, under the supervision of Prof. Josef Krieglstein
09/1999-12/2001	Practical Ph.D. work in the laboratory of Prof. Pak H. Chan, Department of Neurosurgery, School of Medicine, Stanford University, Palo Alto, USA
01/2002-12/2002	Practical Ph.D. work in the laboratory of Prof. J. Krieglstein Faculty of Pharmacy, Institute of Pharmacology and Toxicology, Philipps-University, Marburg

## **Professional experience**

- 05/1998-11/1998      Practical work, Bayer AG, Division Tropon CNS-Research, Cologne, Germany
- 11/1998-04/1999      Practical work, Pharmacy store “Pelikan”, Giessen, Germany
- 1/2002-12/2002      Scientific co-worker, Institute of Pharmacology and Toxicology, Philipps-University, Marburg

## **Erklärung**

Ich versichere, daß ich meine Dissertation

**„On the role of superoxide dismutase and protein phosphatase type-2C $\beta$  in neuronal cell death”**

selbstständig und ohne unerlaubte Hilfe angefertigt habe und mich dabei keiner anderen als der von mir ausdrücklich bezeichneten Quellen bedient habe.

Die Dissertation wurde in der jetzigen oder einer ähnlichen Form noch bei keiner anderen Hochschule eingereicht und hat noch keinen sonstigen Prüfungszwecken gedient.

Marburg, den 10. 03. 2003

Susanna Grzeschik